

Universal bounds on fluctuations in thermal machines and thermal transport junctions

A thesis

Submitted in partial fulfillment of the requirements of the degree of
Doctor of Philosophy

by

Sushant Saryal

Registration ID-20173558



Department of Physics

Indian Institute Of Science Education And Research

Pune-411008, India

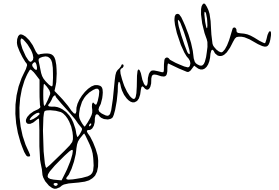
September 2, 2022

*Dedicated to my Parents,
Sunita Devi and Bhagwan Singh Rana.*

Certificate

Certified that the work incorporated in the thesis entitled “**Universal bounds on fluctuations in thermal machines and thermal transport junctions**” submitted by **Sushant Saryal** was carried out by the candidate, under my supervision. The work presented here or any part of it has not been included in any other thesis submitted previously for the award of any degree or diploma from any other university or institution.

Date: September 2, 2022




Prof. Bijay Kumar Agarwalla
(Supervisor)

Declaration

I declare that this written submission represents my ideas in my own words and where others ideas have been included, I have adequately cited and referenced the original sources. I also declare that I have adhered to all principles of academic honesty and integrity and have not misrepresented or fabricated or falsified any idea/data/fact/source in my submission. I understand that violation of the above will be cause for disciplinary action by the Institute and can also evoke penal action from the sources which have thus not been properly cited or from whom proper permission has not been taken when needed.

Date: September 2, 2022


Sushant Saryal
20173558

Acknowledgments

Firstly, I would like to express my sincere gratitude to my advisor Prof. Bijay Kumar Agarwalla for his continuous support, patience, and guidance throughout my PhD. I greatly benefited from his wealth of knowledge, countless discussions and meticulous editing. I am extremely grateful that he took me as his student and always inspired me to work harder.

I would like to especially thank Prof. Deepak Dhar with whom I have collaborated and still collaborating on several exciting projects. He has greatly influenced me to appreciate the scientific enterprise as a whole without falling into the trap of extreme compartmentalization. He is a constant source of inspiration for several generations of physicists and it is a privilege to work with him.

I would like to extend my sincere thanks to my collaborators, Prof. Dvira Segal, Prof. T. S. Mahesh, Hava Meira Friedman, Matthew Gerry, Ilia Khait, Sandipan Mohanta, Onkar Sadekar, and Soham Pal, without them this thesis would not have been possible. I also want to thank all of my former and present group members, Ashrith, Sravya, Bhavesh, Akash, Pranay, Madumita, and Moumita for useful discussions during group meetings. I would also like to thank my other collaborators, Prof. Tridib Sadhu and Juliane Klamsner, with whom I collaborated in early parts of my PhD. I also want to thank my RAC members, Prof. M. S. Santhanam, Prof. G J Sreejith, and Prof. Arnab Saha, for providing insightful feedback on my work. I would also like to thank Aanjaneya for useful discussions on broad range of topics.

I would like to thank all the friends I made in IISER Pune, Anupam, Priya, Bhumika, Chetna, Navita, Uma, Gokul, Pranay, Mayank, Sourabh, Dhruv, Arjit, Projjowal, Sudhasattwa, Naveen and especially Abhishek, with whom I shared my office. They made my stay memorable in IISER. I also want to thank my school and undergraduate friends, Shamema, Anurag, Sumit, Ravi, Sakshi, Soma, Suraj, and especially Rashmi, who stayed in constant touch throughout my Ph.D.

I would like to offer my special thanks to CSIR for providing financial support for

my PhD. I would also like to thank IISER Pune administrative staff for the hassle-free paperwork, especially during Covid.

Last but not least, I would like to thank my parents and my younger brother Prashant for their constant support, advice, encouragement and unconditional love.

Abstract

The second law of thermodynamics forbids the possibility of a perpetual machine of a second kind. It provides a universal upper bound on the efficiency of any thermal machine operating between two heat baths, famously known as *Carnot Efficiency*. But traditional thermodynamics was only concerned with average quantities because typically, fluctuations can be ignored for macro systems, for example, steam engines, automobile engines, etc. With the rapid technological development over the last several decades, we can now investigate systems of sizes that can range from hundreds of nanometers to a few nanometers, such as quantum dots, molecular motors, single atoms, etc, at temperatures that range from micro to nano Kelvin. As a consequence of these advancements, in the past two decades, various small-scale thermal machines have been realized using state-of-the-art experimental techniques like ultra cold atoms, single colloidal particles, single-molecule optomechanical systems, and Paul ion-trap technique, etc. Since these devices operate away from equilibrium, understanding non-equilibrium thermodynamic properties of such small-scale systems is an active area of research where one can no longer ignore the role of fluctuations of thermal and/or quantum origins and therefore a proper probabilistic description is required. Thus, a natural question arises that whether any universal bound exists on the fluctuations as well?

In this thesis, we attempt to shed light on understanding properties of fluctuations in non-equilibrium systems and its impact on the performance of thermal machines by providing universal bounds on the fluctuations of the underlying currents. We will first show that, for a time-reversal symmetric continuous thermal machines, the relative fluctuation of the output current is always greater than the relative fluctuations of the input current in linear response. As a consequence, the ratio between the fluctuations of the output and input currents are bounded both from above and below, where the lower (upper) bound is given by the square of the averaged efficiency (square of the Carnot efficiency) of the thermal machine. Then we will generalize our findings to the machines with broken time-reversal

symmetry. Later we elaborate an extension of our work to the finite-time quantum cycles, in particular for quantum Otto machines. All of these above studies and obtained universal results uncover a novel relationship among the recently discovered trade-off relations for individual currents, famously known as Thermodynamic Uncertainty Relation (TUR). TUR provides bound on relative fluctuations of individual current in terms of associated entropy production. Our work in the context of thermal machines reveals that TUR for individual currents are not independent of each other but follow a strict hierarchy in the operational regime.

In the later part of the thesis we will focus our attention on the fate of of the TUR relation in steady-state and transient-state transport junctions. For steady-state transport following the universal non-equilibrium steady-state fluctuation relations, we derive a general condition on the validity of the TUR for both classical and quantum systems. For transient-state situation we explore TUR in the context of energy transport in a bipartite setting for three exactly solvable toy model systems, two coupled harmonic oscillators, two coupled qubits, and a hybrid coupled oscillator-qubit system, and analyze the role played by the underlying statistics of the transport carriers in the TUR.

List of Publications

1. **S. Saryal**, S. Mohanta, and B. K. Agarwalla, *Bounds on fluctuations for machines with broken time-reversal symmetry: A linear response study*, [Phys. Rev. E 105, 024129 \(2022\)](#).
2. S. Mohanta, **S. Saryal**, and B. K. Agarwalla, *Universal bounds on cooling power and cooling efficiency for autonomous absorption refrigerators*, [Phys. Rev. E 105, 034127 \(2022\)](#).
3. **S. Saryal**, M. Gerry, I Khait, D. Segal, and B.K.Agarwalla, *Universal Bounds on Fluctuations in Continuous Thermal Machines*, [Phys. Rev. Lett. 127, 190603 \(2021\)](#).
4. **S. Saryal** and B. K. Agarwalla , *Bounds on fluctuations for finite-time quantum Otto cycle*, [Phys. Rev. E 103, L060103 \(2021\)](#).
5. **S. Saryal**, O. Sadekar, and B. K. Agarwalla , *Thermodynamic uncertainty relation for energy transport in a transient regime: A model study*, [Phys. Rev. E 103, 022141 \(2021\)](#).
6. S. Pal, **Sushant Saryal**, D. Segal, T. S. Mahesh, and Bijay Kumar Agarwalla *Experimental study of the thermodynamic uncertainty relation*, [Phys. Rev. Research 2, 022044\(R\) \(2020\)](#).
7. **S. Saryal**, H. M. Friedman, D. Segal, and B K. Agarwalla , *Thermodynamic uncertainty relation in thermal transport*, [Phys. Rev. E 100, 042101 \(2019\)](#).

This thesis is based on Ref. 1, 3, 4, 5, and 7, and excludes Ref. 2 and 6.

Contents

Declaration	iii
Acknowledgments	iv
Abstract	vi
List of Publications	viii
1 Introduction	1
1.1 Motivations	1
1.2 A short survey about fluctuation	2
1.2.1 Evans–Searles and Gallavotti-Cohen Fluctuation Theorems	3
1.2.2 Jarzynski Equality and Crooks Fluctuation Theorem	4
1.2.3 Exchange Fluctuation Theorem (XFT)	5
1.2.4 Quantum Fluctuation Theorems	6
1.3 Thermodynamic Uncertainty Relations	9
1.4 Thermal machines	11
1.4.1 Continuous thermal machines	11
1.4.2 Discrete thermal machines	13
1.5 Outline of the thesis	14
2 Universal bounds on fluctuations in continuous thermal machines	17
2.1 Introduction	18
2.2 Linear irreversible thermodynamics	19
2.3 Universal bounds on efficiency and fluctuations for time-reversal symmetric systems	21
2.4 Connection with thermodynamic uncertainty relation	24
2.4.1 Connection between the bounds on efficiency following the TUR and following Eq. (2.20)	25
2.5 Example 1: Steady-state thermoelectric transport in two-terminal systems	27

2.6	Example 2: Quantum Absorption Refrigerator	35
2.7	Summary	40
3	Universal bounds on fluctuations for continuous machines with broken time-reversal symmetry	42
3.1	Introduction	42
3.2	Universal bounds in absence of time-reversal symmetry	43
3.3	Connection with generalized thermodynamic uncertainty relation	47
3.4	Bounds on relative fluctuations in forward and reversed processes	48
3.5	Example: Quantum thermoelectric transport in a three-dot setup in the presence of an external magnetic field	49
3.6	Summary	53
4	Bounds on fluctuations for finite-time quantum Otto cycle	56
4.1	Introduction	56
4.2	Quantum Otto Cycle	57
4.3	Joint probability distribution for input heat and output work in quantum Otto engine	59
4.4	Quasistatic limit	61
4.5	Beyond quasistatic limit	62
4.5.1	Working fluid consisting of a qubit	62
4.5.2	Working fluid consisting of a harmonic oscillator(HO)	66
4.6	Connection with the finite-time TUR	68
4.7	Summary	68
5	Thermodynamic uncertainty relation for steady-state thermal transport junctions	71
5.1	Introduction	71
5.2	Perturbative expansion for the TUR from fluctuation symmetry	74
5.3	Coupled harmonic oscillators: Proof for the validity of the TUR	77
5.4	Thermal transport of noninteracting electrons: TUR violation in the resonant transport regime	79
5.5	Fate of single-affinity TUR in presence of magnetic field	84

5.6	Summary	86
6	Thermodynamic uncertainty relation for energy transport in transient regime	88
6.1	Introduction	89
6.2	Models and TUR	90
6.2.1	Two-oscillator system	90
6.2.2	Two-qubit system	98
6.2.3	Hybrid spin-oscillator system	102
6.3	Proof of T-TUR for generic bipartite systems in the weak coupling regime .	105
6.4	Comparison with Quadratic Bound	110
6.5	Summary	112
7	Concluding remarks and Future prospects	115
A	Quantum XFT in thermal-coupling limit	119
B	Tight-coupling limit beyond linear response	121
C	Single affinity limit in time-reversal symmetric continuous machines	123
D	Harmonic junctions in the classical limit	124
	References	125

1.1 Motivations

The quest to build most efficient and powerful heat engine led Sadi Carnot [1] to pioneer the subject what is known today as *Thermodynamics* [2]. Although the initial development of the subject was motivated by engineering optimal thermal machines, thermodynamics remains one of the fundamental physical theory in science. In fact its core principles have survived both relativity and quantum revolution. One of the central result of thermodynamics is that for any engine operating between hot and cold reservoirs with temperatures T_h and T_c respectively, efficiency, which is the ratio between the average heat input and average work output, is upper bounded by Carnot efficiency, $\eta_C = 1 - T_c/T_h$, irrespective of the fact that the underlying system is time-reversal symmetric or not. Traditionally thermodynamics was only concerned with average quantities as typically fluctuations can be ignored for large systems, for example, steam engines, automobile engines, etc. But with the rapid technological development over the last several decades, we can now investigate systems of sizes that can range from hundreds of nanometers to a few nanometers, such as quantum dots, molecular motors, single atom etc, at temperatures that range can range from micro to nano Kelvin.

As a consequence of these advancements, in past two decades various small scale thermal machines have been realized using microelectromechanical systems [3], piezoresistive effect [4], ultra cold atoms [5], single colloidal particle [6–8], single molecule optomechanical systems [9], Paul ion-trap technique [10–12], NV centers [13], NMR setup [14, 15], and quasi-spin system driven by atomic collision [16]. Since these devices operate away from equilibrium, understanding non-equilibrium thermodynamic properties of such small-scale systems is an active area of research where one can no longer ignore the role of fluctuations of thermal and/or quantum origins and therefore a proper probabilistic description is

required.

In this thesis, we aim to shed light on understanding properties of fluctuations in non-equilibrium systems and its impact on the performance of thermal machines by providing universal bounds on the fluctuations of the underlying currents. We investigate non-equilibrium systems that are either in the transient regime or reside in a non-equilibrium steady state and can further operate under a time-reversal breaking situation. This thesis exposes the relationship between various proposed bounds on the non-equilibrium fluctuations for general, quantum or classical thermal machines and also assesses the validity of these bound under very general conditions. Before we proceed to the core of the thesis let us briefly survey some of the central results that exist in the literature for non-equilibrium fluctuations which will also be essential for this thesis.

1.2 A short survey about fluctuation

Over a century ago, pioneering work by Sutherland [17, 18] and Einstein [19–21] provided the first illustration of the celebrated *Fluctuation-Dissipation Relations*. In these works, it was shown that in the presence of external force mobility of a Brownian particle is related to its diffusion constant which encodes the information about equilibrium fluctuations in absence of external force. Later in 1928 it was shown by Johnson [22] and Nyquist [23] that resistance of a circuit is related to the current-fluctuations in the circuit in the absence of a voltage bias. Such relations suggest that the linear response of a system (mobility, resistance, etc.) to an externally applied force can be inferred from the equilibrium fluctuations of the system in absence of external applied force. In the 1950s these findings were rigorously systematized within the quantum-mechanical framework, starting from the work of Callen and Welton [24] and later by Green [25, 26] and Kubo [27]. These works are collectively known today as *Linear Response Theory* (LRT). One of the main assumptions in the LRT is that the system is prepared in thermal equilibrium before driving it out of equilibrium by applying external force. Hänggi and Thomas [28, 29] later showed that even for system far from equilibrium the linear response of the system is related to the two-point correlation functions evaluated at non-equilibrium steady state of the system in the absence of externally applied force.

In the last three decades, the discovery of *Fluctuations Theorems* (FTs) has revolutionized our understanding of fluctuations for a large class of systems driven arbitrarily far from equilibrium. Instead of thinking of fluctuations as some undesirable noise due to small system size, FTs have unraveled the fact that the fluctuations for non-equilibrium observables follow interesting universal relations. Below I briefly summarize some of the fundamental consequence of FTs:

- FTs quantify the onset of irreversibility for systems driven arbitrarily far from equilibrium even when the underlying dynamics is time-reversal symmetric.
- FTs provide the probability of violation of second law of thermodynamics at the trajectory level for a large class of systems.
- In the linear response regime, FTs reproduce all the known results, such as, the Onsager-Casimir relations, the Green-Kubo formula, etc.
- Needless to mention that the FTs are now extensively verified employing state-of-art experiments [30–35].

Due to the wide range of applicability of FTs across many disciplines there exist a huge amount of research literature. Here we will discuss only few that are relevant to the thesis. Before we proceed further, it is important to point out that, the FTs for out-of-equilibrium systems are followed primarily on the following two assumptions: (i) Initial state of a system or bath is described by the equilibrium Gibbs canonical state, and (ii) Principle of micro-reversibility in the underlying dynamics.

1.2.1 Evans–Searles and Gallavotti-Cohen Fluctuation Theorems

Both, Evans–Searles and Gallavotti-Cohen FTs, were motivated by the numerical studies based on shear stress model [36]. Evans–Searles FT [37] states that, if a system initially prepared in equilibrium is driven out of equilibrium to a steady state then,

$$\frac{p_T(\Sigma)}{p_T(-\Sigma)} = e^\Sigma, \quad (1.1)$$

where $p_T(\Sigma)$ is the probability distribution of entropy production Σ produced up to time T . This is also known as *transient fluctuation theorem* (TFT). This implies that the probability

of positive entropy production is exponentially larger than the probability of the corresponding negative entropy production. This provides the probabilistic foundations for the second law and also quantifies the violation of second law. After a simple manipulation one show that,

$$\langle e^{-\Sigma} \rangle = 1 \quad (1.2)$$

Where angular bracket represents ensemble average taken with respect to $p_T(\Sigma)$. This is similar to the well known Jarzynski equality in the context of work fluctuation (see next subsection). Also following Jensen's inequality we receive,

$$\langle \Sigma \rangle \geq 0 \quad (1.3)$$

Thus we recover we recover the traditional second law of thermodynamics at the level of ensemble average. Later, Gallavotti and Cohen considered a system initially prepared in a non-equilibrium steady state and showed that [38],

$$\lim_{T \rightarrow \infty} \frac{1}{T} \ln \left[\frac{p_T(\sigma)}{p_T(-\sigma)} \right] = \sigma, \quad (1.4)$$

where $\sigma = \frac{\Sigma}{T}$ is the entropy production rate, time averaged over a single randomly chosen time duration T . This result is also known in the literature as the *steady state fluctuation theorem* (SSFT). As in the case of TFT this relation also suggest that the probability of positive entropy production rate is exponentially larger than the probability of the corresponding negative entropy production rate. One can similarly derive relations analogous to Eqs.(1.2) and (1.3),

$$\lim_{T \rightarrow \infty} \frac{1}{T} \ln \langle e^{-T\sigma} \rangle = 0, \quad (1.5)$$

$$\text{and} \quad \langle \sigma \rangle \geq 0. \quad (1.6)$$

1.2.2 Jarzynski Equality and Crooks Fluctuation Theorem

Consider an isolated system initially prepared in Gibbs canonical state at inverse temperature β which is driven out of equilibrium by some external work protocol $\lambda(t)$ starting from some macrostate A (like volume, pressure, trap frequency, etc) with hamiltonian $H[\lambda(0)]$ to some macrostate B at time T with hamiltonian $H[\lambda(T)]$. Then work done on the system

by external source is given by,

$$\begin{aligned} W &= \int_0^T dt \dot{\lambda} \frac{\partial H(\lambda)}{\partial \lambda} \\ &= H[\lambda(T)] - H[\lambda(0)] \end{aligned} \quad (1.7)$$

This work done W is a stochastic quantity as initially the system is prepared in the Gibbs state. For such setup Jarzynski showed that [39],

$$\langle e^{-\beta W} \rangle = e^{-\beta \Delta F}, \quad (1.8)$$

where ΔF is the free energy difference between state A and state B both at inverse temperature β . Angular bracket represents the average taken over the different realizations of work for fixed protocol. This relation is known as Jarzynski Equality in literature. Note that in general state B reached by the system after time T is not in equilibrium. This remarkable result allows us to infer equilibrium information (ΔF) of the system from the system driven arbitrarily far from equilibrium. This is similar to the fluctuation-dissipation relation which was proved in the linear response regime. One can also prove the Jarzynski equality, Eq.(1.8), even when the system is in contact with the thermal bath prepared at inverse temperature β [40–42].

Later Crooks derived a more general relation for this setup. He showed that the probability distribution of work W is constrained by a symmetry relation, given by,

$$\frac{p_F(W, \lambda(t))}{p_R(-W, \tilde{\lambda}(t))} = e^{\beta(W - \Delta F)} \quad (1.9)$$

where subscript F and R represent time-forward, $\lambda(t)$, and time-reversed, $\tilde{\lambda}(t)$, protocols respectively and $\tilde{\lambda}(t) = \lambda(\tau - t)$. This relation is also known as Crooks fluctuation theorem. One can easily derive Jarzynski equality, Eq.(1.8), from above relation. Also note its resemblance with TFT, Eq.(1.1), with Σ replaced by $\beta(W - \Delta F)$.

1.2.3 Exchange Fluctuation Theorem (XFT)

Exchange Fluctuation Theorem (XFT) is a symmetry relation similar to TFT, Eq.(1.1), but in a different context. XFT restrict the probability distribution of heat exchange between two finite bodies initially prepared at different temperatures. More precisely, consider two

systems A and B initially prepared at inverse temperatures β_A and β_B , then they put in thermal contact for some time duration T and then separate them. Let Q be the amount of heat that flows from system A to system B during the contact. Then XFT states that,

$$\ln \left[\frac{p_T(Q)}{p_T(-Q)} \right] = \Delta\beta Q, \quad (1.10)$$

where $p_T(Q)$ is the probability distribution of heat exchange between A and B and $\Delta\beta = \beta_B - \beta_A$ is the corresponding thermal affinity responsible to heat exchange. In order to prove this relation one needs two ingredients, (i) underlying dynamics is time-reversal symmetric, and (ii) energy corresponding to the coupling between the systems is very small as compared to the energy of each system.

1.2.4 Quantum Fluctuation Theorems

FTs were first proved for classical systems. It was not straightforward to extend these relations to quantum regime as there were difficulties in identifying work and heat. Earlier works [43–49] defined a work operator to derive Jarzynski equality for quantum systems but led to quantum correction to the Jarzynski equality. Later, Talkner, Lutz and Hänggi showed that the work is not an observable [50, 51] i.e, we cannot assign a hermitian operator corresponding to it. This observation is consistent with the thermodynamic definition where work is not a state function but depends upon the details of the process which drive the system from the initial state to a final non-equilibrium state. Similarly, integrated energy current, heat current and the associated entropy production are not observables. This problem is circumvented by introducing two-point measurement scheme. This measurement scheme assigns energy change (work or heat) of the system due to a process to the difference in the energy eigenvalues measured at the start and end of the process. This scheme reproduces all of the FTs mentioned previously [50, 52–56]. Next, we will illustrate this two-point measurement scheme by deriving quantum version of XFT as it will be relevant in chapter 6 of this thesis.

Quantum Exchange Fluctuation Theorem

Consider two systems with Hamiltonians H_1 and H_2 that are initially ($t = 0^-$) decoupled with composite density matrix given by a product state, $\rho(0) = \rho_1 \otimes \rho_2$, with

$\rho_i = \exp[-\beta_i H_i] / \mathcal{Z}_i$, $i = 1, 2$ being the initial Gibbs thermal state with inverse temperature $\beta_i = 1/T_i$ (we set $k_B = \hbar = 1$) and $\mathcal{Z}_i = \text{Tr}[e^{-\beta_i H_i}]$ is the corresponding canonical partition function. To allow energy exchange, an interaction term between the two systems, denoted as V , is suddenly switched on at $t = 0$ and suddenly switched off after a duration of $t = T$. The composite system in this interval evolves unitarily with the total Hamiltonian $H = H_1 + H_2 + V$.

As mentioned above, quantities such as integrated energy current, work, or the associated entropy production are not direct observables but rather depends on the measurements of relevant Hamiltonians at the initial and final time of the process. Therefore, to construct the probability distribution function (PDF) [51, 57, 58] for energy exchange, projective measurements of the system Hamiltonians H_1 and H_2 should be carried out simultaneously in the beginning and at the end of the process. Following this, the joint PDF, $p_T(\Delta E_1, \Delta E_2)$, corresponding to the energy change (ΔE_i , $i = 1, 2$) of both the systems can be constructed as

$$p_T(\Delta E_1, \Delta E_2) = \sum_{m,n} \left(\prod_{i=1}^2 \delta(\Delta E_i - (\epsilon_m^i - \epsilon_n^i)) \right) p_{m|n}^T p_n^0, \quad (1.11)$$

where $p_n^0 = \prod_{i=1}^2 e^{-\beta_i \epsilon_n^i} / \mathcal{Z}_i$ corresponds to the probability to find the system initially in the common energy eigenstate $|n\rangle = |n_1, n_2\rangle$ of the composite system where $|n_i\rangle$ and ϵ_n^i are energy eigenstate and eigenvalue respectively of system i after the first projective measurement. The second projective measurement at the final time ($t = T$) leads to the collapse of the state of composite system to another common energy eigenstate $|m\rangle = |m_1, m_2\rangle$. The transition probability between these states is given by $p_{m|n}^T = |\langle m | \mathcal{U}(T, 0) | n \rangle|^2$ with $\mathcal{U}(t, 0) = e^{-iHt}$ being the global unitary propagator with the total Hamiltonian H . Now one can show that for autonomous and time-reversal invariant quantum systems evolving unitarily $p_{m|n}^T = p_{n|m}^T$. This condition is also known as the principle of micro-reversibility in the literature [51, 57]. Using this condition in Eq. (1.11) one receives the following universal symmetry for this joint PDF,

$$p_T(\Delta E_1, \Delta E_2) = e^{\beta_1 \Delta E_1 + \beta_2 \Delta E_2} p_T(-\Delta E_1, -\Delta E_2). \quad (1.12)$$

At this junction, it is important to point out that under general coupling scenario the energy change of an individual system can not be interpreted as heat as part of the energy change

may be used in turning on and off the interaction (V) between the two systems. However, in the weak-coupling limit ($V \ll H_{1,2}$), it is safe to interpret this energy change as heat. One can then define heat as $Q = -\Delta E_1 \approx \Delta E_2$ which following Eq. (1.12) leads to a heat exchange fluctuation relation (XFT), given as

$$p_T(Q) = e^{\Delta\beta Q} p_T(-Q), \quad (1.13)$$

where $\Delta\beta = \beta_2 - \beta_1$. As per our convention, heat flowing out from system 1 to system 2 is considered as positive. The characteristic function (CF) corresponding to the PDF for energy exchange can be obtained by performing a Fourier transformation (FT) of the probability distribution:

$$\begin{aligned} Z_T(u) &= \int dQ e^{iuQ} p_T(Q) \\ &= \text{Tr} \left[\mathcal{U}^\dagger(T, 0) (e^{-iuH_1} \otimes 1_2) \mathcal{U}(T, 0) (e^{iuH_1} \otimes 1_2) \rho(0) \right], \end{aligned} \quad (1.14)$$

where u is a variable conjugate to Q . In terms of the CF, the XFT for heat in Eq. (1.13) translates to [59–62].

$$Z_T(u) = Z_T(-u + i\Delta\beta). \quad (1.15)$$

It is important to note that, for a special choice of the coupling Hamiltonian V , satisfying the commutation relation $[V, H_1 + H_2] = 0$, the total internal energy $H_1 + H_2$ is a constant of motion which imply that the change of energy for one system is exactly compensated by the other one. In other words, there is no energy cost involved in turning on and off the interaction between the systems. Such type of coupling is known as the thermal coupling [63]. Therefore, under this symmetry condition the definition for heat $Q = -\Delta E_1 = \Delta E_2$ becomes exact for arbitrary coupling strength. In other words, under the thermal coupling limit the XFT is valid for arbitrary coupling strength between two systems and for arbitrary time duration of energy exchange as shown in Appendix A.

1.3 Thermodynamic Uncertainty Relations

Thermodynamic Uncertainty Relations (TURs) are recently discovered trade-off relations for systems driven out of equilibrium [64–76]. They provide the lower bound on the relative fluctuations of currents/integrated-currents (heat, particle, energy, etc.) in terms of the net entropy production. In other words, TUR restricts optimization of relative fluctuations and entropy production in an arbitrary manner by providing a trade-off relation between these quantities. These relations have provided unique insight in small-scale thermal machines [68] and thermodynamic inference [76, 77]. Most common form of TUR is given by,

$$\langle \sigma \rangle \frac{\langle I_j^2 \rangle_c}{\langle I_j \rangle^2} \geq 2. \quad (1.16)$$

where, subscript j indexes the different currents like heat, particle, etc. $\langle I_j \rangle$ is the average current, $\langle I_j^2 \rangle_c$ is the second cumulant of current quantifying fluctuations from the mean behaviour, and the total $\langle \sigma \rangle$ is the average entropy production rate. It is easy to see that this bound is saturated in equilibrium following the fluctuation-dissipation relation [78]. Barato and Seifert first proved this bound for multi-affinity systems in steady-state in linear response regime and based on extensive numerical simulations on multi-cyclic Markov network, conjectured it to be true for all Markov processes driven far from equilibrium. Later, this bound was rigorously proven for continuous-time markov process in steady state [64, 65] using large deviation theory [79]. Since then several TURs have been proposed for, discrete-time, discrete-state Markov processes [67], finite-time statistics [66, 80, 81], Brownian motion [82–86], periodically driven systems [87, 88], vector-valued observables [89], molecular motors [90], biochemical oscillations [91], interacting oscillators [92], run-and-tumble processes [93], measurement and feedback control [94, 95], broken time-reversal symmetry systems [69, 94, 96–98], first-passage times [99, 100], quantum transport problems [70, 73, 74, 101, 102], systems satisfying fluctuation relations [71, 72]. Tighter bounds have also been reported for some stochastic currents [103].

In chapter 2 we will show that, for continuous thermal machines operating in steady-state, TUR for different currents is not independent but follows a strict hierarchy. Also in

chapter 5 we will assess the validity of Eq (1.16) starting from the steady-state fluctuation theorem. We will refer to the TUR given in Eq.(1.16) as T-TUR as it provides a tighter bound than other TURs. In a recent experiment [104] validity of T-TUR is assessed using atomic-scale quantum conductors and no violation of T-TUR has been reported. Now we briefly discuss some of the TURs that are relevant to this thesis.

Following the geometry of quantum non-equilibrium steady-states [105, 106] and the Cramer-Rao bound [107, 108], a TUR was derived beyond linear response regime, which we refer to as Q-TUR [74], and is given by,

$$\langle \sigma \rangle \frac{\langle I_j^2 \rangle_c}{\langle I_j \rangle^2} \geq 1 \quad (\text{Q-TUR}), \quad (1.17)$$

which is two times looser than the T-TUR (Eq. (1.16)). Note that this bound does not saturate in the equilibrium limit.

One can rewrite the T-TUR in terms of integrated current Q (measured upto finite-time T) as,

$$\langle \Sigma \rangle \frac{\langle Q^2 \rangle_c}{\langle Q \rangle^2} \geq 2, \quad (1.18)$$

Where $\langle \Sigma \rangle$ is the net entropy production. This result was again rigorously proved for continuous-time Markov process in a steady state [66]. In chapter 6 we will investigate the validity of Eq.(1.18) for various model systems. Also, in one of our works, the validity of Eq.(1.18) has been experimentally examined in [109] using NMR setup, and violations have been reported in a very good agreement with the theoretical prediction.

Interestingly, for systems satisfying exchange fluctuation theorem (XFT), there exists two TURs for any integrated current Q , namely,

$$\langle \Sigma \rangle \frac{\langle Q^2 \rangle_c}{\langle Q \rangle^2} \geq \frac{2\langle \Sigma \rangle}{\exp \langle \Sigma \rangle - 1}, \quad (\text{G-TUR1}) \quad (1.19)$$

$$\langle \Sigma \rangle \frac{\langle Q^2 \rangle_c}{\langle Q \rangle^2} \geq \langle \Sigma \rangle f(\langle \Sigma \rangle), \quad (\text{G-TUR2}) \quad (1.20)$$

where $f(x) = \text{cosech}^2(g(x/2))$ and $g(x)$ is the inverse function of $x \tanh(x)$. We refer to these TURs as G-TUR1 and G-TUR2, where G stands for generalized as these TURs are valid for a very large variety of systems satisfying XFT. It turns out that G-TUR2 is tighter

than G-TUR1. We will elaborate more on this in chapter 6.

1.4 Thermal machines

Now we turn our attention to the thermal machines that in general operate out-of-equilibrium and thus provide an ideal test bed for studying fluctuations. Thermal machines are energy conversion devices that primarily employ heat energy in its operation like, thermoelectric device, photovoltaic cell, refrigerator, etc. A generic thermal machine consists of a working medium, heat and/or particle reservoirs, and a work source, which is used for consuming/extracting energy. In general, irrespective of underlying dynamics, thermal machines can be classified as, (i) Continuous thermal machines, and (ii) Discrete thermal machines [110, 111]. In the next two subsections, we will briefly discuss these two types of thermal machines and provide some paradigmatic examples.

1.4.1 Continuous thermal machines

In continuous thermal machines all the constituents are coupled to the working medium at the same time operating in a steady state. For example, thermoelectric junction, absorption refrigerator, etc. We now discuss two particular continuous thermal machines that will be later revised in the thesis to illustrates our results.

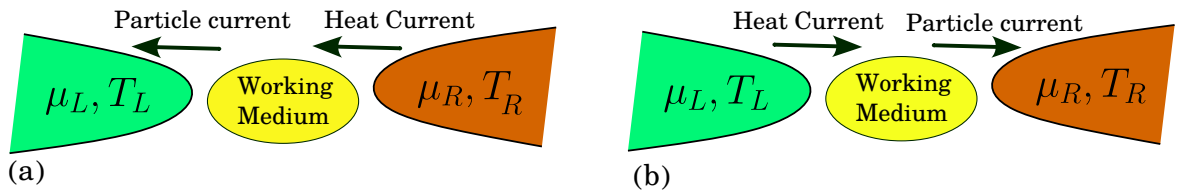


Figure 1.1: Thermoelectric junction with arbitrary working medium connected to two reservoirs maintained at different chemical potentials and temperatures $\mu_{L,R}$ and $T_{L,R}$ respectively. As a result there will be flow of particle and heat currents. We assume that $T_R > T_L$ and $\mu_L > \mu_R$. (a) Thermoelectric Engine: Heat current drives the particle current against the spontaneous flow and hence generate finite work output. (b) Thermoelectric Refrigerator: Particle current is used to extract heat from cold bath and dump it into hot bath.

Thermoelectric Junction

Thermoelectric junction [112] consists of a working medium connected to two reservoirs simultaneously. These reservoirs are maintained at different temperatures and chemical

potential, that drive the system to a non-equilibrium steady-state (NESS). A schematic is given in Fig.1.1. This setup can work as engine, refrigerator or heat pump depending upon direction of heat and particle currents. It works as an engine when heat current drives the particle current against the spontaneous flow and hence generate finite work output against the chemical bias, as shown in Fig.1.1(a). It works as a refrigerator when particle current is used to extract heat from cold bath and dump it on the hot bath, as shown in 1.1(b). Note that we have explicitly assumed $T_R > T_L$ and $\mu_L > \mu_R$ in Fig. 1.1.

Thermoelectric effects have been discovered very long ago in the 19th century and known by Seebeck Effect, Peltier Effect, and Thomson Effect [112]. These effects were seen in macroscopic working medium. But now thermoelectric device has been realized where working medium is of meso/nano scale [113–117] and as a result fluctuations play major role in determining the performance of the device.

Absorption refrigerator

Absorption refrigerator (AR) is an autonomous three-terminal setup that operates in nonequilibrium steady state and continuously directs energy to flow from the cold (C) to the hot (H) terminal by absorbing energy from the ultrahot work (W) terminal a shown in Fig. 1.2. Absorption refrigerators were first realized for industrial purpose by Carré brothers in 19th

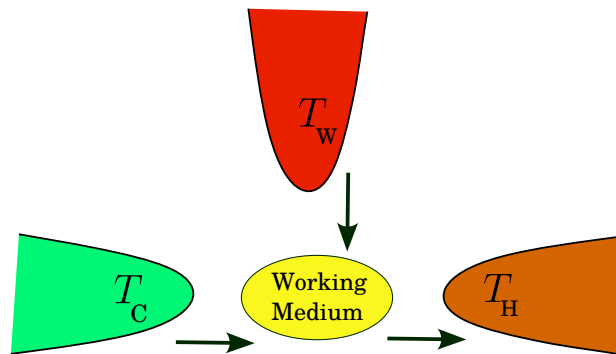


Figure 1.2: Absorption Refrigerator: The setup consists of three heat baths, work, hot, and cold, maintained at temperatures T_W, T_H , and T_C respectively, such that $T_W > T_H > T_C$. Arrows represent the direction of heat currents when the setup is working as an absorption refrigerator.

century [118]. In recent years various efforts directed towards understanding and realizing the smallest possible ARs [110, 119–123] that can operate with the maximum cooling efficiency and power possible, by taking advantage of possible quantum resources. Various proposals to realize quantum ARs using platforms such as superconducting qubits and ar-

rays of quantum dots have been put forward [124–127]. Recently, a AR is realized using three trapped ions in [12].

In chapters 2 and 3 we will investigate autonomous continuous thermal machines, in particular thermoelectric junction and quantum absorption refrigerators in presence of time-reversal symmetry or under broken time-reversal symmetry respectively, and provide universal bounds on the fluctuations. We will analyze how the underlying fluctuations dictate the performance of such machines.

1.4.2 Discrete thermal machines

In discrete thermal machines all the components are not connected to working medium simultaneously. Most familiar discrete thermal machines are *four stroke cycle* like Carnot and Otto cycle [2]. Carnot cycle consists of two adiabatic strokes, in which the working medium is isolated from the baths, and two isothermal strokes, in which the working medium is put in thermal contact with the reservoirs. Similarly Otto cycle comprises two isochoric strokes, in which system is connected to the bath provided no work is done, and two adiabatic strokes. Recently Otto engine is realized in couple of experiments with aid of NV centers [13], NMR setup [14] and trapped ion technique [11]. Hence quantum-mechanical treatment becomes inevitable for these setups. Fig. 1.3 illustrates the quantum analog of Otto engine. In chapter 5 we will examine the quantum Otto engine in more detail and obtain universal bounds on fluctuations for a large class of working medium.

Another class of discrete thermal machines is a *two-stroke cycle* [129, 130]. In first stroke working medium is connected to the heat baths and then the system is decoupled from the heat baths. In the second stroke, work is extracted from the quantum system via a coupling to an external field. For example, in first stroke a three level is connected to the hot and cold bath in such a way to attain population inversion and then in second stroke population inversion is used to extract some useful work [131]. Another well known two-stroke engine is a SWAP engine which has been studied extensively over the years [129, 130, 132–134] and a solid-state implementation has been also proposed for it [134].

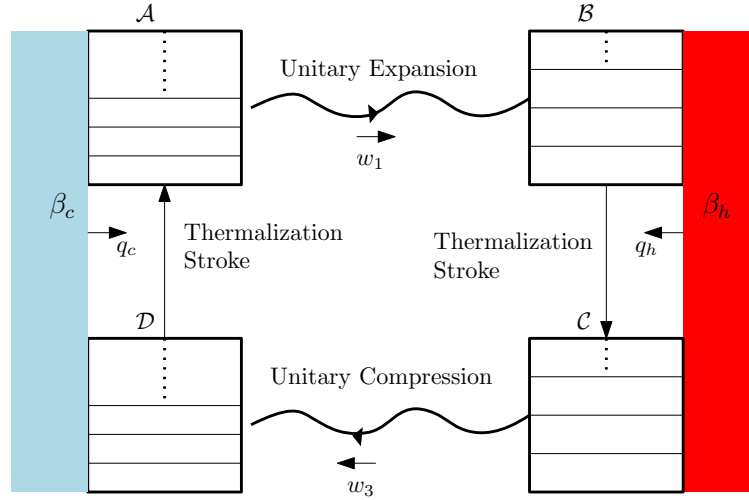


Figure 1.3: Schematic for a four-stroke Quantum Otto cycle. Figure reproduced with permission from Ref.[128].

1.5 Outline of the thesis

In chapter 2 we investigate the bounds for continuous time-reversal symmetric autonomous thermal machines in linear response regime. Invoking the principles of linear irreversible thermodynamics we show that the relative fluctuations of the output current (power output) is always lower bounded by the relative fluctuations of the input current (heat current absorbed from the hot bath). As an immediate consequence, thermodynamic uncertainty relation for input and output current receives strict hierarchy. Furthermore, we show that the obtained upper bound on the efficiency is tighter than the upper bound obtained using the thermodynamic uncertainty relations.

Next, in chapter 3 we generalize our findings of chapter 2 to broken time-reversal symmetric thermal machines. We show that in the linear response regime the relative fluctuation of the sum of output currents for time-forward and time-reversed processes is always lower bounded by the corresponding relative fluctuation of the sum of input currents. This bound is received when the same operating condition, for example, engine, refrigerator, or pump, is imposed on both the forward and the reversed processes. Furthermore, we establish a connection between our results and the generalized thermodynamic uncertainty relations for time-reversal symmetry-broken systems.

In chapter 4 we examine the bounds on the fluctuations for finite-time quantum Otto

cycle which is an instance of discrete thermal machine. We provide exact full statistics of heat and work for a class of working fluids that follow a scale-invariant energy eigenspectra. Equipped with the full joint statistics we go on to derive a universal expression for the ratio of n th cumulant of output work and input heat in terms of the Otto efficiency. Furthermore, for nonadiabatic driving of quantum Otto engine with working fluid consisting of either (i) a qubit or (ii) a harmonic oscillator, we show that the relative fluctuation of output work is always greater than the corresponding relative fluctuation of input heat absorbed from the hot bath that we also obtained for time-reversal symmetric continuous thermal machines in chapter 2.

In chapter 5 we shift our attention to the single affinity driven steady-state thermal transport. We use the fundamental non-equilibrium steady state fluctuation symmetry and derive a condition on the validity of T-TUR for single affinity driven systems. We test the condition and study the breakdown of the TUR in different thermal transport junctions of bosonic and electronic degrees of freedom. We show that the TUR is feasibly violated by tuning e.g. the hybridization energy of the chain to the metal leads. These results manifest that the validity of the T-TUR relies on the statistics of the participating carriers.

In chapter 6 we assess the validity of transient version of T-TUR. We explore T-TUR in the context of energy transport in a bipartite setting for three exactly solvable toy model systems (two coupled harmonic oscillators, two coupled qubits, and a hybrid coupled oscillator-qubit system) and analyze the role played by the underlying statistics of the transport carriers in the TUR. Interestingly, for all these models, depending on the statistics, the TUR ratio can be expressed as a sum or a difference of a universal term which is always greater than or equal to 2 and a corresponding entropy production term. We find that the generalized versions of the TUR, originating from the universal fluctuation symmetry (G-TUR1 and G-TUR2), is always satisfied. We also provide a rigorous proof following the nonequilibrium Green's function approach that the tighter bound is always satisfied in the weak-coupling regime for generic bipartite systems.

Finally in chapter 7 we conclude this thesis with our central results and outline future prospects.

CHAPTER 2

Universal bounds on fluctuations in continuous thermal machines

Abstract

We investigate the bounds on the fluctuations in steady-state time-reversal-symmetric energy conversion devices. Starting from the general principles of linear irreversible thermodynamics along with the fluctuation dissipation theorem, we prove that the relative fluctuations of the output current (power output) is always lower bounded by the relative fluctuations of the input current (heat current absorbed from the hot bath). As a consequence, the ratio between the fluctuations of the output and input currents are bounded both from above and below, where the lower (upper) bound is determined by the square of the averaged efficiency (square of the Carnot efficiency) of the engine. The saturation of the lower bound is achieved in the tight-coupling limit when the determinant of the Onsager response matrix vanishes. Our analysis can be applied to different operational regimes, including engines, refrigerators, and heat pumps. Furthermore, we show that the obtained upper bound on the efficiency is tighter than the upper bound obtained using the *thermodynamic uncertainty relations*. We illustrate our findings for two types of continuous engines: two-terminal coherent thermoelectric junctions and three-terminal quantum absorption refrigerators. Numerical simulations in the far-from-equilibrium regime suggest that these bounds apply more broadly, beyond linear response.

Reported in

S. Saryal, M. Gerry, I Khait, D. Segal, and B.K. Agarwalla, *Universal Bounds on Fluctuations in Continuous Thermal Machines*, [Phys. Rev. Lett. 127, 190603 \(2021\)](#).

2.1 Introduction

The second law of thermodynamics forbids the conversion of all of the heat energy to work. As a consequence of that one cannot build any heat engine, operating between a cold and a hot heat baths, whose efficiency is greater than the famous *Carnot efficiency* [1]. However, the *Carnot efficiency* is never attained for any practical heat engine because in order to attain it all the processes during the operation of the engine should be quasi-static, which amounts to zero output power. In addition, classical laws of thermodynamics, written for macroscopic systems, do not provide any information about how fluctuations influence the operation of the devices, which becomes crucial to consider for engines with few degrees of freedom and operating at low temperatures. Therefore it becomes imperative to understand the role of fluctuations for small scale devices.

Intense efforts in the field of stochastic thermodynamics [135] are now dedicated towards characterizing nanoscale systems by incorporating fluctuations of thermodynamic quantities such as currents [64, 136], entropy production, [80, 137, 138] and efficiency [139–142]. As an example, there has been a great deal of activity in recent times in deriving bounds on relative fluctuations of observables for out-of-equilibrium systems. The so-called *thermodynamic uncertainty relations* (TUR) [64, 65, 68–73, 75] provide a trade-off bound on such relative fluctuation, can also be quantified as the precision, and the entropy production which is the cost to drive the system away from equilibrium. The TUR further constrains the performance of a thermal engine, providing a trade-off between output power, power fluctuations and the engine’s efficiency [68]. In addition, it was recently shown in Ref. [143] that for finite-time four-stroke heat engines, the ratio between fluctuations of output work (W) and input heat (Q) is upper bounded, and the bound solely depends on the temperatures of the hot (T_h) and cold heat baths (T_c). More precisely, the relation was given as $\eta^{(2)} \equiv \frac{\langle W^2 \rangle_c}{\langle Q^2 \rangle_c} \leq \eta_C^2$, where $\eta_C = 1 - \frac{T_c}{T_h}$ is the Carnot efficiency and $\langle A^2 \rangle_c = [\langle A^2 \rangle - \langle A \rangle^2]$ is the second cumulant, or the fluctuations, of an observable A . Furthermore, a tighter-than-Carnot efficiency bound was recently derived for classical continuous engines expressed in terms of high order cumulants of the power [144]. Our work, in this chapter, exposes the relationship between these different bounds on non-equilibrium fluctuations for general quantum or classical thermal machines. In this and the next chapter

we will primarily focus on continuous thermal machines such as, thermoelectric junctions, quantum absorption refrigerators, and provide universal bounds on fluctuations and will further make interesting connections with the TUR. In this chapter we will first focus on the autonomous time-reversal symmetric systems and the consequence of the breakdown of this symmetry on fluctuations will be discussed in the next chapter.

We organize this chapter as follows: We will first introduce the basic framework of *linear irreversible thermodynamics* in section 2.2. Next we will prove the universal bounds on fluctuations and efficiency based on general principles of *linear irreversible thermodynamics* in section 2.3. In section 2.4 we unravel the consequence of our results on recently discovered *thermodynamic uncertainty relations* (TUR) and also show that the bound we obtained on efficiency is tighter than the obtained from TUR. We illustrate our results in section 2.5 using single-quantum dot thermoelectric junction. Finally we conclude this chapter in section 2.6.

2.2 Linear irreversible thermodynamics

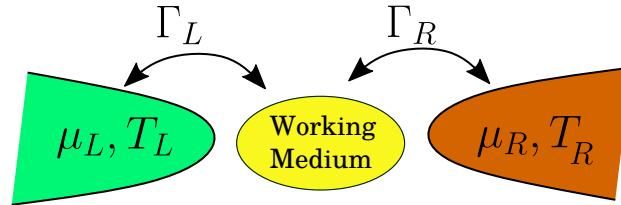


Figure 2.1: Thermoelectric junction with arbitrary working medium connected to two reservoirs that are maintained at different chemical potentials and temperatures $\mu_{L,R}$ and $T_{L,R}$. $\Gamma_{L,R}$ denotes the coupling between the system and the left (L) and the right (R) reservoirs. For such a generic setup, in the long-time limit a non-equilibrium steady state will be attained with steady particle and heat currents flowing across the system. This setup can work as engine, refrigerator or heat pump depending upon the direction of particle and heat current.

As the central results obtained in this chapter are based on the principles of linear irreversible thermodynamics, we will first briefly outline the basic framework. Let us consider a small-scale continuous device (such as shown in Fig.(2.1)): where a system of interest is subjected to multiple affinities, A_i ($i = 1, 2, \dots, n$), which produces time-integrated stochastic currents J_i . In the context of Fig. (2.1), there are two thermodynamic affinities, $A_1 = 1/T_L - 1/T_R$, and $A_2 = \mu_R/T_R - \mu_L/T_L$, that generates conjugate currents J_1 (heat)

and J_2 (particle) across the junction. The affinities, which depend upon quantities like temperature, chemical potential, etc., are properties of the reservoirs and as thermodynamic variables, they negligibly fluctuate. In contrast, the currents may suffer from significant fluctuations. In steady state, typically, cumulants of integrated currents scale extensively with the operation time t , $\langle J_i^n \rangle_c = t \langle I_i^n \rangle_c$. Note that the subscript c symbolizes the cumulant of the given observable. In the linear response regime, the time-intensive average currents are proportional to the affinities and therefore can be expressed in terms of the Onsager response matrix [2, 145–147] as,

$$\langle I_i \rangle = \sum_{j=1}^n \mathcal{L}_{ij} A_j. \quad (2.1)$$

\mathcal{L}_{ij} are the matrix elements of the Onsager matrix \mathcal{L} and are often referred to as the kinetic coefficients, defined as $\mathcal{L}_{ij} = \partial_{A_i} \langle I_j \rangle |_{A=0}$. Note that, as per our convention, average currents $\langle I_i \rangle$ are positive when flowing towards the system. The steady-state entropy production rate, $\langle \sigma \rangle$, can be expressed as,

$$\langle \sigma \rangle = \sum_{i=1}^n I_i A_i = \sum_{i,j=1}^n \mathcal{L}_{ij} A_i A_j, \quad (2.2)$$

which is always non-negative, in accordance with the Second law of thermodynamics. This particular condition ($\langle \sigma \rangle \geq 0$), imposes two strict constraints on the Onsager kinetic coefficients.

First, since $\langle \sigma \rangle \geq 0$ is true for any possible values of A_i 's, we make all affinities zero except A_i . Then $\langle I_i \rangle = \mathcal{L}_{ii} A_i$ and as a result $\langle \sigma \rangle = \mathcal{L}_{ii} A_i^2 \geq 0$. This simply implies that $\mathcal{L}_{ii} \geq 0$. This can be done for other i 's as well and leads to the conclusion that the diagonal Onsager coefficients are always non-negative i.e.,

$$\boxed{\mathcal{L}_{ii} \geq 0 \quad \forall i} \quad (2.3)$$

Second constraint can be obtained as follows. We can write the Onsager matrix as a sum of symmetric and antisymmetric parts,

$$\mathcal{L} = \frac{\mathcal{L} + \mathcal{L}^T}{2} + \frac{\mathcal{L} - \mathcal{L}^T}{2} = \mathcal{L}^S + \mathcal{L}^A \quad (2.4)$$

where superscript T stands for transpose of a matrix. The entropy production rate then given as,

$$\langle \sigma \rangle = \sum_{i,j=1}^n \mathcal{L}_{ij}^S A_i A_j + \sum_{i,j=1}^n \mathcal{L}_{ij}^A A_i A_j. \quad (2.5)$$

It can be easily shown that $\sum_{i,j=1}^n \mathcal{L}_{ij}^A A_i A_j = 0$ due the antisymmetric nature of the matrix \mathcal{L}^A . Thus, we receive $\sum_{i,j=1}^n \mathcal{L}_{ij}^S A_j A_i \geq 0$, implying \mathcal{L}^S is a positive semi-definite matrix [148] and as a consequence its determinant is always non-negative i.e.,

$$\det[\mathcal{L}^S] \geq 0 \quad (2.6)$$

In what follows, we will investigate the situation when $n = 2$ i.e. a two-affinity setup that generate two independent currents and can potentially act as a useful machine (heat engine, refrigerator, or pump). This particular simple situation allows us to uniquely identify the input and output currents. We will first consider the time-reversal symmetric situation for which the Onsager reciprocity relation is given as, [145, 146],

$$\mathcal{L}_{ij} = \mathcal{L}_{ji}, \quad (2.7)$$

which further implies that for a two-affinity driven time-reversal symmetric system,

$$\mathcal{L}_{11}\mathcal{L}_{22} - \mathcal{L}_{12}^2 \geq 0. \quad (2.8)$$

2.3 Universal bounds on efficiency and fluctuations for time-reversal symmetric systems

Let us consider fluctuations of currents around their mean values, $\langle I_i^2 \rangle_c = \langle I_i^2 \rangle - \langle I_i \rangle^2$, and define the squared relative uncertainty for individual currents as,

$$\epsilon_i^2 = \frac{\langle I_i^2 \rangle_c}{\langle I_i \rangle^2}. \quad (2.9)$$

We now construct the ratio between the uncertainties of the two currents and write in the linear response regime,

$$\mathcal{Q} \equiv \frac{\epsilon_2^2}{\epsilon_1^2} = \frac{\mathcal{L}_{22}}{\mathcal{L}_{11}} \frac{\sum_{ij} \mathcal{L}_{1i} \mathcal{L}_{1j} A_i A_j}{\sum_{ij} \mathcal{L}_{2i} \mathcal{L}_{2j} A_i A_j}. \quad (2.10)$$

Note that, as the currents are linear in affinities, the fluctuation of currents are replaced by their corresponding equilibrium values in the linear response limit,

$$[\langle I_i^2 \rangle_c]_{\text{eq}} = \mathcal{L}_{ii}, \quad (2.11)$$

ensuing the fluctuation-dissipation relation in equilibrium [19, 78]. After simple algebraic manipulations, Eq. (2.10) reduces to

$$\mathcal{Q} = 1 + \frac{1}{\mathcal{L}_{11} \langle I_2 \rangle^2} \sum_{i,j=1}^2 \left[\mathcal{L}_{1i} \mathcal{L}_{1j} \mathcal{L}_{22} - \mathcal{L}_{2i} \mathcal{L}_{2j} \mathcal{L}_{11} \right] A_i A_j. \quad (2.12)$$

Interestingly, the above summation does not contribute for $i \neq j$ and therefore reduces to

$$\begin{aligned} \mathcal{Q} &= 1 + \frac{1}{\mathcal{L}_{11} \langle I_2 \rangle^2} \sum_i \left[\mathcal{L}_{1i}^2 \mathcal{L}_{22} - \mathcal{L}_{2i}^2 \mathcal{L}_{11} \right] A_i^2 \\ &= 1 + \frac{1}{\mathcal{L}_{11} \langle I_2 \rangle^2} (\mathcal{L}_{11} \mathcal{L}_{22} - \mathcal{L}_{12}^2) (\mathcal{L}_{11} A_1^2 - \mathcal{L}_{22} A_2^2) \end{aligned} \quad (2.13)$$

We now focus on the second term which is a product of three terms and in general can take positive or negative value. However, the first term, $\frac{1}{\mathcal{L}_{11} \langle I_2 \rangle^2}$, is always non-negative because of Eq.(2.3), and for the time-reversal symmetric systems the second term, $(\mathcal{L}_{11} \mathcal{L}_{22} - \mathcal{L}_{12}^2)$, is also non-negative because of Eq.(2.8). Only the sign of the third term, $(\mathcal{L}_{11} A_1^2 - \mathcal{L}_{22} A_2^2)$, is not directly restricted by any of the fundamental laws of physics. But so-far, we have not imposed any restriction on the operational behavior of the system. As a result \mathcal{Q} can either be less than unity or greater than unity. However, upon imposing the condition that the steady-state setup operates as a thermal machine, it turns out the first term in the above product is also positive, i.e., $(\mathcal{L}_{11} A_1^2 - \mathcal{L}_{22} A_2^2) > 0$. This can be shown as follows:

To realize a steady-state thermal machine, we assign I_1 as the *input* current and I_2 as the *output* current. Recall that, as per our convention, the current flowing into the system is considered as positive. We therefore demand that

$$\langle I_1 \rangle A_1 > 0, \quad \text{and} \quad -\langle I_2 \rangle A_2 > 0. \quad (2.14)$$

The condition $\langle I_1 \rangle A_1 > 0$ in the linear response generates a constraint, $\mathcal{L}_{11} A_1^2 > -\mathcal{L}_{12} A_1 A_2$. Similarly, the other condition, $-\langle I_2 \rangle A_2 > 0$, yields another constraint, $-\mathcal{L}_{12} A_1 A_2 >$

$\mathcal{L}_{22}A_2^2$. A combination of these two constraints provides an interesting inequality

$$\mathcal{L}_{11}A_1^2 - \mathcal{L}_{22}A_2^2 > 0 \quad (2.15)$$

Note that the above inequality holds as long as the steady-state setup operates as a thermal machine. From this result, following Eq. (2.13), we immediately conclude that for continuous thermal machines in linear response

$$\mathcal{Q} \geq 1. \quad (2.16)$$

This is one of the central results of this chapter. Note that our result is universal and independent of the nature of the working medium and therefore valid in both classical and quantum regimes. Because of the strict inequality in Eq.(2.15) saturation of Eq.(2.16) can be only be achieved when $(\mathcal{L}_{11}\mathcal{L}_{22} - \mathcal{L}_{12}^2) = 0$ that is only possible when determinant of Onsager matrix \mathcal{L} is zero, which corresponds to tight coupling situation (see Appendix B for more details) i.e., $\langle I_1 \rangle \propto \langle I_2 \rangle$.

The above result provide two immediate interesting observations:

- $\mathcal{Q} \geq 1$ immediately implies that, in any operational regime, the ratio between fluctuations of output and input current gets lower-bounded by the square of the average efficiency, $\langle \eta \rangle = |\langle I_2 \rangle|/|\langle I_1 \rangle|$. More precisely we get,

$$\eta^{(2)} \equiv \frac{\langle I_2^2 \rangle_c}{\langle I_1^2 \rangle_c} \geq \langle \eta \rangle^2 \quad (2.17)$$

- The inequality in Eq. (2.15), further provides an upper bound for $\eta^{(2)}$, as defined in Eq. (2.17). Following the fluctuation-dissipation relation, we can replace $\mathcal{L}_{22} = \langle I_2^2 \rangle_c$ and $\mathcal{L}_{11} = \langle I_1^2 \rangle_c$. From this we can simply conclude that

$$\eta^{(2)} = \frac{\mathcal{L}_{22}}{\mathcal{L}_{11}} < \left(\frac{A_1}{A_2} \right)^2. \quad (2.18)$$

Applying the above results for an arbitrary continuous steady-state heat engine operating between a hot and a cold reservoir with temperatures T_h and T_c , respectively, we get $A_1 =$

η_C/T_c , and $A_2 = 1/T_c$ where $\eta_C = 1 - \frac{T_c}{T_h}$ is the Carnot efficiency. As a result $\frac{A_1}{A_2} = 1 - \frac{T_c}{T_h} = \eta_C$. Thus for continuous heat engines we receive the following universal upper and lower bounds on fluctuation,

$$\langle \eta \rangle^2 \leq \eta^{(2)} < \eta_C^2 \quad (2.19)$$

Interestingly, this inequality further provides a tighter bound (tighter than the Seminal Carnot bound) on the average efficiency of a heat engine

$$\langle \eta \rangle \leq \sqrt{\eta^{(2)}} < \eta_C \quad (2.20)$$

solely in terms of current fluctuations. Following the same analysis, similar bounds can also be obtained for other operational regimes such as refrigerator and heat pump, as given explicitly in table 2.1.

Table 2.1: Input (I_1) and output (I_2) currents, their affinities, average efficiency and ratio of fluctuations in different operational regimes following the notation of Ref. [139]. The delivered power is given by $-I_2$. $\eta_C = 1 - T_c/T_h$ is the Carnot efficiency.

	Heat Engine	Refrigerator	Heat Pump
I_1	I_q^h	I_w	I_w
A_1	η_C/T_c	$1/T_h$	$1/T_c$
I_2	I_w	$-I_q^c$	I_q^h
A_2	$1/T_c$	η_C/T_c	η_C/T_c
$\langle \eta \rangle$	$\frac{ \langle I_w \rangle }{ \langle I_q^h \rangle } \leq \eta_C$	$\frac{ \langle I_q^c \rangle }{ \langle I_w \rangle } \leq \frac{(1-\eta_C)}{\eta_C}$	$\frac{ \langle I_q^h \rangle }{ \langle I_w \rangle } \leq \frac{1}{\eta_C}$
$\eta^{(2)}$	$\langle \eta \rangle_{\text{eng}}^2 \leq \eta_{\text{eng}}^{(2)} \leq \eta_C^2$	$\langle \eta \rangle_{\text{ref}}^2 \leq \eta_{\text{ref}}^{(2)} \leq \left(\frac{1-\eta_C}{\eta_C}\right)^2$	$\langle \eta \rangle_{\text{pump}}^2 \leq \eta_{\text{pump}}^{(2)} \leq \frac{1}{\eta_C^2}$

2.4 Connection with thermodynamic uncertainty relation

Following the definition for \mathcal{Q} [Eq. 2.10], our central result $\mathcal{Q} \geq 1$ implies that the relative fluctuation of output current is always greater than the relative fluctuation of the input current, i.e.,

$$\frac{\langle I_2^2 \rangle_c}{\langle I_2 \rangle^2} \geq \frac{\langle I_1^2 \rangle_c}{\langle I_1 \rangle^2}. \quad (2.21)$$

One can immediately connect this result with the TUR by multiplying the above equation with the steady-state entropy production rate $\langle\sigma\rangle$ (Note that $\langle\sigma\rangle \geq 0$), which results in

$$\langle\sigma\rangle \frac{\langle I_2^2 \rangle_c}{\langle I_2 \rangle^2} \geq \langle\sigma\rangle \frac{\langle I_1^2 \rangle_c}{\langle I_1 \rangle^2}. \quad (2.22)$$

Our result therefore put forward an important connection with the TUR product $\left(\langle\sigma\rangle \frac{\langle I_i^2 \rangle_c}{\langle I_i \rangle^2}\right)$ for the output current being always lower-bounded by the corresponding TUR product for the input current. Note that earlier studies [64, 65, 71] derived independent TUR bounds for the individual currents for generic classes of steady-state systems (both Markovian and non-Markovian). In contrast, Eq. (2.60) establishes that the TUR bounds for different currents are not independent in the operational regimes but follow a strict hierarchy. In other words, in the operational regime of a non-equilibrium setup, the following universal result hold in the linear-response regime

$$\boxed{\langle\sigma\rangle \frac{\langle I_2^2 \rangle_c}{\langle I_2 \rangle^2} \geq \langle\sigma\rangle \frac{\langle I_1^2 \rangle_c}{\langle I_1 \rangle^2} \geq 2} \quad (2.23)$$

2.4.1 Connection between the bounds on efficiency following the TUR and following Eq. (2.20)

Interestingly, the TUR relation provides a bound on average efficiency of a machine and is tighter than the Carnot bound [68]. We show here that our bound on the efficiency following Eq. (2.20) is tighter than the bound following the TUR. For that purpose, we first present the bound that follows from the TUR. For details please see Ref. [68].

Let us derive the bound for a steady state heat engine operating between hot and cold reservoirs with temperatures T_h and T_c , respectively. Due to the steady state condition and the first law of thermodynamics we have,

$$-\langle I_w \rangle = \langle I_q^h \rangle + \langle I_q^c \rangle \quad (2.24)$$

where $-\langle I_w \rangle$ is the average output power as per our convention. $\langle I_q^h \rangle$ and $\langle I_q^c \rangle$ are the average heat currents from hot and cold bath respectively. Then the average entropy production

rate can be written as,

$$\langle \sigma \rangle = -\frac{\langle I_q^h \rangle}{T_h} - \frac{\langle I_q^c \rangle}{T_c} = \frac{-\langle I_w \rangle}{T_c} \left[\frac{\eta_C}{\langle \eta \rangle} - 1 \right] \quad (2.25)$$

where $\langle \eta \rangle = \frac{-\langle I_w \rangle}{\langle I_q^h \rangle}$ is the average efficiency. Note that in order for this setup to work as an engine both input heat current and output power have to be positive i.e., $-\langle I_w \rangle, \langle I_q^h \rangle > 0$.

Now the TUR for work current or power output of given by

$$\langle \sigma \rangle \frac{\langle I_w^2 \rangle_c}{\langle I_w \rangle^2} \geq 2. \quad (2.26)$$

Inserting the average entropy production rate from Eq.(2.25) into the above equation and after some manipulations we get,

$$\langle \eta \rangle \leq \frac{\eta_C}{1 - \frac{2\langle I_w \rangle T_c}{\langle I_w^2 \rangle_c}} \equiv \eta_{\text{TUR}} \quad (2.27)$$

Note that this bound is tighter than the Carnot efficiency as $-\langle I_w \rangle > 0$. This non-trivial bound was first obtained in Ref. [68]. Now in what follows we show that this bound is looser than our bound on efficiency in the linear response regime.

Following our convention for input and output currents, in this example, $\langle I_w \rangle$ corresponds to $\langle I_2 \rangle$ (output) and $\langle I_q^h \rangle$ corresponds to $\langle I_1 \rangle$ (input), and $A_1 = \eta_C/T_c$ and $A_2 = 1/T_c$. Also $\langle I_w^2 \rangle_c = 2\mathcal{L}_{22}$. Given this, after some manipulations η_{TUR} , defined in Eq. (2.27) simplifies to,

$$\eta_{\text{TUR}} = -\frac{\mathcal{L}_{22}}{\mathcal{L}_{21}} \quad (2.28)$$

Since $A_1, A_2 > 0$, therefore engine operating condition, $-I_2 A_2 > 0$, implies that $-\mathcal{L}_{21} > 0$. Along with this information, positivity of the entropy production rate implies,

$$-\frac{1}{\mathcal{L}_{21}} \geq \frac{1}{\sqrt{\mathcal{L}_{11}\mathcal{L}_{22}}} \quad (2.29)$$

Putting this in Eq.(2.28) we get,

$$\eta_{\text{TUR}} = -\frac{\mathcal{L}_{22}}{\mathcal{L}_{21}} \geq \sqrt{\frac{\mathcal{L}_{22}}{\mathcal{L}_{11}}} = \sqrt{\eta^{(2)}} \quad (2.30)$$

This shows that our bound on efficiency is tighter than η_{TUR} . Thus we have ,

$$\boxed{\langle \eta \rangle \leq \sqrt{\eta^{(2)}} \leq \eta_{\text{TUR}} < \eta_C} \quad (2.31)$$

In what follows, we will illustrate our findings using two types of continuous thermal machines, two-terminal coherent thermoelectric junctions and three-terminal quantum absorption refrigerators.

2.5 Example 1: Steady-state thermoelectric transport in two-terminal systems

As an illustration of our results we consider a two-terminal thermoelectric device as shown in Fig.(2.1). The junction consists of an elastic scatterer (e.g., array of quantum dots), which is connected to two fermionic reservoirs. Hamiltonian for this non-interacting setup is given by,

$$\begin{aligned} \hat{H} &= \hat{H}_C + \hat{H}_L + \hat{H}_R + \hat{\mathcal{V}}_L + \hat{\mathcal{V}}_R \\ &= \sum_{\nu=L,C,R} \hat{c}_\nu^\dagger h^\nu \hat{c}_\nu + \sum_{\nu=L,R} \left(\hat{c}_\nu^\dagger V_e^\nu \hat{c}_C + \text{h.c.} \right). \end{aligned} \quad (2.32)$$

Here, \hat{H}_C , \hat{H}_L and \hat{H}_R denotes the Hamiltonian of the isolated central system, and the left, and the right reservoirs. $\hat{\mathcal{V}}_{L,R}$ corresponds to the interaction between system and the left (right) reservoirs. \hat{c}_ν^\dagger (\hat{c}_ν) is the row (column) vector consisting of electronic creation (annihilation) operators in the ν region, with h^ν the single-particle Hamiltonian matrix in that domain. The baths ($\nu = L, R$) and the central system are initially decoupled and are prepared at their respective grand canonical equilibrium state with temperature T_ν and chemical potential μ_ν . For such a non-interacting setup, the exact steady-state cumulant generating function (CGF) for both charge and energy currents can be obtained exactly using a scattering matrix formalism. It is given by the celebrated Levitov-Lesovik formula [61, 149, 150]. The characteristic function for the joint integrated charge and energy currents is defined as

$$Z(\chi_e, \chi_u) = \langle \exp(i\chi_e J_e + i\chi_u J_u) \rangle, \quad (2.33)$$

where χ_e and χ_u are the counting fields that keep track of net charge J_e and energy J_u flowing out of one of the terminals, say the right (R) terminal. In the long-time limit, as the CGF scales extensively with the integrated time t one can define the corresponding scaled cumulant generating function (CGF) as,

$$\mathcal{G}(\chi_e, \chi_u) = \lim_{t \rightarrow \infty} \frac{1}{t} \ln Z(\chi_e, \chi_u). \quad (2.34)$$

This scaled CGF for such a non-interacting setup is obtained exactly as,

$$\begin{aligned} \mathcal{G}(\chi_e, \chi_u) = & \int_{-\infty}^{\infty} \frac{d\epsilon}{2\pi} \ln \left(1 + \mathcal{T}(\epsilon) \left\{ f_R(\epsilon) [1 - f_L(\epsilon)] [e^{i(\chi_e + \epsilon \chi_u)} - 1] \right. \right. \\ & \left. \left. + f_L(\epsilon) [1 - f_R(\epsilon)] [e^{-i(\chi_e + \epsilon \chi_u)} - 1] \right\} \right), \end{aligned} \quad (2.35)$$

where $f_\nu(\epsilon) = [e^{\beta\nu(\epsilon - \mu\nu)} + 1]^{-1}$, $\nu = L, R$ is the equilibrium Fermi-Dirac distribution function for the reservoirs. $\mathcal{T}(\epsilon)$ is the transmission function, which indicates the probability for electrons to transfer from the right to the left reservoir via the elastic scattering region. It can be computed from the retarded and advanced Green's function of the system and from the self-energy matrix originating due to the interaction of the central system with the two reservoirs [151]. The formal expression for the transmission is given by,

$$\mathcal{T}(\epsilon) = \text{Tr}[G^r(\epsilon)\Gamma_L(\epsilon)G^a(\epsilon)\Gamma_R(\epsilon)], \quad (2.36)$$

where $G^r(\epsilon)$ is the retarded Green's function of the central system in presence of the reservoirs, $G^a(\epsilon) = [G^r(\epsilon)]^\dagger$ is the corresponding advanced Green's function and $\Gamma_{L,R}$ are the hybridization matrices that include the coupling to the reservoirs L and R .

From the CGF, we obtain cumulants of currents, flowing out of the right reservoir, by taking derivatives with respect to the corresponding counting fields, and obtain

$$\langle I_K \rangle = \int_{-\infty}^{\infty} \frac{d\epsilon}{2\pi} \xi_K \mathcal{T}(\epsilon) [f_R(\epsilon) - f_L(\epsilon)], \quad (2.37)$$

where $\xi_K = 1$ or ϵ for particle(e) or energy(u) currents respectively. Fluctuations i.e., the second order cumulants are given by,

$$\langle I_K^2 \rangle_c = \int_{-\infty}^{\infty} \frac{d\epsilon}{2\pi} \xi_K^2 \mathcal{T}(\epsilon) \{ f_L(\epsilon) [1 - f_R(\epsilon)] + f_R(\epsilon) [1 - f_L(\epsilon)] \} - \mathcal{T}^2(\epsilon) [f_R(\epsilon) - f_L(\epsilon)]^2 \quad (2.38)$$

Note that the heat current (q) cumulants can be simply obtained by setting $\xi_q = \epsilon - \mu_R$. In the linear response regime, one considers the limit $|\Delta T| \ll T$ and $|\Delta\mu| \ll T$. Here, $\Delta\mu = \mu_L - \mu_R$, $\Delta T = T_R - T_L$, and $T = (T_L + T_R)/2$, $\mu = (\mu_L + \mu_R)/2$ being the average temperature and average chemical potential, respectively. The currents can then be expressed in terms of Onsager's transport coefficients,

$$\begin{aligned}\langle I_e \rangle &= \mathcal{L}_{ee} \left(\frac{-\Delta\mu}{T} \right) + \mathcal{L}_{eq} \left(\frac{\Delta T}{T^2} \right), \\ \langle I_q \rangle &= \mathcal{L}_{qe} \left(\frac{-\Delta\mu}{T} \right) + \mathcal{L}_{qq} \left(\frac{\Delta T}{T^2} \right),\end{aligned}\quad (2.39)$$

where we used $-\frac{\partial f}{\partial \epsilon} = f(1-f)\beta$. Here, $f(\epsilon)$ is the equilibrium distribution function evaluated at T and μ . The various transport coefficients are given by

$$\begin{aligned}\mathcal{L}_{ee} &= \int_{-\infty}^{\infty} \frac{d\epsilon}{2\pi} \mathcal{T}(\epsilon) f(\epsilon) [1 - f(\epsilon)], \\ \mathcal{L}_{eq} &= \mathcal{L}_{qe} = \int_{-\infty}^{\infty} \frac{d\epsilon}{2\pi} (\epsilon - \mu) \mathcal{T}(\epsilon) f(\epsilon) [1 - f(\epsilon)], \\ \mathcal{L}_{qq} &= \int_{-\infty}^{\infty} \frac{d\epsilon}{2\pi} (\epsilon - \mu)^2 \mathcal{T}(\epsilon) f(\epsilon) [1 - f(\epsilon)].\end{aligned}\quad (2.40)$$

In the equilibrium limit ($\Delta\mu = \Delta T = 0$), one recovers the standard equilibrium fluctuation-dissipation relation from Eq. (2.38),

$$\left[\langle I_q^2 \rangle_c \right]_{\text{eq}} = \mathcal{L}_{qq}, \quad \left[\langle I_e^2 \rangle_c \right]_{\text{eq}} = \mathcal{L}_{ee}. \quad (2.41)$$

To realize different operational regimes, we set the thermodynamic parameters for the reservoirs as $T_R > T_L$ and $\mu_L > \mu_R$. As a result all the expressions for currents obtained above are from the hot reservoir i.e., the right terminal. Also note that due to the steady state condition once we know the charge and energy currents flowing out of the hot reservoir (right), one can immediately compute the currents from the cold reservoir (left) employing the current conservation. Recall that the above results are valid for arbitrary coherent junction. In what follows we illustrate our findings for three different operational regimes i.e., engine, refrigerator, and pump for a working medium made out of a single quantum dot.

1. Thermoelectric engine: In order to operate the setup as a thermoelectric engine the heat current absorbed from the hot terminal (right terminal) can be used to drive charge

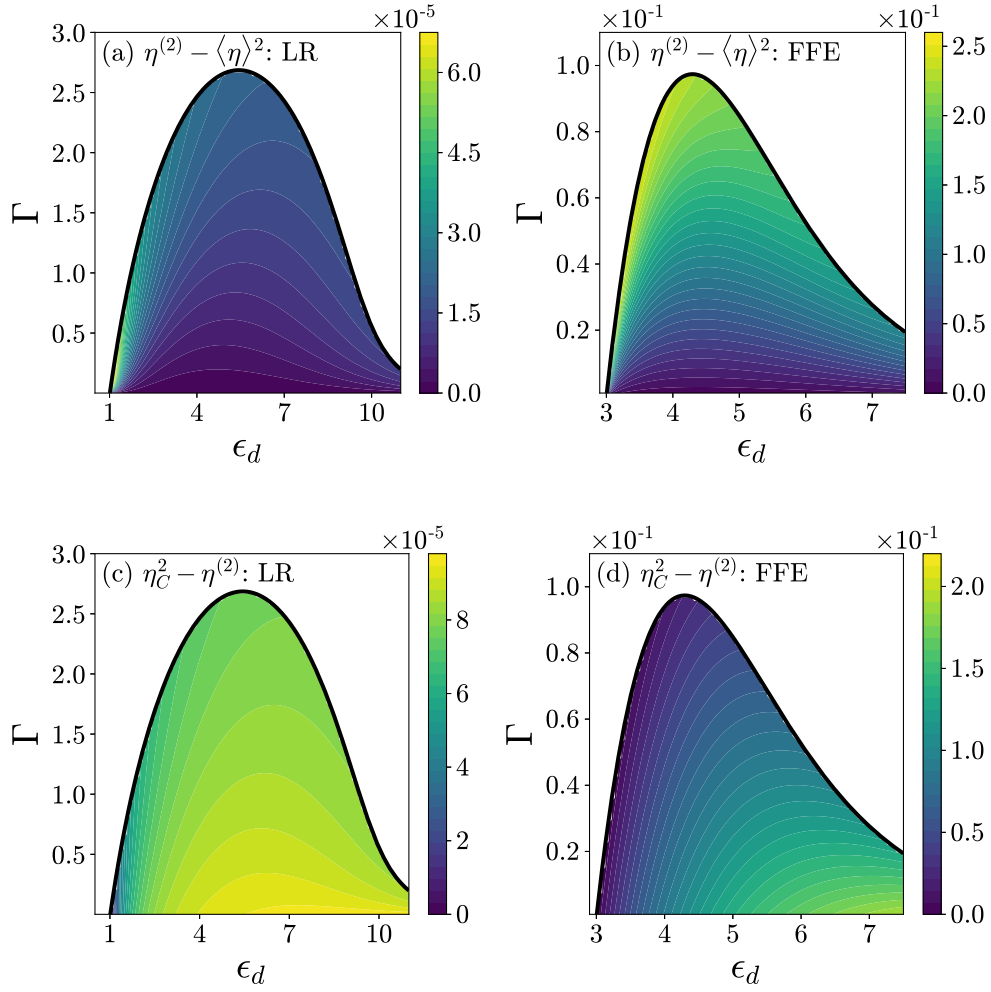


Figure 2.2: Single-dot thermoelectric engine. (a)-(b) Test of the lower bound, $\eta^{(2)} \geq \langle \eta \rangle^2$, and (c)-(d) the upper bound, $\eta_C^2 \geq \eta^{(2)}$, for a single-dot thermoelectric system within linear response (LR) and far from equilibrium (FFE). We focus on the ranges of ϵ_d and Γ at which the system operates as an engine. Positive values signify that bounds are satisfied (see Table 2.1). We use $\beta_L = 1.01$, $\beta_R = 1$, $\mu_L = 0.01$, $\mu_R = 0$ for (a) and (c) and $\beta_L = 2$, $\beta_R = 1$, $\mu_L = 1$, $\mu_R = -1$ for (b) and (d). Figure reproduced with permission from Ref.[152].

current against the chemical bias. Following the stochastic thermodynamics framework we can write,

$$\langle I_q^h \rangle = \langle I_q^\alpha \rangle = \langle I_u \rangle - \mu_R \langle I_e \rangle > 0 \quad (2.42)$$

$$-\langle I_w \rangle = (\mu_L - \mu_R) \langle I_e \rangle > 0. \quad (2.43)$$

The corresponding efficiency is then $\langle \eta \rangle_{\text{eng}} = \frac{-\langle I_w \rangle}{\langle I_q^h \rangle}$. In Fig. 2.2 we display contour plots to assess the validity of lower (a)-(b) $\eta^{(2)} - \langle \eta \rangle^2$ and upper (c)-(d) $\eta_C^2 - \eta^{(2)}$ bounds for a thermoelectric engine both in linear response (LR) and far from equilibrium (FFE). We use a single quantum dot as the scatter with the dot energy ϵ_d and the hybridization strength $\Gamma_{L,R}(\epsilon)$ which is assumed to be independent of energy (wide-band approximation) and equal in magnitude for both the left and the right leads i.e., $\Gamma_L = \Gamma_R = \Gamma$. To generate the contour plot we tune ϵ_d and Γ over a broad window. Note that, to compute the Onsager coefficients following Eq. (2.40), we need the expression for transmission function which can be analytically obtained for the single dot case following Eq. (2.36). In this case, the retarded Green's function component is given as,

$$G^r(\epsilon) = \frac{1}{\epsilon - \epsilon_d + i\Gamma} \quad (2.44)$$

and as a result the transmission function is given as,

$$\mathcal{T}(\epsilon) = \frac{\Gamma^2}{(\epsilon - \epsilon_d)^2 + \Gamma^2} \quad (2.45)$$

We show the validity of our bounds in the linear response regime. Interestingly, our numerical simulation over a wide range of parameters further suggest the validity of the lower and upper bounds beyond the linear response regime.

2. Refrigerator: In the refrigerator regime, heat current from the cold (left) reservoir is extracted by using the charge current flowing from high to low bias i.e., $\langle I_q^c \rangle = -\langle I_u \rangle + \mu_L \langle I_e \rangle \geq 0$ and $\langle I_e \rangle \leq 0$. The efficiency is given as $\langle \eta \rangle_{\text{ref}} = \frac{\langle I_q^c \rangle}{\langle I_w \rangle}$. In Fig. 2.3 we display the validity for the lower, $\langle \eta \rangle^2 \leq \eta^{(2)}$, and upper, $\eta^{(2)} \leq \left(\frac{1 - \eta_C}{\eta_C}\right)^2$, bounds in both linear response and far-from-equilibrium regimes.

3. Heat pump: To realize a heat pump, we demand that the heat current should flow

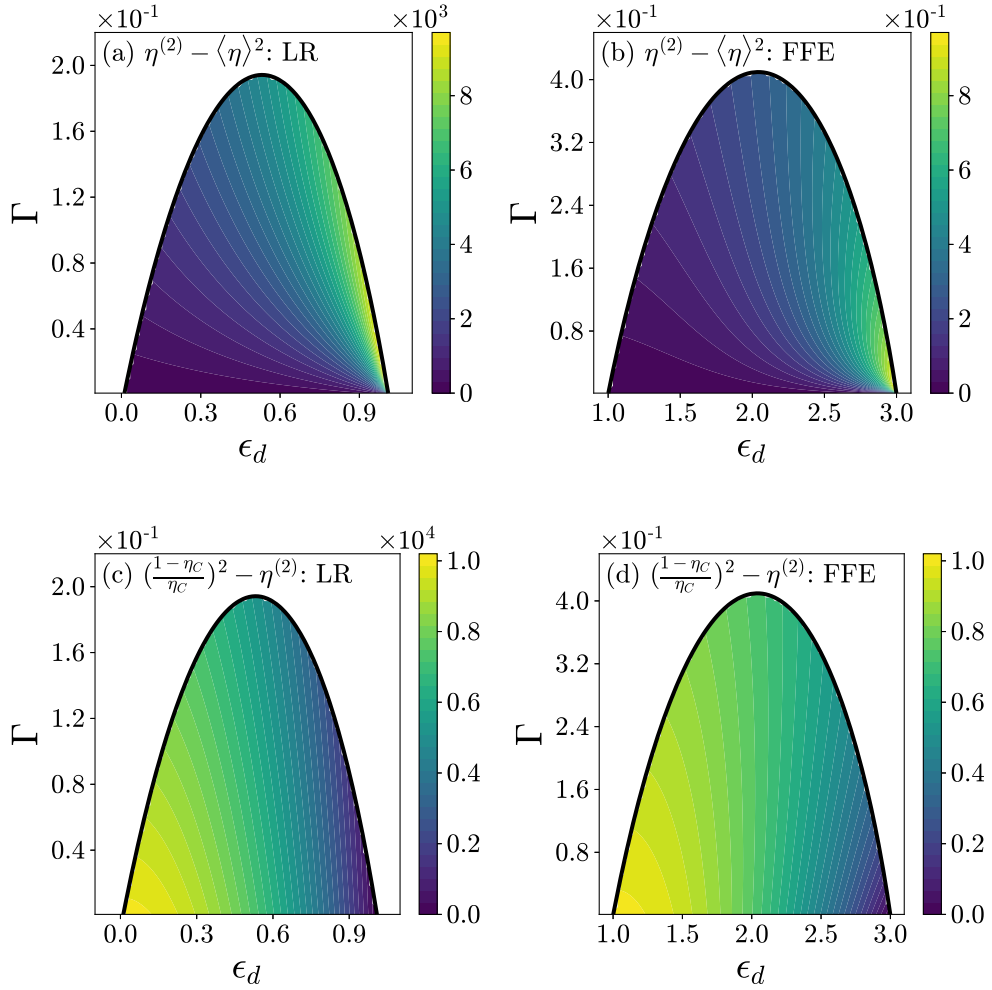


Figure 2.3: Single-dot thermoelectric refrigerator. (a)-(b) Test of the lower bound, $\eta^{(2)} \geq \langle \eta \rangle^2$ within linear response and far from equilibrium. (c)-(d) Test of the upper bound, $\left(\frac{1-\eta_C}{\eta_C}\right)^2 \geq \eta^{(2)}$, for the same system. We focus on relevant ranges of ϵ_d and Γ at which the system operates as a refrigerator. Positive values signify that the bound is satisfied. We used $\beta_L = 1.01$, $\beta_R = 1$, $\mu_L = 0.01$, $\mu_R = 0$ for (a) and (c) and $\beta_L = 2$, $\beta_R = 1$, $\mu_L = 1$, $\mu_R = -1$ for (b) and (d). Figure reproduced with permission from Ref.[152].

towards the (right) hot reservoir, $\langle I_q^h \rangle \leq 0$, by using the charge current, $\langle I_e \rangle \leq 0$. The corresponding efficiency is $\langle \eta \rangle_{\text{pump}} = \frac{-\langle I_q^h \rangle}{\langle I_w \rangle}$. Figure 2.4 once again shows the validity of upper and lower bounds both in linear response and far-from-equilibrium regimes.

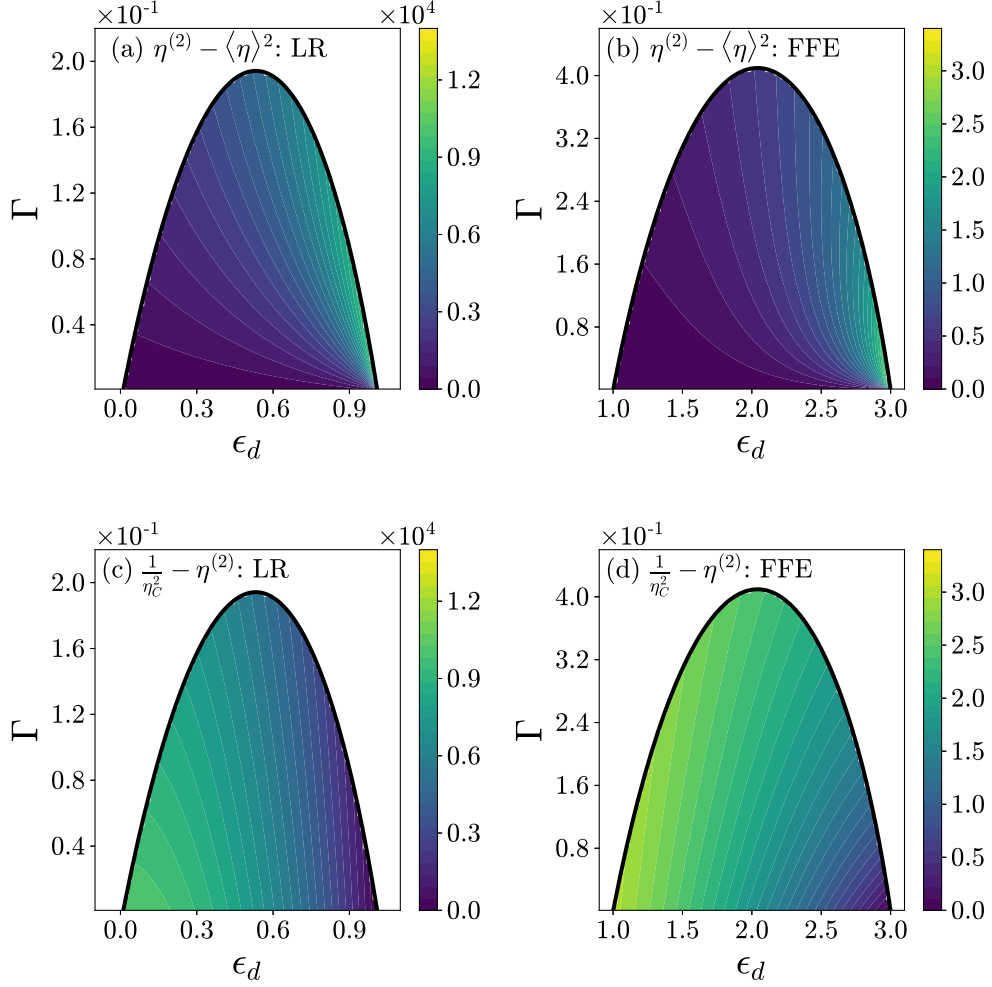


Figure 2.4: (Color online) Single-dot thermoelectric heat pump. (a)-(b) Test of the lower bound, $\eta^{(2)} \geq \langle \eta \rangle^2$ within linear response and far from equilibrium. (c)-(d) Test of the upper bound, $\frac{1}{\eta_c} \geq \eta^{(2)}$, for the same system. We focus on relevant ranges of ϵ_d and Γ at which the system operates as a heat pump. Positive values signify that the bound is satisfied (see Table in main text). We used $\beta_L = 1.01$, $\beta_R = 1$, $\mu_L = 0.01$, $\mu_R = 0$ for (a) and (c) and $\beta_L = 2$, $\beta_R = 1$, $\mu_L = 1$, $\mu_R = -1$ for (b) and (d). Figure reproduced with permission from Ref.[152].

In Fig. 2.5, we show the \mathcal{Q} ratio both in the linear and beyond linear response regime. We observe the existence of the lower bound i.e., $\mathcal{Q} \geq 1$ in both the engine (E) and the refrigerator (R) regimes.

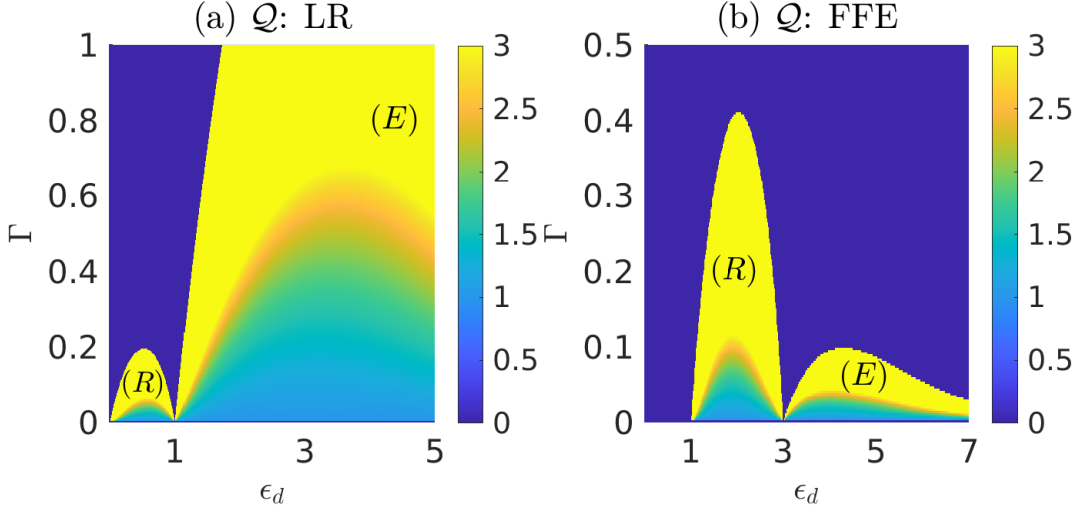


Figure 2.5: (Color online) Plot of the ratio Q for a single dot thermoelectric system within and beyond linear response. We display both the engine (E) and refrigerator (R) regimes for the relevant ranges of ϵ_d and Γ . (a) Linear response simulations with $\beta_L = 1.01$, $\beta_R = 1$, $\mu_L = 0.01$, $\mu_R = 0$. (b) Beyond linear response simulations with $\beta_L = 2$, $\beta_R = 1$, $\mu_L = 1$, $\mu_R = -1$. We confirm that in both the engine and refrigerator regimes, $Q \geq 1$. For clarity of presentation, values of $Q > 3$ were assigned the value 3. Figure reproduced with permission from Ref.[152].

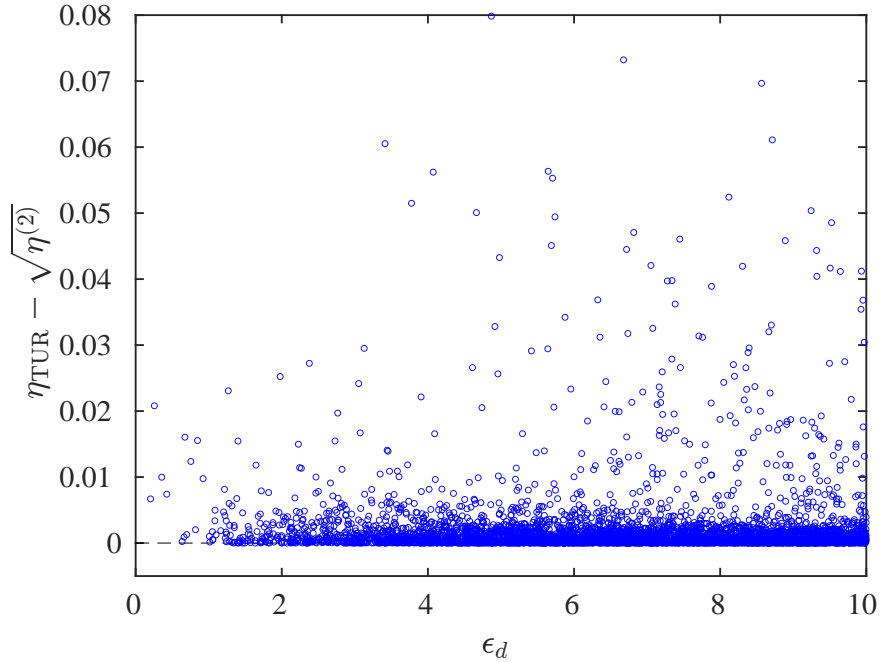


Figure 2.6: Scatter plot for difference between the bounds, $\eta_{\text{TUR}} - \sqrt{\eta^{(2)}}$ for single dot thermoelectric engine. We perform numerical simulation over a broad parameter regime by choosing the different model parameters randomly. We choose all the parameters from uniform random distribution. $T_L \in [0, 4]$, $T_R \in [4, 6]$, $\mu_R \in [0, 4]$, $\mu_L \in [4, 6]$, $\Gamma \in [0, 3]$, and $\epsilon_d \in [0, 10]$.

In section 2.4 we provided a proof that the upper bound on the engine efficiency, $\langle \eta^2 \rangle$,

that we obtained is tighter than the one obtained following TUR, see Eq.(2.31). In Fig. 2.6 we provide scatter plot for single-dot thermoelectric engine by choosing different model parameters randomly, which once again agrees with our findings.

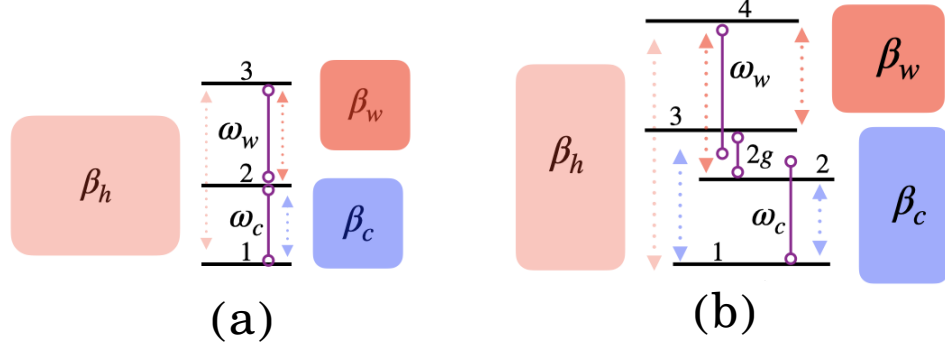


Figure 2.7: Schematic for (a) three-level and (b) four-level models for quantum absorption refrigerators. In both cases the inverse temperature of the baths follow the sequence $\beta_c > \beta_h > \beta_w$. The baths induced incoherent transitions are shown by the dashed arrows. The energy gaps between the states are indicated by solid lines. In the population dynamics, the different baths induced transition rates contributes in the additive manner. Fig. 2.7(b) reproduced with permission from Ref.[153].

2.6 Example 2: Quantum Absorption Refrigerator

As a second example, we consider a quantum absorption refrigerator (QAR) setup. Models for QAR have served a crucial role in establishing working principles of autonomous quantum thermal machines [110, 119–123] with recent experiments realizing such models using trapped ions [12]. In QARs, heat is extracted from a cold (c) bath and released into a hot (h) environment by utilizing heat from a so-called work (w) bath. The reversed operation realizes a heat engine. We identify three inverse-temperatures, $\beta_w < \beta_h < \beta_c$ in a QAR, and three heat currents, $I_{c,h,w}$, defined positive when flowing out from the respective baths, with two affinities, $\beta_h - \beta_c$ and $\beta_h - \beta_w$. Schematic diagrams of three-level and four-level QARs are displayed in Figs. 2.7(a) and 2.7(b), respectively. The cooling efficiency of QARs is defined as $\langle \eta \rangle = \langle I_c \rangle / \langle I_w \rangle$. It is bounded by $\langle \eta \rangle \leq \eta_{\text{cool}}$ where $\eta_{\text{cool}} \equiv \frac{(\beta_h - \beta_w)}{\beta_c - \beta_h} \xrightarrow{T_w \gg T_h} (1 - \eta_C) / \eta_C$ [154].

In what follows, we limit our discussion to the weak system-bath coupling limit, Markovian reservoirs, and decoupled coherence population dynamics (secular approximation), which

can be handled within a perturbative quantum Master equation (QME) approach . Following the QME, a first-order differential equation for the characteristic function (CF) $|\mathcal{Z}(\chi, t)\rangle$, corresponding to the counting-fields dressed population dynamics can be obtained as,

$$\frac{d|\mathcal{Z}(\chi, t)\rangle}{dt} = \hat{\mathcal{W}}(\chi)|\mathcal{Z}(\chi, t)\rangle, \quad (2.46)$$

where counting parameters $\chi = (\chi_w, \chi_h, \chi_c)$ keep track of the energy flowing out from the respective terminals. $\hat{\mathcal{W}}(\chi)$ is the dressed rate matrix. The steady-state cumulant generating function (CGF) hands over the cumulants for currents which can be received from the CF as

$$\mathcal{G}(\chi) = \lim_{t \rightarrow \infty} \frac{1}{t} \ln \langle I | \mathcal{Z}(\chi, t) \rangle \quad (2.47)$$

with $\langle I | = \langle 11..1 |$ being a unit vector for the n -level QAR. The mean currents and the fluctuations are determined by taking the first and second derivative of the CGF with respect to the respective counting fields.

For three-level QAR, Fig. 2.7(a), one can obtain the analytical form of current and noise for the above mentioned approximation. $\hat{\mathcal{W}}(\chi)$ for three-level QAR is given by,

$$\hat{\mathcal{W}}(\chi) = \begin{pmatrix} -k_{1 \rightarrow 2}^c - k_{1 \rightarrow 3}^h & k_{2 \rightarrow 1}^c e^{-i\chi_c \omega_c} & k_{3 \rightarrow 1}^h e^{-i\chi_h \omega_h} \\ k_{1 \rightarrow 2}^c e^{i\chi_c \omega_c} & -k_{2 \rightarrow 1}^c - k_{2 \rightarrow 3}^w & k_{3 \rightarrow 2}^w e^{-i\chi_w \omega_w} \\ k_{1 \rightarrow 3}^h e^{i\chi_h \omega_h} & k_{2 \rightarrow 3}^w e^{i\chi_w \omega_w} & -k_{3 \rightarrow 2}^w - k_{3 \rightarrow 1}^h \end{pmatrix}. \quad (2.48)$$

Here, we count the three levels (bottom to top) by 1,2,3, with energies $\epsilon_{1,2,3} = (0, \omega_c, \omega_w)$. Assuming that the baths comprise collections of harmonic oscillators, which are coupled to the quantum system through the displacements of the oscillators, the rate constant due to the b bath is given by the product

$$k_{i \rightarrow j}^b = J_b(\epsilon_j - \epsilon_i) n_b(\epsilon_j - \epsilon_i). \quad (2.49)$$

Here, $n_b(\Delta) = (e^{\beta_b \Delta} - 1)^{-1}$ is the Bose-Einstein distribution function and $J_b(\Delta) = \gamma_b \Delta e^{-|\Delta|/\Lambda}$ is the spectral density function of the b bath. For simplicity, we assume Ohmic spectral functions and take the cutoff frequency to be large, $\Lambda \gg \omega_{c,w}, 1/\beta$.

The statistics for all the currents is determined by the largest eigenvalue (real part) of this

characteristic polynomial. The characteristic polynomial for the largest eigenvalue satisfy the equation

$$\lambda_{\max}^3 - a_1 \lambda_{\max}^2 + a_2 \lambda_{\max} - a_3(\chi) = 0 \quad (2.50)$$

with the condition that $\lambda_{\max}(\chi = 0) = 0$. Here,

$$\begin{aligned} a_1 &= w_{0,0} + w_{1,1} + w_{2,2}, \\ a_2 &= w_{0,0}w_{1,1} + w_{0,0}w_{2,2} + w_{1,1}w_{2,2} - w_{0,1}(\chi_c) w_{1,0}(\chi_c) - w_{0,2}(\chi_h) w_{2,0}(\chi_h) \\ &\quad - w_{1,2}(\chi_w) w_{2,1}(\chi_w), \\ a_3(\chi) &= w_{0,0} w_{1,1} w_{2,2} - w_{0,0} w_{1,2}(\chi_w) w_{2,1}(\chi_w) - w_{0,1}(\chi_c) w_{1,0}(\chi_c) w_{2,2} \\ &\quad + w_{0,1}(\chi_c) w_{1,2}(\chi_w) w_{2,0}(\chi_h) + w_{0,2}(\chi_h) w_{2,1}(\chi_w) w_{1,0}(\chi_c) \\ &\quad - w_{0,2}(\chi_h) w_{2,0}(\chi_h) w_{1,1}, \end{aligned} \quad (2.51)$$

where $w_{i,j}$ are the elements of the matrix $\hat{\mathcal{W}}(\chi)$ [155]. Notice that, a_1 is counting field independent. Moreover, the counting field dependent phase factors exactly cancels out in a_2 . As a result, a_3 is the only counting field dependent term in Eq. (2.50). We can obtain analytical expression for the current for bath α as

$$\langle I_\alpha \rangle = \frac{1}{a_2} \frac{\partial a_3}{\partial (ix_\alpha)} \Big|_{\chi=0}, \quad \alpha = h, c, w. \quad (2.52)$$

It can be easily checked that the currents are proportional to each other and given by

$$\begin{aligned} \langle I_c \rangle &= \frac{\omega_c}{a_2} \left[w_{0,2} w_{2,1} w_{1,0} - w_{0,1} w_{1,2} w_{2,0} \right], \\ \langle I_w \rangle &= \frac{\omega_w}{\omega_c} \langle I_c \rangle \end{aligned} \quad (2.53)$$

The corresponding noise for bath α is given as

$$\frac{\langle I_\alpha^2 \rangle_c}{2} = \frac{1}{2 a_2} \left[\frac{\partial^2 a_3}{\partial (ix_\alpha)^2} + \frac{2 a_1}{a_2^2} \left(\frac{\partial a_3}{\partial (ix_\alpha)} \right)^2 \right] \Big|_{\chi=0}. \quad (2.54)$$

As a result, the relative fluctuation simplifies to

$$\frac{\langle I_\alpha \rangle_c}{\langle I_\alpha \rangle^2} = \frac{a_1}{a_2} + \frac{a_2}{2} \frac{a_3''}{(a_3')^2}, \quad (2.55)$$

where the primes indicate the order of the derivative with respect to the respective counting field χ_α . Notice that a_1 and a_2 remains the same for any current. Interestingly, it turns out

the second term $a_3''/(a_3')^2$ is also the same for any current and is given by

$$\frac{a_3''}{(a_3')^2} = \frac{w_{0,2} w_{2,1} w_{1,0} + w_{0,1} w_{1,2} w_{2,0}}{(w_{0,2} w_{2,1} w_{1,0} - w_{0,1} w_{1,2} w_{2,0})^2}. \quad (2.56)$$

We therefore see that the relative fluctuation of currents for output and input currents are the same, i.e.,

$$\frac{\langle I_c \rangle_c}{\langle I_c \rangle^2} = \frac{\langle I_w \rangle_c}{\langle I_w \rangle^2}. \quad (2.57)$$

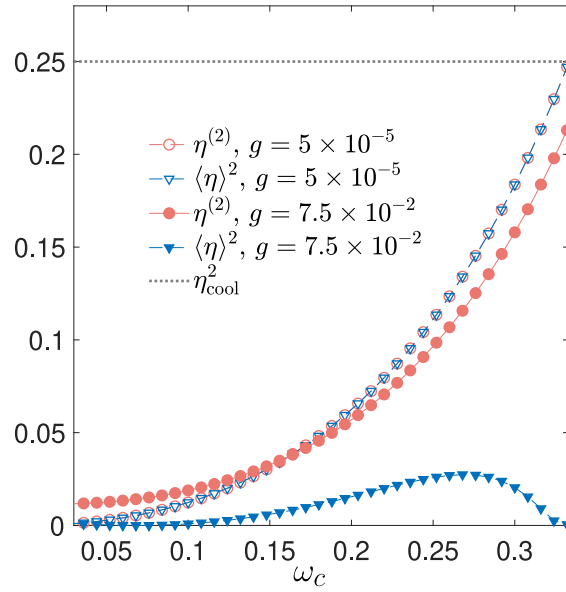


Figure 2.8: Simulations of $\eta^{(2)}$ for the four-level model. Here, we use $\beta_w = 2.5$, $\beta_h = 5$, $\beta_c = 10$, with the maximum cooling efficiency $\eta_{\text{cool}} \equiv \frac{\beta_h - \beta_w}{\beta_c - \beta_h} = 0.5$. The spectral function of the baths are chosen as Ohmic, $J_b(\omega) = \gamma_b \omega e^{-|\omega|/\Lambda}$, with $\gamma_h = 2 \times 10^{-3}$, $\gamma_{w,c} = 10^{-3}$, and $\Lambda = 50$. Figure reproduced with permission from Ref.[152].

Similarly, for four-level system, Fig. 2.7(b), dressed rate matrix $\hat{\mathcal{W}}(\chi)$ is given by,

$$\hat{\mathcal{W}}(\chi) = \begin{pmatrix} -k_{1 \rightarrow 2}^c - k_{1 \rightarrow 3}^c - k_{1 \rightarrow 4}^h & k_{2 \rightarrow 1}^c e^{-i\chi_c(\omega_c - g)} & k_{3 \rightarrow 1}^c e^{-i\chi_c(\omega_c + g)} & k_{4 \rightarrow 1}^h e^{-i\chi_h(\omega_c + \omega_w)} \\ k_{1 \rightarrow 2}^c e^{i\chi_c(\omega_c - g)} & -k_{2 \rightarrow 1}^c - k_{2 \rightarrow 4}^w & 0 & k_{4 \rightarrow 2}^w e^{-i\chi_w(\omega_w + g)} \\ k_{1 \rightarrow 3}^c e^{i\chi_c(\omega_c + g)} & 0 & -k_{3 \rightarrow 1}^c - k_{3 \rightarrow 4}^w & k_{4 \rightarrow 3}^w e^{-i\chi_w(\omega_w - g)} \\ k_{1 \rightarrow 4}^h e^{i\chi_h(\omega_c + \omega_w)} & k_{2 \rightarrow 4}^w e^{i\chi_w(\omega_w + g)} & k_{3 \rightarrow 4}^w e^{i\chi_w(\omega_w - g)} & -k_{4 \rightarrow 1}^h - k_{4 \rightarrow 2}^w - k_{4 \rightarrow 3}^w \end{pmatrix} \quad (2.58)$$

with $k_{i \rightarrow j}^\alpha$ being the transition rate between states i and j due to terminal α . The energy levels are labelled from bottom to top as 1 to 4 with energies given by $\epsilon_{1,2,3,4} = (0, \omega_c -$

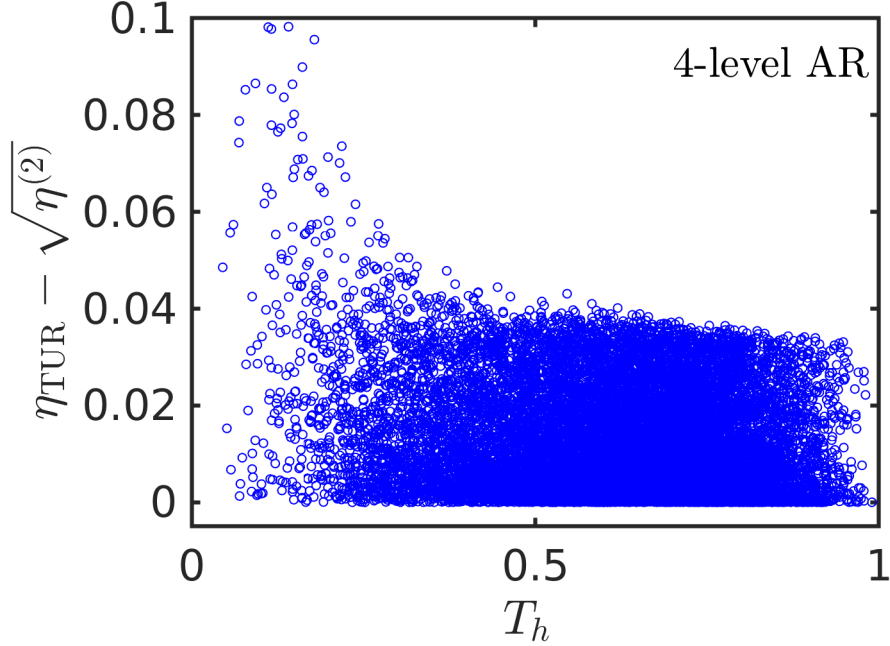


Figure 2.9: Scatter plot of the difference in the bounds $\eta_{\text{TUR}} - \sqrt{\eta^{(2)}}$ for the 4-level quantum AR. We simulate the system over a broad parameter regime and observe that $\eta_{\text{TUR}} - \sqrt{\eta^{(2)}} > 0$. We perform the simulation over 1 million random points and select those data points for which we realise a refrigerator. Here we choose the temperature of all three baths within the interval $[0.1, 1]$ randomly and set the linear response regime by demanding that the ratio $\Delta T/T$ is always smaller than 0.05 where ΔT is the temperature difference between any two terminals and T is the average temperature for the same two terminals. The value of g is chosen within the interval $[0, 0.05]$. We kept other parameters fixed with values for $\omega_c = 0.3$ and $\omega_w = 0.6$.

$g, \omega_c + g, \omega_c + \omega_w$). For $\chi = 0$, the rate matrix describes the standard population dynamics for the system states. For this system we can no longer obtain analytical form of average current and noise. Therefore we have to rely on the numerical methods to compute the current and its corresponding fluctuation. In Fig 2.8 we further verify our findings for four-level QAR. We once again notice that the bounds we obtained are also valid beyond the linear response regime.

In Fig. 2.9 we provide scatter plot for 4-level QAR by choosing different model parameters randomly to verify Eq.(2.31) in the context of QAR. Note that for QAR, upper bound on efficiency obtained from TUR modifies to,

$$\eta_{\text{TUR}} \equiv \frac{\eta_{\text{cool}}}{1 + \frac{2\langle I_c \rangle}{(\beta_c - \beta_h)\langle I_w^2 \rangle_c}}, \quad (2.59)$$

where $\eta_{\text{cool}} \equiv \frac{(\beta_h - \beta_w)}{\beta_c - \beta_h}$. Fig. 2.9 once again verifies our findings for 4-level QAR.

We also want to point out that in our recent work Ref. [153], we further generalized our findings for QAR and obtained a strict hierarchy between the relative fluctuations of heat currents from each terminal. More precisely we found out that,

$$\frac{\langle I_c^2 \rangle_c}{\langle I_c \rangle^2} \geq \frac{\langle I_h^2 \rangle_c}{\langle I_h \rangle^2} \geq \frac{\langle I_w^2 \rangle_c}{\langle I_w \rangle^2} \quad (2.60)$$

Further, the three universal bounds on the mean cooling power, obtained following the thermodynamic uncertainty relations [68] in the context of absorption refrigerator, receive a strict hierarchy [153].

2.7 Summary

In summary, in this chapter following the framework of linear irreversible thermodynamics we showed that for a two-affinity continuous thermal machines, relative fluctuation of the output current (for example, power output for heat engines) is always larger than the relative fluctuations of the input current (for example, heat current absorbed by the system from hot bath). As a consequence of this interesting result, we immediately uncovered universal lower and upper bounds on $\eta^{(2)}$, the ratio between the fluctuations of output and input currents. We also made an interesting connection with the thermodynamic uncertainty relation and further showed that the bound on efficiency following from our result is tighter than the bound obtained following the TUR. We illustrated our findings in two paradigmatic setups that had been realized in experiments. Our numerical results further suggests the validity of these bounds beyond the linear response regime. Our result are universal, albeit in the linear response regime, and completely independent of the underlying dynamics and the nature of the working medium whether it is classical or quantum.

CHAPTER 3

Universal bounds on fluctuations for continuous machines with broken time-reversal symmetry

Abstract

For a generic class of thermal machines with broken time-reversal symmetry we show that in the linear response regime the relative fluctuation of the sum of output currents for time-forward and time-reversed processes is always lower bounded by the corresponding relative fluctuation of the sum of input currents. This bound is received when the same operating condition, for example, engine, refrigerator, or pump, is imposed on both the forward and the reversed processes. As a consequence, universal upper and lower bounds for the ratio between fluctuations of output and input current are obtained. Furthermore, we establish a connection between our results and the *generalized* thermodynamic uncertainty relations for time-reversal symmetry-broken systems. We illustrate these findings for a steady-state three-terminal quantum thermoelectric setup in presence of an external magnetic field.

Reported in

S. Saryal, S. Mohanta, and B. K. Agarwalla, *Bounds on fluctuations for machines with broken time-reversal symmetry: A linear response study*, [Phys. Rev. E 105, 024129 \(2022\)](#).

3.1 Introduction

In the previous chapter we focused on continuous thermal machines respecting time-reversal symmetry and obtained universal bounds on the fluctuations and as a result a bound on the thermodynamic efficiency. A natural question that arises immediately is that what happens to these bounds when the time-reversal symmetry is broken? In this chapter, we answer this

question by generalizing our findings of the previous chapter. Note that breakdown of time-reversal symmetry is quite common in many different scenarios, for example, thermoelectric transport in presence of an external magnetic field [98, 156, 157] or cyclic heat engines driven in a time-asymmetric manner [158, 159]. Notably, a plethora of studies [156, 160–162] had been devoted towards understanding the performance of thermal machines under such situations with the possibility of achieving the Carnot bound with finite power output [162]. But in the context of thermoelectric setup, a universal tighter bound on the Onsager coefficients is provided which has ruled out the possibility of achieving finite output power at the Carnot efficiency [160]. We here provide a deep deep understanding of such bounds in the context of fluctuations.

The plan of this chapter is as follows: In section 3.2 we investigate a general class of machines in the absence of time-reversal symmetry and provide universal bounds on fluctuations. In section 3.3 we now make the connection of these universal bounds with the so-called *generalized* thermodynamic uncertainty relations (GTUR), derived for time-reversal symmetry-broken systems [96]. In section 3.4 we discuss these bounds for individual time-forward and time-reversed processes in the different operational regimes. In section 3.5 we illustrate our findings using a steady-state three-terminal quantum thermoelectric setup in presence of an external magnetic field. Finally we summarize our main findings in section 3.6.

3.2 Universal bounds in absence of time-reversal symmetry

We once again consider a steady-state thermal device, operating in the linear response regime, but now in absence of the time-reversal symmetry. This implies that the Onsager symmetry $\mathcal{L}_{12} = \mathcal{L}_{21}$ is not respected, which was crucial for establishing the results of the previous chapter. In general, for time-reversal symmetry broken (TRB) systems one can always associate a time-forward (F) and a corresponding time-reversed (R) process. As an example, in case of a continuous steady-state transport setup, a time-reversed process is simply realized by reversing the direction of the external magnetic field. We express the

currents in both F and the R processes as,

$$\begin{aligned}\langle I_i \rangle &= \sum_{j=1,2} \mathcal{L}_{ij} A_j \\ \langle \bar{I}_i \rangle &= \sum_{j=1,2} \bar{\mathcal{L}}_{ij} A_j\end{aligned}\quad (3.1)$$

where \mathcal{L}_{ij} and $\bar{\mathcal{L}}_{ij}$ are the kinetic coefficients for the F and R processes, respectively. The Onsager reciprocity relation for TRB systems is given by the symmetry [147, 156, 162, 163]

$$\mathcal{L}_{ij} = \bar{\mathcal{L}}_{ji}. \quad (3.2)$$

Note that, here we have assumed the thermodynamic affinities A_1, A_2 to be time-reversal symmetric.

We follow a similar procedure as done in the previous chapter, but now consider the fluctuations of currents for both F and R processes. We define the squared relative uncertainty for individual current i that involves a combination of F and R processes as,

$$\epsilon_i^2 = \frac{\langle I_i^2 \rangle_c + \langle \bar{I}_i^2 \rangle_c}{(\langle I_i \rangle + \langle \bar{I}_i \rangle)^2}. \quad (3.3)$$

Then the ratio between the relative uncertainties of the two currents in the LR regime can be expressed solely in terms of the symmetric components of the Onsager coefficients of the F-process. We finally receive

$$\mathcal{Q} \equiv \frac{\epsilon_2^2}{\epsilon_1^2} = \frac{\mathcal{L}_{22}^S \sum_{ij} \mathcal{L}_{1i}^S \mathcal{L}_{1j}^S A_i A_j}{\mathcal{L}_{11}^S \sum_{ij} \mathcal{L}_{2i}^S \mathcal{L}_{2j}^S A_i A_j}. \quad (3.4)$$

To obtain this expression we exploit the symmetry relation in Eq. (3.2). Here \mathcal{L}^S is the symmetric part of the \mathcal{L} matrix. Also note that in the LR regime we substitute the current fluctuations by their corresponding kinetic coefficients i.e., $\langle I_i^2 \rangle_c = \langle \bar{I}_i^2 \rangle_c = 2 \mathcal{L}_{ii}^S$, which is the standard fluctuation-dissipation relation in equilibrium [19, 78]. One can further manipulate the above expression and re-write

$$\mathcal{Q} - 1 = \frac{4}{\mathcal{L}_{11}^S (\langle I_2 \rangle + \langle \bar{I}_2 \rangle)^2} \sum_{i,j=1}^2 \left[\mathcal{L}_{22}^S \mathcal{L}_{1i}^S \mathcal{L}_{1j}^S - \mathcal{L}_{11}^S \mathcal{L}_{2i}^S \mathcal{L}_{2j}^S \right] A_i A_j. \quad (3.5)$$

The above summation can be expanded and the finite contributions come only from $i = j$

term. As a result, we receive

$$Q - 1 = \frac{4}{\mathcal{L}_{11}^S (\langle I_2 \rangle + \langle \bar{I}_2 \rangle)^2} [\mathcal{L}_{11}^S A_1^2 - \mathcal{L}_{22}^S A_2^2] [\mathcal{L}_{11}^S \mathcal{L}_{22}^S - (\mathcal{L}_{12}^S)^2]. \quad (3.6)$$

Interestingly, the last term in the above expression is the determinant of the symmetric part of the Onsager's matrix which is always non-negative and directly follows from the positivity of entropy-production rate $\langle \sigma \rangle \geq 0$. So-far, the analysis has been general with no condition imposed on the direction of the currents flowing across the system. As before, to realise a useful operational regime such as an engine or a refrigerator or a pump, we need to identify the directions of input and output currents. To do this, from here onwards, we identify $\langle I_1 \rangle$ and $\langle I_2 \rangle$ as the input and the output currents in the F process and similarly $\langle \bar{I}_1 \rangle$ and $\langle \bar{I}_2 \rangle$ as the input and output currents in the R process. First focusing on the input current in the F (R) process, we demand that $\langle I_1 \rangle A_1 > 0$, ($\langle \bar{I}_1 \rangle A_1 > 0$), which in the LR regime generates a condition involving the affinities and the kinetic coefficients as $\mathcal{L}_{11} A_1^2 > -\mathcal{L}_{12} A_1 A_2$ ($\mathcal{L}_{11} A_1^2 > -\mathcal{L}_{21} A_1 A_2$). A combination of these two conditions now yields

$$\mathcal{L}_{11}^S A_1^2 > -\mathcal{L}_{12}^S A_1 A_2. \quad (3.7)$$

We next demand that in the operational regime, the setup delivers output in both the F and R processes and thus $\langle I_2 \rangle A_2 < 0$, ($\langle \bar{I}_2 \rangle A_2 < 0$) which translates to another condition in the LR regime,

$$-\mathcal{L}_{12}^S A_1 A_2 > \mathcal{L}_{22}^S A_2^2. \quad (3.8)$$

Combining Eqs. (3.7) and (3.8), we receive an important inequality

$$\mathcal{L}_{11}^S A_1^2 - \mathcal{L}_{22}^S A_2^2 > 0. \quad (3.9)$$

This is exactly one of the terms that appears in Eq. (3.6). As a result of this inequality and positivity of entropy production rate, we arrive at an important conclusion that for a generic out-of-equilibrium setup, operating as a useful device in both the F and the R processes, $Q \geq 1$.

Because of the strict inequality in Eq.(3.9), $Q = 1$ in Eq. (3.6) can only be reached when the determinant of the symmetric part of the Onsager's matrix vanishes. This corresponds

to a situation when $(\langle I_1 \rangle + \langle \bar{I}_1 \rangle) \propto (\langle I_2 \rangle + \langle \bar{I}_2 \rangle)$, which is a generalized version of the so-called tight-coupling limit as it involves both forward and reversed currents. For time-reversal symmetric systems this generalized tight coupling corresponds to the usual tight coupling limit i.e., $\langle I_1 \rangle \propto \langle I_2 \rangle$ [152]. Interestingly, $\langle I_1 \rangle \propto \langle I_2 \rangle$ can never be attained in the broken time reversal situation as it violates the standard second law of thermodynamics. This can be shown as follows,

In tight-coupling limit $\langle I_1 \rangle = \alpha \langle I_2 \rangle$, where α is a proportionality constant. This condition implies following relations among the Onsager's kinetic coefficients,

$$\mathcal{L}_{11} = \alpha \mathcal{L}_{21} \quad , \quad \mathcal{L}_{12} = \alpha \mathcal{L}_{22} \quad (3.10)$$

Given these relations determinant of the symmetric part of the Onsager's matrix (\mathcal{L}^s) reduces to,

$$\begin{aligned} \det[\mathcal{L}^s] &= \mathcal{L}_{11}\mathcal{L}_{22} - \frac{(\mathcal{L}_{12} + \mathcal{L}_{21})^2}{4} \\ &= \alpha \mathcal{L}_{21} \frac{\mathcal{L}_{12}}{\alpha} - \frac{(\mathcal{L}_{12} + \mathcal{L}_{21})^2}{4} \\ &= \frac{(4\mathcal{L}_{12}\mathcal{L}_{21} - \mathcal{L}_{12}^2 + \mathcal{L}_{21}^2 - 2\mathcal{L}_{12}\mathcal{L}_{21})}{4} \\ &= -\frac{(\mathcal{L}_{12} - \mathcal{L}_{21})^2}{4} \\ &\leq 0 \end{aligned} \quad (3.11)$$

where the equality is achieved only when $\mathcal{L}_{12} = \mathcal{L}_{21}$ which corresponds to a time-reversal symmetric situation. For broken time-reversal case, in general, this violates the standard second law of thermodynamics that always requires $\det[\mathcal{L}^s] \geq 0$. Hence tight coupling limit can never be achieved in broken time-reversal systems.

A few important outcomes follow immediately from the above derived central result $\mathcal{Q} \geq 1$. Just like in the case of time-reversal symmetric setup, $\eta^{(2)}$ gets lower bounded in terms of generalized efficiency defined as,

$$\langle \eta \rangle_G = \frac{|\langle I_2 \rangle + \langle \bar{I}_2 \rangle|}{|\langle I_1 \rangle + \langle \bar{I}_1 \rangle|} \quad (3.12)$$

which following $\mathcal{Q} \geq 1$ then gives a universal lower bound,

$$\eta^{(2)} = \bar{\eta}^{(2)} \geq \langle \eta \rangle_G^2. \quad (3.13)$$

Furthermore, for $\eta^{(2)}$ an universal upper bound also exists due to the inequality in Eq. (3.9), employing which we receive,

$$\eta^{(2)} = \bar{\eta}^{(2)} = \frac{\mathcal{L}_{22}^S}{\mathcal{L}_{11}^S} < \frac{A_1^2}{A_2^2}. \quad (3.14)$$

Interestingly, the same upper bound was received for continuous engines [152] in time reversal symmetric case. Our result therefore implies that the upper bound for $\eta^{(2)}$ is robust even in the absence of time-reversal symmetry [164]. Note that, in the context of thermal engines (ENG) with a working fluid operating between a hot and a cold reservoir with fixed temperatures T_h and T_c , respectively, Eq. (3.14) translates to

$$\eta_{\text{ENG}}^{(2)} = \bar{\eta}_{\text{ENG}}^{(2)} < \eta_C^2. \quad (3.15)$$

This result can be easily extended to other operational regimes like refrigerator or pump.

3.3 Connection with generalized thermodynamic uncertainty relation

Our central result, $\mathcal{Q} \geq 1$, provides a strong and deep connection with the recently obtained generalized thermodynamic uncertainty relation (GTUR) [96] for time-reversal broken systems. The GTUR in the LR regime provides a universal lower bound on the relative fluctuations ϵ_i^2 of individual currents in terms of the associated entropy production rate. The GTUR reads [96],

$$\left(\langle \sigma \rangle + \langle \bar{\sigma} \rangle \right) \epsilon_i^2 \geq 2, \quad i = 1, 2. \quad (3.16)$$

The proof of GTUR in the LR regime requires only the non-negativity condition of the symmetric part of the Onsager's matrix. Once again, the equality here corresponds to a generalized tight-coupling situation. In general, no obvious relation exists between the GTUR for different currents. However as shown in this work, in the operational regime, $\epsilon_2^2 \geq \epsilon_1^2$, immediately implies a strict hierarchy for the GTUR between the output and the

input currents,

$$\left(\langle\sigma\rangle+\langle\bar{\sigma}\rangle\right)\epsilon_2^2\geq\left(\langle\sigma\rangle+\langle\bar{\sigma}\rangle\right)\epsilon_1^2\geq 2. \quad (3.17)$$

Note that, in the LR regime the entropy production rate are the same for both F and R processes. Therefore the above expression further simplifies to,

$$\boxed{\langle\sigma\rangle\epsilon_2^2\geq\langle\sigma\rangle\epsilon_1^2\geq 1} \quad (3.18)$$

3.4 Bounds on relative fluctuations in forward and reversed processes

So far we have discussed the bounds only on the quantities that contain contribution from both forward and reversed processes. In this section we discuss the bounds on relative fluctuations in individual forward and reversed processes. Without any loss of generality, we first assume that $A_1, A_2 > 0$. Then from operational regime conditions of the machine, i.e., $\langle I_1 \rangle A_1 (\langle \bar{I}_1 \rangle A_1) > 0$ and $-\langle I_2 \rangle A_2 (-\langle \bar{I}_2 \rangle A_2) > 0$, one receives $\langle I_1 \rangle \langle \bar{I}_1 \rangle > 0$ and $\langle I_2 \rangle \langle \bar{I}_2 \rangle < 0$. Let us now consider a situation where $\langle \eta \rangle < \langle \bar{\eta} \rangle$, i.e., the mean thermodynamic efficiency of the forward process is smaller than the mean thermodynamic efficiency of the reversed process. This leads to the following inequality

$$\frac{\langle \bar{I}_2 \rangle}{\langle I_2 \rangle} > \frac{\langle \bar{I}_1 \rangle}{\langle I_1 \rangle}. \quad (3.19)$$

We have shown that whenever a setup works as a thermal machine in both forward and reversed processes, $\mathcal{Q} > 1$ (defined in Eq. (3)). This means that the generalized relative output fluctuation is always greater than the generalized input fluctuation in the operational regime. As a result we receive the following pair of relations:

$$\begin{aligned} \frac{\langle\langle I_2^2 \rangle\rangle}{\langle I_2 \rangle^2} &> z \frac{\langle\langle I_1^2 \rangle\rangle}{\langle I_1 \rangle^2} \\ \frac{\langle\langle \bar{I}_2^2 \rangle\rangle}{\langle \bar{I}_2 \rangle^2} &> \bar{z} \frac{\langle\langle \bar{I}_1^2 \rangle\rangle}{\langle \bar{I}_1 \rangle^2} \end{aligned} \quad (3.20)$$

where z and \bar{z} are given as

$$z = \left(\frac{1+x}{1+y} \right)^2, \quad (3.21)$$

$$\bar{z} = \left(\frac{1+1/x}{1+1/y} \right)^2, \quad (3.22)$$

and $x = \frac{\langle \bar{I}_2 \rangle}{\langle I_2 \rangle}$, $y = \frac{\langle \bar{I}_1 \rangle}{\langle I_1 \rangle}$. Note that, $x > 0$ and $y > 0$ as we are in the useful operational regime in both forward and reversed processes. Moreover, as we have assumed $\langle \eta \rangle < \langle \bar{\eta} \rangle$, we always have $x > y$ following Eq. (3.19). Thus interestingly, if $\langle \eta \rangle < \langle \bar{\eta} \rangle$, we always receive $z > 1$ and $\bar{z} < 1$. This leads to an important conclusion that, if the forward process is less efficient than the corresponding reversed process, then in the forward process, relative output fluctuation is always going to be larger than the relative input fluctuation. This also means that all the bounds obtained for time-reversal symmetric case will hold true for the forward process. In other words, for the forward process, we will receive $\langle \eta \rangle^2 \leq \eta^{(2)} \leq \eta_C^2$. However, for the corresponding reversed process there exist regimes where relative input fluctuation may surpass relative output fluctuations, and as a result the lower bounds for $\eta^{(2)}$ may not be fulfilled. The upper bound, however, remains intact. Our result therefore implies that the bounds exactly like the time-reversal symmetric case will hold true for at least one of the processes. Eqs. (3.13), (3.14), (3.17), and (3.20) are the other central results of this paper. We would like to stress that the results obtained here are universal in the LR regime and valid for both classical and quantum systems. In what follows, we illustrate these results for an autonomous steady-state quantum dot setup where time-reversal symmetry is broken via an external magnetic field.

3.5 Example: Quantum thermoelectric transport in a three-dot setup in the presence of an external magnetic field

As an illustration of our findings, we consider a mesoscopic triple quantum dot (QD) thermoelectric setup which is arranged in a triangular geometry and is additionally subjected to an Aharonov-Bohm magnetic flux Φ (Fig. 3.1). Each dot is further in contact with its own thermochemical reservoir which is maintained in equilibrium at a fixed temperature T_i and a chemical potential μ_i , where $i = 1, 2, 3$ corresponds to left, right, and probe terminals,

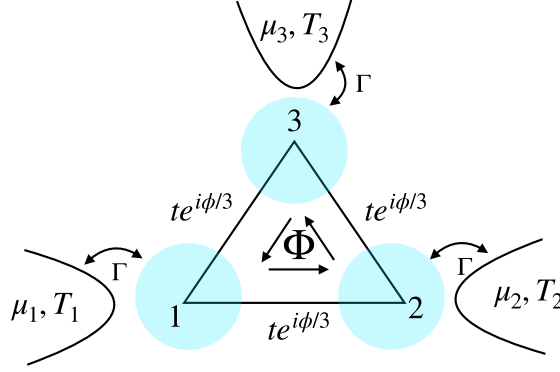


Figure 3.1: Schematic of a thermoelectric setup consisting of three quantum dots with each dot further in contact with its own thermochemical bath. The third bath acts as a Büttiker probe whose temperature T_3 and chemical potential μ_3 are fixed by imposing zero net heat and particle currents from the probe. Figure reproduced with permission from Ref. [165].

respectively. The Hamiltonian of this entire setup is given by,

$$H = H_d + H_b + H_{tun} \quad (3.23)$$

where

$$H_d = \sum_{i=1}^3 \epsilon_i c_i^\dagger c_i + te^{i\phi/3} (c_2^\dagger c_1 + c_3^\dagger c_2 + c_1^\dagger c_3) + \text{h.c.}, \quad (3.24)$$

is the Hamiltonian for the three QD's. Here $c_i (c_i^\dagger)$ is the electronic annihilation (creation) operator for the i -th dot, ϵ_i is the onsite energy, t is the hopping parameter between the dots and $\phi = 2\pi\Phi/\Phi_0$ is the phase picked up by the electron by moving around the loop once with Φ being the magnetic flux penetrating the setup and $\Phi_0 = hc/e$ is the flux quantum. The baths are modeled as non-interacting free electron gas with Hamiltonian given by,

$$H_b = \sum_{ik} \epsilon_{ik} b_{ik}^\dagger b_{ik}, \quad (3.25)$$

and

$$H_{tun} = \sum_{ik} V_{ik} c_i^\dagger b_{ik} + \text{h.c.}, \quad (3.26)$$

describes the tunneling of electrons between the dots and the baths. The coupling strength between the baths and the dots is characterized by $\Gamma = \sum_k |V_{ik}|^2 \delta(\epsilon - \epsilon_k)$ which is assumed to be identical and energy independent for all the three baths.

Given the fully non-interacting nature of the setup, the transport properties can be analytically calculated following the standard Landauer-Büttiker formalism [160, 161]. We are interested here to realize a thermoelectric engine that absorbs heat current (input) from the hot bath and push the electrons against the chemical bias and thereby generating electric current (output). We set $T_1 > T_2$ and $\mu_2 > \mu_1$ and fix T_3 and μ_3 for the third bath by demanding that the net charge and heat currents flowing out of this bath is zero. The third bath therefore acts as a Büttiker probe that allows to simulate elastic and inelastic scattering processes within the central QD system [166, 167]. As a result of this probe condition, it is sufficient for our analysis to consider currents flowing out either of the left or the right bath. We consider the right bath as reference and define the affinities for heat current $A_q = 1/T_2 - 1/T_1 > 0$ and particle current $A_c = (\mu_1 - \mu_2)/T_2 < 0$ and write the current flowing out of left bath as $\langle I_\alpha \rangle = \sum_{\beta=c,q} \mathcal{L}_{\alpha\beta} A_\beta$, $\alpha = (c, q)$ for the F process. Analogous expression for the R process is obtained by reversing the phase $\phi \rightarrow -\phi$ in the dot Hamiltonian H_d . The presence of the magnetic field and the Büttiker probe ensures $\mathcal{L}_{cq}(\phi) \neq \mathcal{L}_{qc}(\phi)$, in general. It can be easily checked numerically that the Onsager-Casimir relation remains intact i.e., $\mathcal{L}_{cq}(\phi) = \mathcal{L}_{qc}(-\phi)$, as expected.

In Fig. (3.2(a)) we display the forward ($\langle I_q \rangle, \langle I_c \rangle$) and the reversed currents ($\langle \bar{I}_q \rangle, \langle \bar{I}_c \rangle$) as a function of ϕ , fulfilling the engine condition ($\langle I_q \rangle \geq 0, \langle I_c \rangle \geq 0$) in F and ($\langle \bar{I}_q \rangle \geq 0, \langle \bar{I}_c \rangle \geq 0$) R processes. Fig. (3.2(b)) shows the validity of one of our central results (Eq. (3.17)) with GTUR product $\left((\langle \sigma \rangle + \langle \bar{\sigma} \rangle) \epsilon_c^2 \right)$ for the output charge current is always larger than the corresponding GTUR product of the input heat current $\left((\langle \sigma \rangle + \langle \bar{\sigma} \rangle) \epsilon_q^2 \right)$ from the hot bath in the engine regime. The inset displays the off-diagonal Onsager coefficients, indicating the broken time-reversal symmetry due to the presence of magnetic field and the Büttiker probe. In Fig. (3.2(c)) we show the validity of the universal upper bound for $\eta_{\text{ENG}}^{(2)} \equiv \frac{\langle I_w^2 \rangle_c}{\langle I_q^2 \rangle_c} < \eta_C^2$ by choosing the parameters of the model randomly (please see Fig. (3.2) caption for more details). For the thermoelectric setup, nth cumulant of work is identified as $\langle I_w^n \rangle_c = (\mu_2 - \mu_1)^n \langle I_c^n \rangle_c$.

This setup can also work as refrigerator provided by extracting heat current from the cold bath (output) by investing the work current. Since we have set $T_1 > T_2$ and $\mu_2 > \mu_1$, the refrigeration condition demands that ($\langle I_q^{(2)} \rangle \geq 0, \langle I_c^{(2)} \rangle \geq 0$) in F and ($\langle \bar{I}_q^{(2)} \rangle \geq 0,$

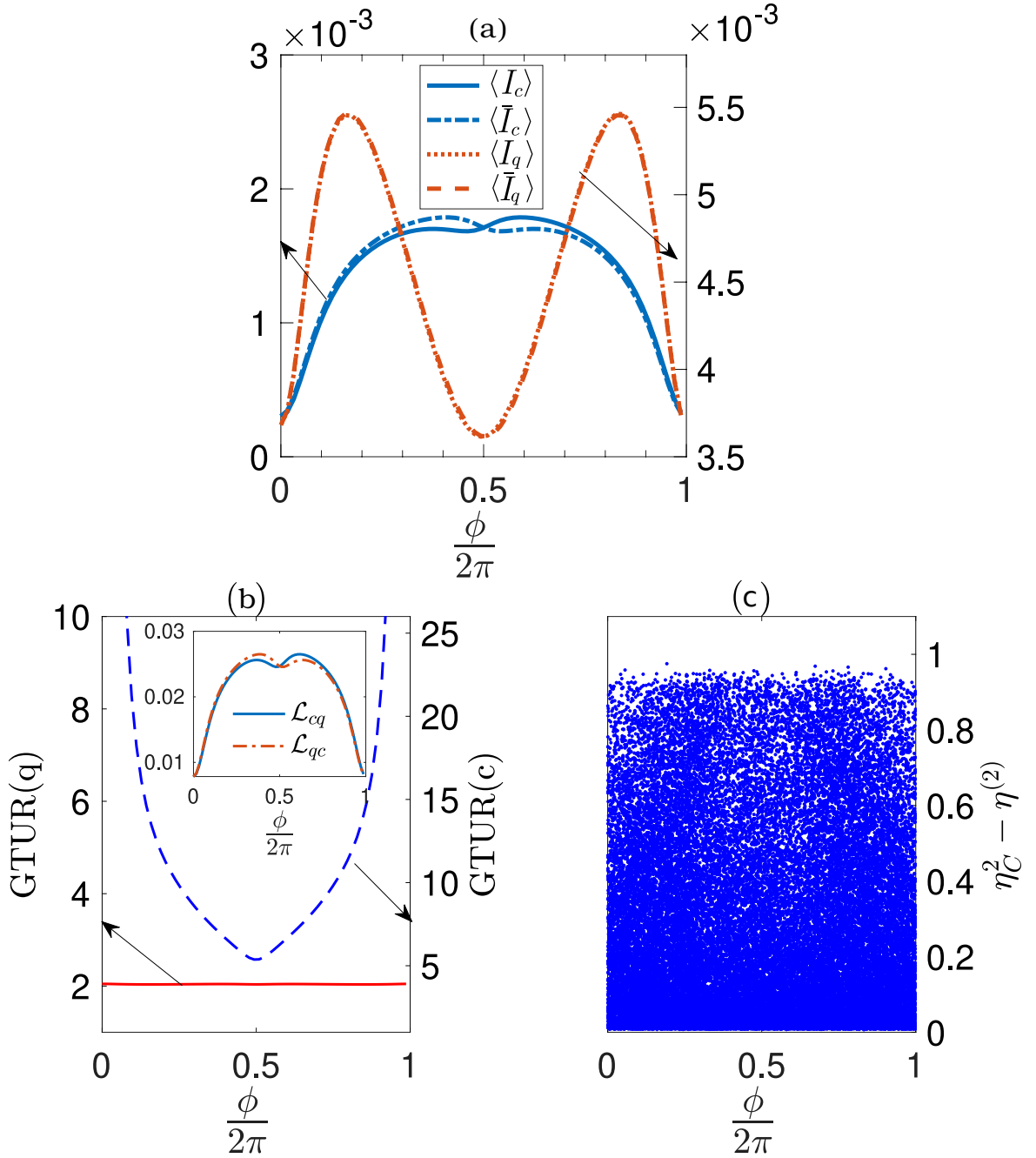


Figure 3.2: (a) Plot for steady-state heat and charge currents flowing out of the left bath in F ($(\langle I_q \rangle, \langle I_c \rangle)$) and R ($(\langle \bar{I}_q \rangle, \langle \bar{I}_c \rangle)$) processes, as a function of the phase ϕ . As per our convention and with the bias settings $T_1 > T_2$ and $\mu_2 > \mu_1$, the setup works as a thermoelectric engine in both F and R processes when $\langle I_q \rangle, \langle I_c \rangle, \langle \bar{I}_q \rangle, \langle \bar{I}_c \rangle > 0$. (b) The generalized TUR (GTUR) ratio for input heat current from the left (hot) bath and the output charge current. The inset in (c) shows the off-diagonal elements of the Onsager matrix as a function of the phase ϕ . (c) A scatter plot showing the validity of the upper bound for $\eta^{(2)}$. We display $\eta_C^2 - \eta^{(2)}$ as a function of ϕ over 50000 sample points chosen randomly. For figures (b) and (c) the parameters are chosen as $\epsilon_1 = 2.0, \epsilon_2 = 1.3, \epsilon_3 = 0.9, t = -1$ and $\Gamma = 0.5, T_1 = 1.1, T_2 = 1, \mu_1 = -0.01, \mu_2 = 0.01$. For the plot (d), $\epsilon_1, \epsilon_2,$ and ϵ_3, Γ, T_2 are chosen randomly in the interval between $[0, 1], t$ is chosen between $[-1, 0], \mu_1$ is chosen from $[-0.01, 0]$ and μ_2 is chosen from $[0, 0.01]$. Figure reproduced with permission from Ref.[165].

$\langle \bar{I}_c^{(2)} \rangle \geq 0$) R processes, where the superscript 2 refers to current flowing out of the second terminal. In Fig. 3.3(a) we show that the GTUR ratio for extracted heat current from the cold bath (output) is always larger than the corresponding GTUR product of the input work current in the refrigerator regime. Note that, in the linear response regime, as $\langle I_q^{(2)} \rangle = -\langle I_q^{(1)} \rangle$, the GTUR product for both these currents are the same. In Fig. 3.3(b) we show the validity of the universal upper bound for $\eta_{\text{REF}}^{(2)} \equiv \frac{\langle I_q^{(2)} \rangle_c}{\langle I_w^{(2)} \rangle_c} < (1 - \eta_C)^2 / \eta_C^2$ by choosing the parameters of the model randomly (please see Fig. 3.3 caption for more details).

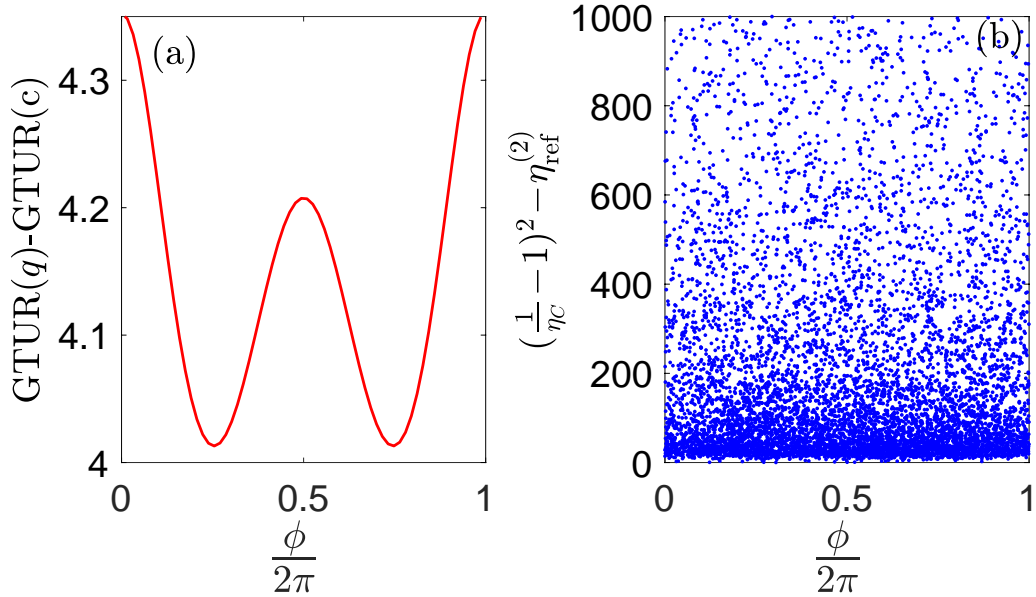


Figure 3.3: (Color online): (a) The difference between the generalized TUR (GTUR) for extracted cold current from the cold (right) bath and the input charge current in the refrigerator regime. (b) A scatter plot showing the validity of the upper bound for $\eta_{\text{REF}}^{(2)}$. We display $(1 - \eta_C^2) / \eta_C^2 - \eta_{\text{REF}}^{(2)}$ as a function of ϕ over 20000 sample points chosen randomly. For figure (a) the parameters are $\epsilon_1 = 4.0$, $\epsilon_2 = 1$, $\epsilon_3 = 4.8$, $t = 0.7$ and $\Gamma = 3.6$, $T_1 = 1.01$, $T_2 = 1$, $\mu_1 = -0.1$, $\mu_2 = 0.1$. For figure (b) ϵ_1 , ϵ_2 , and ϵ_3 , Γ are chosen randomly in the interval between $[0, 1]$, t is chosen between $[-1, 0]$, μ_1 is chosen from $[-0.2, 0]$ and μ_2 is chosen from $[0, 0.2]$, T_1 is chosen between $[1, 1.1]$ and T_2 is chosen between $[0.9, 1]$. For better presentation, we set the y axis to 1000. Figure reproduced with permission from Ref.[165].

3.6 Summary

In this chapter we have generalised the study of previous chapter on universal bounds on fluctuations for machines in a significant way by incorporating time-reversal symmetry breaking situation. We show that even in this general situation non-trivial universal upper and lower bounds for $\eta^{(2)}$ exist whenever a setup operates as a useful machine both in the

forward and the reversed processes. However in order to receive such bounds the relative fluctuations of the sum of forward and reversed currents must be taken into account. As a consequence of the lower bound ($Q \geq 1$), we further able to establish the hierarchy in the GTUR bounds between the output and input current. $Q \geq 1$ also provides physically relevant bounds on individual forward and backward processes. As a consequence of this, we also show that the bounds exactly like the time-reversal symmetric case will hold true for at least one of the processes. We again emphasize that the results obtained here are universal and do not depend on the details of the underlying dynamics and the nature of the working medium (classical or quantum).

CHAPTER 4

Bounds on fluctuations for finite-time quantum Otto cycle

Abstract

For quantum Otto engine driven quasistatically, we provide exact full statistics of heat and work for a class of working fluids that follow a scale-invariant energy eigenspectra. Equipped with the full joint statistics we go on to derive a universal expression for the ratio of n th cumulant of output work and input heat in terms of the mean Otto efficiency. Furthermore, for nonadiabatic driving of quantum Otto engine with working fluid consisting of either (i) a qubit or (ii) a harmonic oscillator, we show that the relative fluctuation of output work is always greater than the corresponding relative fluctuation of input heat absorbed from the hot bath. As a result, the ratio between the work fluctuation and the input heat fluctuation receives a lower bound in terms of the square value of the average efficiency of the engine. The saturation of the lower bound is received in the quasistatic limit of the engine.

Reported in

S. Saryal and B. K. Agarwalla , *Bounds on fluctuations for finite-time quantum Otto cycle*, [Phys. Rev. E \(Letter\)](#), 103, L060103 (2021).

4.1 Introduction

In the previous two chapters we uncovered universal bounds for continuous steady-state thermal machines. It is natural to ask what happens to these bounds for finite-time discrete machines such as, Otto cycles, Carnot cycle etc.? In this chapter we will answer this question for a paradigmatic example of discrete thermal machine, finite-time quantum Otto cycle. Otto cycle was first proposed in 19th century by a German inventor Nikolaus Otto as a internal combustion four stroke engine. Even today almost all of the automobile makers use Otto cycle to make their engines, also famously known as *gasoline engines*. With the

great advancement in miniaturization technology, Otto engine is realized recently in a couple of experiments with aid of NV centers [13], NMR setup [14] and trapped ion technique [11]. Hence quantum-mechanical treatment becomes inevitable for these systems. In this chapter we will examine the quantum analog of Otto engine and obtain universal bounds on fluctuations for a large class of working medium.

We first introduce the quantum Otto cycle along with the projective measurement scheme that allows us to construct the probability distribution function to study fluctuations in section 4.2. We follow a similar scheme, as proposed in Ref. [168], to construct the joint probability distribution of heat and work in section 4.3. However, in our work, we will be primarily focusing on the higher order statistics/cumulants of heat and work instead of the stochastic efficiency which was the main focus of Ref. [168]. In section 4.4 for the quasi-static driving case, we derive a general joint cumulant generating function of heat and work for scale-invariant driven Hamiltonian and show that the ratio of n th cumulant of output work and n th cumulant of input heat is exactly equal to the n th power of the average efficiency and consequently upper bounded by the n th power of the Carnot efficiency. Then we provide two paradigmatic examples [a two-level system (TLS) and a harmonic oscillator (HO)] of non-adiabatic driving of the quantum Otto cycle and show that relative fluctuations of work are always lower bounded by relative fluctuations of heat whenever the Otto cycle works as engine in section 4.5. In section 4.6 we point out the consequence of our results on thermodynamic uncertainty relations for finite-time thermal machines [71]. Finally we summarize our central results in section 4.7.

4.2 Quantum Otto Cycle

We consider a standard four-stroke quantum Otto cycle, as illustrated in Fig. (4.1). The working fluid is initially ($t = 0$) thermalized by placing it in a weak contact with a cold reservoir at inverse temperature $\beta_c = 1/T_c$ (k_B is set to unity). The fluid is then separated from the bath and is subjected to four strokes.

1. Unitary expansion Stroke ($A \rightarrow B$) – In this stroke, the working fluid expands unitarily under a time-dependent driving that takes the initial hamiltonian H_0 to a final hamiltonian H_τ in a time duration τ . The working fluid, in this step, consumes an amount of work

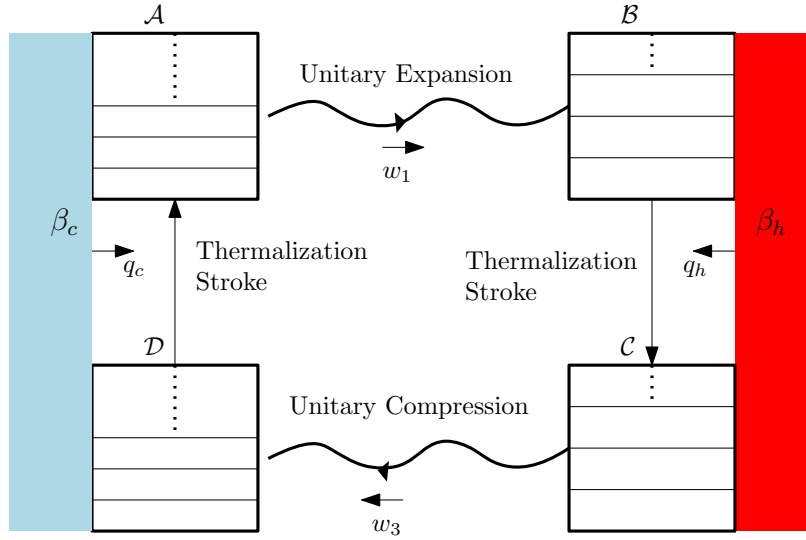


Figure 4.1: (Color online): Schematic of a four-stroke Quantum Otto cycle consisting of two unitary and two thermalization strokes. As per our convention, energy flowing towards the working fluid is considered as positive. The cycle operates as a heat engine when the net work $\langle w \rangle = \langle w_1 \rangle + \langle w_3 \rangle < 0$ and the input heat $\langle q_h \rangle > 0$. In a similar fashion, it is possible to realize a refrigerator. Figure reproduced with permission from Ref. [128].

w_1 which is not a fixed number but rather a stochastic quantity due to the random thermal initial condition and possible quantum fluctuations during the unitary evolution.

2. Isochoric heating stroke ($B \rightarrow C$)– During this step, the working medium is put in weak contact with a hot bath at inverse temperature β_h to achieve full thermalization. The Hamiltonian for the working fluid therefore remains the same while the fluid absorbs an amount of heat q_h . Here, we assume that the interaction time with the bath is long enough to achieve equilibration.

3. Unitary compression Stroke ($C \rightarrow D$) – In the next stroke, the system is detached from the hot bath and unitarily compressed via driving the working fluid back to the initial Hamiltonian H_0 starting from H_τ while the fluid consuming an amount of work w_3 . For simplicity, we assume that the time duration for this stroke is the same as the expansion stroke.

4. Isochoric cooling Stroke ($D \rightarrow A$) – In the final stroke, the fluid is put in contact with a cold bath at inverse temperature β_c to reach equilibrium and thereby closing the cycle.

It is important to note that, as per our convention (see Fig. (4.1)), energy flowing into the fluid is always considered to be positive. From here onwards, we denote $w = w_1 + w_3$ as the net work performed on the working fluid.

4.3 Joint probability distribution for input heat and output work in quantum Otto engine

In the quantum regime, a thermodynamically consistent way of studying fluctuations for non-equilibrium systems is via the two-point projective measurement scheme [50, 51]. Such a measurement scheme is also consistent with the fluctuation relations [51, 57]. This measurement scheme assigns energy change of the system due to a process, like unitary stroke or isochore stroke, to the difference in the energy eigenvalues measured at the start and end of the process. Very recently, following this scheme, an expression for efficiency statistics for Otto cycle with arbitrary working fluid was obtained [168]. We follow a similar procedure here and as in this work we are interested only in the heat engine regime, we construct the joint probability distribution $p(w_1, q_h, w_3)$ by performing projective measurement of the respective Hamiltonian involved in the first three strokes ($A \rightarrow B \rightarrow C \rightarrow D$). Formal expression of $p(w_1, q_h, w_3)$ can be easily obtained as follows. From elementary probability theory one can write $p(w_1, q_h, w_3)$ as

$$p(w_1, q_h, w_3) = p(w_3|q_h, w_1)p(q_h|w_1)p(w_1), \quad (4.1)$$

where $p(a|b)$ is the conditional probability distribution of event a provided b has happened. Following two-point projective measurement scheme probability distribution of work during unitary expansion stroke ($A \rightarrow B$) is given by,

$$p(w_1) = \sum_{nm} \delta(w_1 - (\epsilon_n^\tau - \epsilon_n^0)) T_{n \rightarrow m}^{\text{exp}} \frac{e^{-\beta_c \epsilon_n^0}}{\mathcal{Z}_0}, \quad (4.2)$$

where ϵ_n^0 (ϵ_n^τ) are the energy eigenvalues of initial (final) hamiltonian during the unitary expansion stroke $A \rightarrow B$. Here $\mathcal{Z}_0 = \sum_n \exp(-\beta_c \epsilon_n^0)$ is the partition function corresponding to initial Hamiltonian at inverse temperature β_c . $T_{n \rightarrow m}^{\text{exp}} = |\langle m_\tau | U_{\text{exp}} | n_0 \rangle|^2$ is the transition probability between the final and initial eigenstates during the unitary expansion stroke.

In the same way, conditional probability distribution that during the isochoric heating stroke ($B \rightarrow C$) q_h amount of heat is absorbed from hot bath provided w_1 amount of work

has been during unitary expansion stroke is given by,

$$p(q_h|w_1) = \sum_k \delta\left(q_h - (\epsilon_k^\tau - \epsilon_m^\tau)\right) \frac{e^{-\beta_h \epsilon_k^\tau}}{\mathcal{Z}_\tau}, \quad (4.3)$$

where $\mathcal{Z}_\tau = \sum_n \exp(-\beta_h \epsilon_n^\tau)$ is the partition function corresponding to final hamiltonian at inverse temperature β_h . Similarly, conditional probability distribution that during the unitary compression stroke ($C \rightarrow D$) w_3 amount of work is done provided, q_h amount of heat has been drawn from the hot reservoir during isochoric heating stroke and w_1 amount of work has been done during unitary expansion stroke, is given by

$$p(w_3|q_h, w_1) = \sum_l \delta\left(w_3 - (\epsilon_l^0 - \epsilon_k^\tau)\right) T_{k \rightarrow l}^{\text{com}}, \quad (4.4)$$

where $T_{k \rightarrow l}^{\text{com}} = |\langle l_0 | U_{\text{com}} | k_\tau \rangle|^2$ is the transition probability between the final and initial eigenstates during the unitary compression stroke. As a result the joint probability distribution for q_h , w_1 , and q_3 in a Otto cycle is given by,

$$\begin{aligned} p(w_1, q_h, w_3) &= \sum_{nmkl} \delta\left(w_1 - (\epsilon_m^\tau - \epsilon_n^0)\right) \delta\left(q_h - (\epsilon_k^\tau - \epsilon_m^\tau)\right) \\ &\times \delta\left(w_3 - (\epsilon_l^0 - \epsilon_k^\tau)\right) T_{n \rightarrow m}^\tau T_{k \rightarrow l}^\tau \frac{e^{-\beta_c \epsilon_n^0}}{\mathcal{Z}_0} \frac{e^{-\beta_h \epsilon_k^\tau}}{\mathcal{Z}_\tau}. \end{aligned} \quad (4.5)$$

From the above distribution function, the joint distribution for net work $w = w_1 + w_3$ and input heat q_2 can also be obtained easily. As mentioned before, we focus in the engine regime, (i.e., as per our convention, $\langle w \rangle < 0$ and $\langle q_2 \rangle > 0$) and correspondingly investigate the bound for the ratio for the output work fluctuation to the input heat fluctuation by defining our central quantity

$$\eta^{(2)} = \frac{\langle w^2 \rangle_c}{\langle q_2^2 \rangle_c}. \quad (4.6)$$

In what follows, we first present universal result for $\eta^{(2)}$ for quasi-static Otto cycle with working fluid satisfying scaling relation and then extend our study to the non-adiabatic regime for two paradigmatic models, consisting of (i) a two-level system and (ii) a harmonic oscillator.

4.4 Quasistatic limit

Before discussing the most-general situation, we first focus on the quasi-static (QS) driving limit for the unitary strokes for an Otto cycle. In this limit, one receives universal results for $\eta^{(2)}$. As per the *quantum adiabatic theorem* in the slow-driving limit, the occupation probabilities between the instantaneous energy eigenstates do not change with time which imply for transition probabilities $p_{n \rightarrow m} = \delta_{nm}$ and $p_{k \rightarrow l} = \delta_{kl}$. As a result, following Eq. (4.5) the joint distribution of input heat (q_h) and the net work $w = w_1 + w_3$ simplifies to,

$$p(w, q_h) = \sum_{n,k} \delta(w - [(\epsilon_n^\tau - \epsilon_n^0) + (\epsilon_k^0 - \epsilon_k^\tau)]) \times \delta(q_h - (\epsilon_k^\tau - \epsilon_n^\tau)) \frac{e^{-\beta_c \epsilon_n^0} e^{-\beta_h \epsilon_k^\tau}}{\mathcal{Z}_0 \mathcal{Z}_\tau}. \quad (4.7)$$

Instead of looking at most general eigen-spectra for the driving Hamiltonians, we consider a scale-invariant energy eigen-spectra, which appears in many classes of single particle, non-linear and many-body systems [169–173], given as $\epsilon_n^\tau = \frac{\epsilon_n^0}{\lambda_\tau^2}$ where λ_τ is the scaling factor. In this limit, the corresponding characteristic function $\chi(\alpha_1, \alpha_2)$ where α_1 and α_2 are the counting parameters for w and q_h is given as

$$\chi(\alpha_1, \alpha_2) = \sum_{n,k} e^{i(\epsilon_n^0 - \epsilon_k^0) \left[\frac{1}{\lambda_\tau^2} (\alpha_1 - \alpha_2) - \alpha_1 \right]} \frac{e^{-\beta_c \epsilon_n^0} e^{-\beta_h \epsilon_k^\tau}}{\mathcal{Z}_0 \mathcal{Z}_\tau}. \quad (4.8)$$

A relation between work and heat cumulants immediately follows from it,

$$\langle w^n \rangle_c = (-1)^n (1 - \lambda_\tau^2)^n \langle q_h^n \rangle_c. \quad (4.9)$$

Consequently the n -th order ratio for work and heat fluctuation is given as,

$$\boxed{\eta_{QS}^n = (-1)^n \frac{\langle w^n \rangle_c}{\langle q_h^n \rangle_c} = (1 - \lambda_\tau^2)^n = \langle \eta \rangle^n < \eta_C^n}, \quad (4.10)$$

where $\langle \eta \rangle = -\langle w \rangle / \langle q_h \rangle$ is the standard thermodynamic efficiency which for an Otto engine in the QS limit reduces to $\langle \eta \rangle_{QS} = (1 - \lambda_\tau^2)$. Note that the upper bound can be simply obtained by demanding the positivity of the net entropy production for the Otto cycle. This is

the first central result of this chapter. One can see that similar to continuous engine, we obtained the upper bound on $\langle \eta \rangle$, given by square of Carnot efficiency, while the lower bound is saturated in QS limit. We note that a similar result was obtained for central moments instead of cumulants in Ref. [143] for a classical four stroke engine operating in quasistatic strokes. Interestingly, the results in Eq. (4.9) also hold true for the central moments.

4.5 Beyond quasistatic limit

Beyond the QS limit, it is non-trivial to derive universal bound for arbitrary working fluid. We therefore focus on two paradigmatic models systems to understand the non-adiabatic limit. We consider the working fluid for Otto-engine consisting of i) a two-level system (qubit), and (ii) a simple harmonic oscillator. Interestingly, a TLS as a working fluid was recently implemented and studied from the perspective of an Otto heat engine [14].

4.5.1 Working fluid consisting of a qubit

We first consider a two-level system (TLS) with Hamiltonian evolving unitarily from $H_A = \frac{1}{2}\omega_0\sigma_x$ to $H_B = \frac{1}{2}\omega_\tau\sigma_y$ during the expansion ($A \rightarrow B$) stroke and back to H_A during the compression stroke ($B \rightarrow A$). For the compression stroke we consider here the reverse protocol of the expansion stroke. Here $\sigma_{x,y,z}$ are the standard Pauli matrices, ω_0, τ denote the angular frequencies with $\omega_\tau > \omega_0$ corresponding to the energy gap expansion. The evolution of the density operator during unitary strokes is governed by a unitary operator U which in this case can be arbitrary. For this system we can exactly obtain the the joint characteristic function (CF) for the net work w and q_h , given by [174]

$$\begin{aligned}
\chi_{\text{TLS}}(\alpha_1, \alpha_2) &= \int_{-\infty}^{\infty} \int_{-\infty}^{\infty} dw dq_2 e^{i\alpha_1 w} e^{i\alpha_2 q_2} p(w, q_2) \\
&= \frac{1}{\mathcal{Z}_0 \mathcal{Z}_\tau} \left[2u^2 \cosh(x_0 + x_\tau) + 2v^2 \cosh(x_0 - x_\tau) \right. \\
&\quad + 2uv \cosh(x_\tau) (e^{-2i\alpha_1 y_0} e^{-x_0} + e^{2i\alpha_1 y_0} e^{x_0}) \\
&\quad + u^2 (e^{-x_0 + x_\tau} e^{-2i\alpha_1(y_0 - y_\tau)} e^{-2i\alpha_2 y_\tau} + e^{x_0 - x_\tau} e^{2i\alpha_1(y_0 - y_\tau)} e^{2i\alpha_2 y_\tau}) \\
&\quad + v^2 (e^{-x_0 - x_\tau} e^{-2i\alpha_1(y_0 + y_\tau)} e^{2i\alpha_2 y_\tau} + e^{x_0 + x_\tau} e^{2i\alpha_1(y_0 + y_\tau)} e^{-2i\alpha_2 y_\tau}) \\
&\quad \left. + 2uv \cosh(x_0) (e^{2i(\alpha_1 - \alpha_2)y_\tau} e^{x_\tau} + e^{-2i(\alpha_1 - \alpha_2)y_\tau} e^{-x_\tau}) \right], \quad (4.11)
\end{aligned}$$

where α_1 and α_2 are the counting parameters for $w = w_1 + w_3$ and q_h , respectively. Also, we denote $x_0 = \beta_c \omega_0$, $x_\tau = \beta_h \omega_\tau$, and $v = 1 - u$. All the moments can be obtained from the CF by taking partial derivatives with respect to α_1, α_2 i.e.,

$$\langle w^n q_h^m \rangle = \frac{\partial^n \partial^m}{\partial (i\alpha_1)^n \partial (i\alpha_2)^m} \chi_{\text{TLS}}(\alpha_1, \alpha_2) \Big|_{\alpha_1 = \alpha_2 = 0}. \quad (4.12)$$

Therefore, the first and second order cumulants of heat and work given by

$$\begin{aligned} \langle w \rangle &\equiv \langle w_1 \rangle + \langle w_3 \rangle = \left[\frac{\omega_0}{2} + \frac{\omega_\tau}{2}(1-2u) \right] \tanh\left(\frac{\beta_c \omega_0}{2}\right) + \left[\frac{\omega_\tau}{2} + \frac{\omega_0}{2}(1-2u) \right] \tanh\left(\frac{\beta_h \omega_\tau}{2}\right), \\ \langle q_h \rangle &= -\frac{\omega_\tau}{2} \left[\tanh\left(\frac{\beta_h \omega_\tau}{2}\right) + \tanh\left(\frac{\beta_c \omega_0}{2}\right)(1-2u) \right], \\ \langle w^2 \rangle_c &= \frac{1}{2}(\omega_\tau + \omega_0)^2 - 2u\omega_\tau\omega_0 - \langle w_1 \rangle^2 - \langle w_3 \rangle^2, \\ \langle q_h^2 \rangle_c &= \frac{\omega_\tau^2}{4} \left[2 - \tanh^2\left(\frac{\beta_h \omega_\tau}{2}\right) - (1-2u)^2 \tanh^2\left(\frac{\beta_c \omega_0}{2}\right) \right], \end{aligned} \quad (4.13)$$

where u represents the probability of no transition between the final and the initial states during the unitary strokes. The quasi-static (QS) limit therefore corresponds to $u = 1$. It is easy to check from the above expressions that, in the QS limit, one receives $\eta^{(2)} = \langle \eta \rangle^2 = (1 - \omega_0/\omega_\tau)^2$ matching with the result obtained in the previous section.

Beyond the QS limit, we now provide a rigorous proof that while working as a heat engine i.e., $\langle w \rangle < 0$ and $\langle q_h \rangle > 0$, the following quantity

$$\mathcal{A} = \langle w^2 \rangle_c \langle q_h \rangle^2 - \langle q_h^2 \rangle_c \langle w \rangle^2 \quad (4.14)$$

is always non-negative and the equality sign is achieved in the quasi-static limit $u = 1$.

\mathcal{A} can be simplified as follows,

$$\mathcal{A} = u(u-1)\omega_0\omega_\tau^2 \left[\mathcal{A}_1 + \mathcal{A}_2 \right], \quad (4.15)$$

where

$$\begin{aligned} \mathcal{A}_1 &= \left[1 + (1-2u)\mathbf{t}(\bar{x}_0)\mathbf{t}(\bar{x}_\tau) \right] \left[\omega_\tau \mathbf{t}(\bar{x}_0) \left((1-2u)\mathbf{t}(\bar{x}_0) + \mathbf{t}(\bar{x}_\tau) \right) + \omega_0 \mathbf{t}^2(\bar{x}_0) + (1-2u)\omega_0 \mathbf{t}(\bar{x}_0)\mathbf{t}(\bar{x}_\tau) \right], \\ \mathcal{A}_2 &= \left[(1-2u)\mathbf{t}(\bar{x}_0) + \mathbf{t}(\bar{x}_\tau) \right] \left[\omega_\tau \mathbf{t}(\bar{x}_0) (1 - \mathbf{t}^2(\bar{x}_\tau)) - \omega_0 \mathbf{t}(\bar{x}_\tau) [1 + (1-2u)\mathbf{t}(\bar{x}_0)\mathbf{t}(\bar{x}_\tau)] \right], \end{aligned}$$

where $\bar{x}_0 = \beta_c \omega_0 / 2$ and $\bar{x}_\tau = \beta_h \omega_\tau / 2$ and we have used a simplified notation for tanh function and write it as \mathbf{t} . In the regime of heat engine operation, we demand $\langle q_h \rangle > 0$

which implies the following condition,

$$(1 - 2u)\mathbf{t}(\bar{x}_0) + \mathbf{t}(\bar{x}_\tau) < 0, \quad (4.16)$$

which also leads to a condition

$$1 + (1 - 2u)\mathbf{t}(\bar{x}_0)\mathbf{t}(\bar{x}_\tau) < 1 - \mathbf{t}^2(\bar{x}_\tau). \quad (4.17)$$

In addition to this, $\langle q_c \rangle = -\frac{\omega_0}{2} \left[\mathbf{t}(\bar{x}_0) + \mathbf{t}(\bar{x}_\tau)(1 - 2u) \right] < 0$ implies,

$$1 + (1 - 2u)\mathbf{t}(\bar{x}_0)\mathbf{t}(\bar{x}_\tau) > 1 - \mathbf{t}^2(\bar{x}_0) > 0. \quad (4.18)$$

Furthermore, the requirement that the output work is positive i.e., $\langle w \rangle < 0$ gives the condition

$$\left[\omega_0 \mathbf{t}(\bar{x}_0) + \omega_\tau \mathbf{t}(\bar{x}_\tau) \right] + (1 - 2u) \left[\omega_0 \mathbf{t}(\bar{x}_\tau) + \omega_\tau \mathbf{t}(\bar{x}_0) \right] < 0. \quad (4.19)$$

Multiplying this with $\mathbf{t}(\bar{x}_0)$ and rearranging the terms, one receives,

$$\left[\omega_\tau \mathbf{t}(\bar{x}_0) \left((1 - 2u) \mathbf{t}(\bar{x}_0) + \mathbf{t}(\bar{x}_\tau) \right) + \omega_0 \mathbf{t}^2(\bar{x}_0) + (1 - 2u) \omega_0 \mathbf{t}(\bar{x}_0) \mathbf{t}(\bar{x}_\tau) \right] < 0. \quad (4.20)$$

Similarly combining Eq. (4.18) and Eq. (4.20) confirms that \mathcal{A}_1 is always negative. Now the first part in \mathcal{A}_2 is negative which follows from Eq. (4.16). Let us now look at the second term in \mathcal{A}_2 , which using the condition Eq. (4.17) provides a lower bound, given as

$$\begin{aligned} \mathcal{B} &= \left[\omega_\tau \mathbf{t}(\bar{x}_0) (1 - \mathbf{t}^2(\bar{x}_\tau)) - \omega_0 \mathbf{t}(\bar{x}_\tau) [1 + (1 - 2u)\mathbf{t}(\bar{x}_0)\mathbf{t}(\bar{x}_\tau)] \right], \\ \mathcal{B} &\geq \left[\omega_\tau \mathbf{t}(\bar{x}_0) - \omega_0 \mathbf{t}(\bar{x}_\tau) \right] \left[1 - \mathbf{t}^2(\bar{x}_\tau) \right], \end{aligned} \quad (4.21)$$

while operating as an engine as $\frac{\omega_0}{\omega_\tau} \geq \frac{\beta_h}{\beta_c}$ which means $\mathbf{t}(\bar{x}_0) > \mathbf{t}(\bar{x}_\tau)$ and therefore $\mathcal{B} > 0$.

This completes our proof that $\mathcal{A} \geq 0$. That immediately implies that,

$$\boxed{\eta^{(2)} \equiv \frac{\langle w^2 \rangle_c}{\langle q_h^2 \rangle_c} \geq \frac{\langle w \rangle^2}{\langle q_h \rangle^2} = \langle \eta \rangle^2} \quad (4.22)$$

In other words, in the engine regime, $\eta^{(2)}$ is always lower bounded by square of average efficiency. Another way to interpret the above result is that the relative fluctuation of output

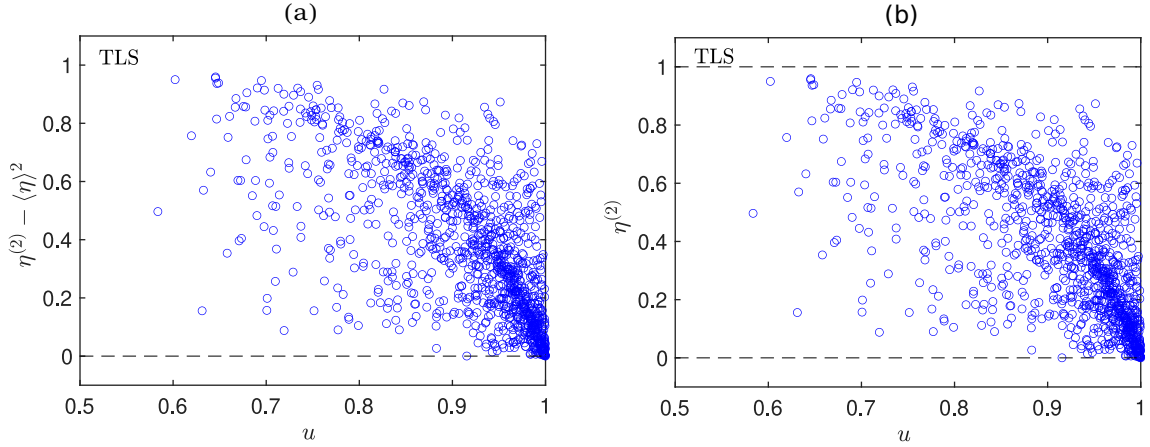


Figure 4.2: Scatter plots of for the TLS Otto cycle while operating as a heat engine. (a) Scatter plot of $\eta^{(2)} - \langle \eta \rangle^2$. (b) Scatter plot of $\eta^{(2)}$. All parameters except u here are chosen randomly in the interval between $[0, 10]$. u is varied randomly between $[0, 1]$. Simulation is done for one million random points. Fig.4.2(a) reproduced with permission from Ref. [128].

work is always greater than relative fluctuations of input heat in the engine regime i.e.,

$$\boxed{\frac{\langle w^2 \rangle_c}{\langle w \rangle^2} \geq \frac{\langle q_h^2 \rangle_c}{\langle q_h \rangle^2}} \quad (4.23)$$

This is the second central result of this chapter. It is interesting to note that we receive exactly the same lower bound on $\eta^{(2)}$ for such finite-time discrete engine as for the steady-state time-reversal symmetric continuous engines. However, the upper bound of $\eta^{(2)}$ in terms of η_C does not exist for such non-adiabatic driving case and a further detailed investigation is required to see the existence of a new upper bound.

In Fig. 4.2(a) we present a scatter plot for $\eta^{(2)} - \langle \eta \rangle^2$ for the two-level system, while operating as a heat engine, by choosing all the parameters randomly. The validity of the lower bound is clear from this scatter plot. As the Hamiltonian here is scale invariant under the driving protocol, we expect that $\eta^{(2)} - \langle \eta \rangle^2$ approaches zero in the quasistatic driving limit which in this case corresponds to $u = 1$. Thus, in Fig. 4.2(a), close to $u = 1$, large number of points cluster around the zero value. In Fig. 4.2(b) scatter plot of $\eta^{(2)}$ is shown and it suggest that the upper bound of $\eta^{(2)}$ is unity. Right now we do not have any analytical proof for this upper bound but extensive numerical simulations suggest this upper bound.

4.5.2 Working fluid consisting of a harmonic oscillator(HO)

We next consider another paradigmatic example with working fluid consisting of a single harmonic oscillator. The time-dependent Hamiltonian for the unitary strokes is given as $H(t) = p^2/2m + \frac{1}{2}m\omega^2(t)x^2$ where in this case, the trapping frequency $\omega(t)$ is modulated as a function of time from ω_0 at $t = 0$ to ω_τ at $t = \tau$ during the stroke $A \rightarrow B$. For the unitary compression stroke $C \rightarrow D$ a reverse protocol is considered which can be obtained from the expansion stroke by replacing t by $\tau - t$.

The CF for this case can be obtained exactly and is given by [175]

$$\begin{aligned} \chi_{\text{HO}}(\alpha_1, \alpha_2) &= \frac{2}{\mathcal{Z}_0 \mathcal{Z}_\tau} \times \frac{1}{\sqrt{\mathcal{Q}(1-u_0^2)(1-v_0^2) + (1+u_0^2)(1+v_0^2) - 4u_0v_0}} \\ &\times \frac{1}{\sqrt{\mathcal{Q}(1-x_0^2)(1-y_0^2) + (1+x_0^2)(1+y_0^2) - 4x_0y_0}}, \end{aligned} \quad (4.24)$$

where

$$\begin{aligned} u_0 &= e^{-\omega_0(\beta_c + i\alpha_1)}, \\ v_0 &= e^{i\omega_\tau(\alpha_1 - \alpha_2)}, \\ x_0 &= e^{-\omega_\tau(\beta_h + i(\alpha_1 - \alpha_2))}, \\ y_0 &= e^{i\omega_0\alpha_1}, \end{aligned} \quad (4.25)$$

and \mathcal{Z}_0 and \mathcal{Z}_τ are the partition functions. Here $\mathcal{Q} \in [1, \infty]$ is the so-called the adiabaticity parameter with the value 1 corresponding to the QS limit.

Thus, we can easily obtain the average and the noise for both absorbed heat and net work in the non-adiabatic limit. The net average work and heat absorbed from the hot bath is given as

$$\langle w \rangle = \frac{1}{2} \left[(\mathcal{Q}\omega_\tau - \omega_0) \coth\left(\frac{\beta_c\omega_0}{2}\right) + (\mathcal{Q}\omega_0 - \omega_\tau) \coth\left(\frac{\beta_h\omega_\tau}{2}\right) \right], \quad (4.26)$$

$$\langle q_h \rangle = \frac{\omega_\tau}{2} \left[\coth\left(\frac{\beta_h\omega_\tau}{2}\right) - \mathcal{Q} \coth\left(\frac{\beta_c\omega_0}{2}\right) \right], \quad (4.27)$$

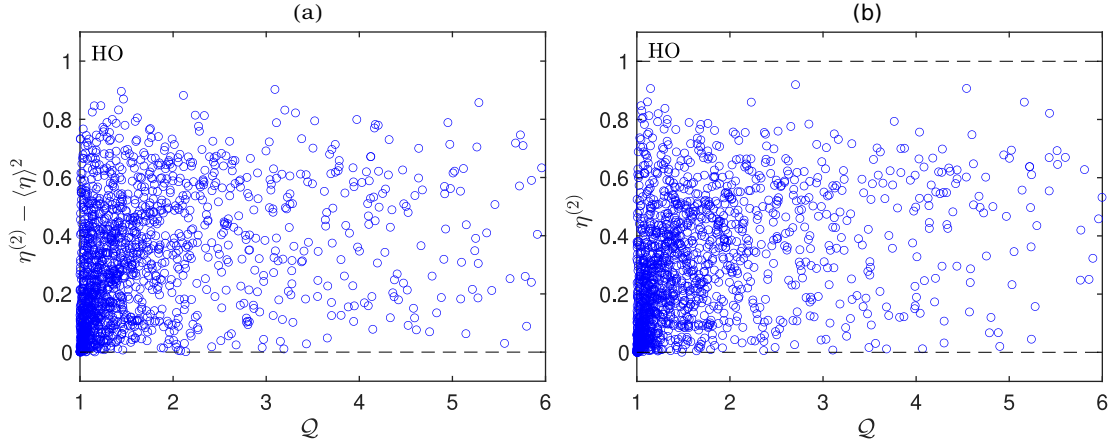


Figure 4.3: Scatter plots for the harmonic oscillator (HO) Otto cycle while operating as a heat engine. (a) Scatter plot of $\eta^{(2)} - \langle \eta \rangle^2$ (b) Scatter plot of $\eta^{(2)}$. All parameters except \mathcal{Q} are chosen randomly in the interval between $[0, 10]$. \mathcal{Q} is varied randomly between $[1, 6]$. Simulation is done for one million random points. Fig. 4.3(a) reproduced with permission from Ref. [128].

Similarly the corresponding fluctuations are given as,

$$\begin{aligned} \langle w^2 \rangle_c &= \langle w_1 \rangle^2 + \langle w_3 \rangle^2 - \frac{1}{2}(\omega_0 - \omega_\tau)^2 + (\mathcal{Q} - 1)\omega_0\omega_\tau + \frac{1}{4}(\mathcal{Q}^2 - 1) \left[\omega_\tau^2 \coth^2 \left(\frac{\beta_c \omega_0}{2} \right) \right. \\ &\quad \left. + \omega_0^2 \coth^2 \left(\frac{\beta_h \omega_\tau}{2} \right) \right], \end{aligned} \quad (4.28)$$

$$\langle q_h^2 \rangle_c = -\frac{\omega_\tau^2}{4} \left[2 - \coth^2 \left(\frac{\beta_h \omega_\tau}{2} \right) - (2\mathcal{Q}^2 - 1) \coth^2 \left(\frac{\beta_c \omega_0}{2} \right) \right]. \quad (4.29)$$

The above expressions are valid for arbitrary protocol of $\omega(t)$. Here $\mathcal{Q} \in [1, \infty]$ is the so-called adiabaticity parameter which characterizes the degree of adiabaticity. The QS limit corresponds to $\mathcal{Q} = 1$ and it is easy to check that $\eta^{(2)}$ saturates the lower bound i.e., $\eta_{\text{QS}}^{(2)} = \langle \eta \rangle_{\text{QS}}^2 = (1 - \omega_0/\omega_\tau)^2$ which is expected as the energy eigenspectra follow the scaling relation. We perform extensive numerical simulation by choosing the parameters randomly and notice that, for this model as well, in the engine regime, the lower bound is always respected. In Fig.4.3(a) we present a scatter plot for $\eta^{(2)} - \langle \eta \rangle^2$ for the HO working fluid in the engine regime with the parameters chosen randomly over a broad range. It is clear that the lower bound is always respected for this model with the difference disappearing in the QS limit i.e., for $\mathcal{Q} = 1$. This suggest that, although we have no proof, $\eta^{(2)}$ gets lower bounded by $\langle \eta \rangle^2$, same as obtained for continuous engine in chapter one. In Fig.4.3(b) scatter plot of $\eta^{(2)}$ is shown and again just like TLS it suggest that upper bound is unity.

4.6 Connection with the finite-time TUR

At this point, it is important to make a connection with the finite-time TUR studies. In Ref. [71] it was shown that if a non-equilibrium process satisfying the finite-time exchange fluctuation theorem [59], which implies for the CF the symmetry $\chi(\alpha_1, \alpha_2) = \chi(-\alpha_1 + i\beta_c, -\alpha_2 + i(\beta_c - \beta_h))$, then the relative fluctuations of individual integrated currents (work, heat, etc.) are lower bounded by a function which solely depends on the total entropy production $\langle \Sigma \rangle = \beta_c \langle w \rangle + (\beta_c - \beta_h) \langle q_h \rangle$. More precisely, the finite-time TUR states,

$$\frac{\langle w^2 \rangle_c}{\langle w \rangle^2} \geq f(\langle \Sigma \rangle) \quad , \quad \frac{\langle q_h^2 \rangle_c}{\langle q_h \rangle^2} \geq f(\langle \Sigma \rangle), \quad (4.30)$$

where $f(x) = \text{csch}^2(g(x/2))$, and $g(x)$ is the inverse function of $x \tanh(x)$. For the two paradigmatic examples studied in this chapter it can be easily checked that the CF's as given in Eq. (4.11) and Eq. (4.24) satisfies the exchange fluctuation theorem. Now as for both the models, in the heat engine regime, the relative fluctuation of total work is always greater than the relative fluctuation of heat absorbed from the hot bath, this implies that these relative fluctuations are not independent of each other but rather follow the following sequence of bounds in the engine regime,

$$\boxed{\frac{\langle w^2 \rangle_c}{\langle w \rangle^2} \geq \frac{\langle q_h^2 \rangle_c}{\langle q_h \rangle^2} \geq f(\langle \Sigma \rangle)}. \quad (4.31)$$

4.7 Summary

In this chapter, we have investigated bounds on the ratio of nonequilibrium fluctuation for output work and input heat for a finite-time quantum Otto cycle operating as an engine. We provide a universal result for the ratio $\eta^{(n)}$ in the quasistatic (QS) driving limit which is exactly equal to the nth power of the corresponding average efficiency $\langle \eta \rangle$. As a consequence of this result, one receives an upper bound on $\eta^{(2)}$ given by the square of the Carnot efficiency. Remarkably, this result is similar to the one that we received for the steady-state continuous engine case with the lower bound on $\eta^{(2)}$ saturating in the QS limit. In the nonadiabatic limit, we show the existence of the lower bound on $\eta^{(2)}$ for two paradigmatic

models. Interestingly, we did not find an upper bound on $\eta^{(2)}$ in terms of Carnot efficiency for these models but extensive numerical simulations suggest that the upper bound is unity. Importantly, our results further connect to the finite-time version of the TUR study where as a consequence of our lower bound, the relative fluctuation of work, always surpass the corresponding relative fluctuation of heat absorbed from the hot bath and follows a hierarchy. It remains an open problem to provide a general proof for the lower bound as well as upper bound for arbitrary working fluid operating as an engine.

CHAPTER 5

Thermodynamic uncertainty relation for steady-state thermal transport junctions

Abstract

We use the fundamental non-equilibrium steady state fluctuation symmetry and derive a condition on the validity of thermodynamic uncertainty relation (TUR) for single affinity driven systems. In particular, we focus on thermal transport where a system of interest is driven out of equilibrium by applying a temperature difference. Our analysis is valid for both classical and quantum systems. We test the condition and study the breakdown of the TUR in different thermal transport junctions of bosonic and electronic degrees of freedom. First, we prove that the TUR is valid in harmonic oscillator junctions. Then, we consider the heat transport by non-interacting electrons in a tight-binding chain model. Here we show that the TUR is feasibly violated by tuning e.g. the hybridization energy of the chain to the metal leads. These results manifest that the validity of the TUR relies on the statistics of the participating carriers.

Reported in

S. Saryal, H. M. Friedman, D. Segal, and B K. Agarwalla , *Thermodynamic uncertainty relation in thermal transport*, [Phys. Rev. E 100, 042101 \(2019\)](#).

5.1 Introduction

So far we focused our attention on thermal machines which are subjected to two thermodynamic affinities and we showed that a strict universal hierarchy exists between relative-fluctuations of input and output currents, in the linear response regime. As a straightforward consequence, thermodynamic uncertainty relation (TUR) also receives a strict hierarchy. In this chapter we direct our attention beyond linear response but focusing on a single affin-

ity driven case and assesses the validity of TUR. We primarily focus on the thermal transport case, implying a system of interest is driven out-of-equilibrium by applying a temperature difference across its boundaries (see Fig. (5.1)).

As mentioned in the introduction, several TURs [64, 65, 68–73, 75] have been proposed after the pioneering work by Barato and Seifert [64] which we refer as the T-TUR, and is given by,

$$\langle \sigma \rangle \frac{\langle I^2 \rangle_c}{\langle I \rangle^2} \geq 2. \quad (5.1)$$

Barato and Seifert conjectured the T-TUR for arbitrary far-from-equilibrium processes in steady-state. Later on this bound was rigorously proven for continuous-time Markov process in the steady state [65]. In this chapter we will only investigate the validity/violation of T-TUR because of the following reasons.

(i) First of all, since T-TUR is only proved rigorously for the Markov process, it is imperative to study its validity for very general dynamics and its violation will definitely imply the onset of non-markovian behaviour making it profoundly useful.

(ii) Next, as mentioned in chapter 1, following the geometry of quantum non-equilibrium steady-states and Cramer-Rao bound, a TUR was derived, which we refer as Q-TUR [74]. For single affinity driven systems Q-TUR reads,

$$\langle \sigma \rangle \frac{\langle I^2 \rangle_c}{\langle I \rangle^2} \geq 1, \quad (5.2)$$

which is two times looser than T-TUR (Eq. (5.1)). At equilibrium the T-TUR becomes an equality, providing a clear reference point to the role of the non-equilibrium condition on the trade-off relation, which is not the case for Q-TUR. As we prove below, harmonic systems exactly satisfy the T-TUR (5.1), making it clear that its validity extends beyond Markovian dynamics to cover more general cases. Also, our simulations below satisfy the Q-TUR, yet we observe that this bound is quite loose, thus suggesting the existence of a tighter bound.

(iii) Finally, since we are interested in steady-state transport, bounds G-TUR1 and G-TUR2 (introduced in chapter 1), which are derived invoking the fluctuation relation $\frac{P(\Sigma)}{P(-\Sigma)} = e^\Sigma$, where Σ is the total entropy production, becomes trivial in the steady state

limit.

In this chapter, we would like to assess the validity of the T-TUR from the perspective of universal steady-state fluctuation symmetries. Note that, such fluctuation symmetry does not rely on underlying dynamics, or statistics of the participating carriers, but only depends on Gibbs state of the reservoirs and the principle of micro-reversibility. Our study here therefore is very general and valid for both quantum and classical systems. Using the nonequilibrium steady state fluctuation symmetry (SSFS), we put together the relative uncertainty of heat current and the associated entropy production rate. The resulting expression recovers the structure of the T-TUR—while allowing its violation—depending on the sign of high order cumulants. We study here both bosonic and fermionic systems, illustrating that the particle statistics plays a central role on this bound.

Our setup includes a central system that is coupled to two heat baths L, R maintained at different temperatures, $T_R > T_L$; there are no other thermodynamical forces (e.g. the chemical potential is fixed). For such a setup, the average steady-state entropy production rate is given by $\langle \sigma \rangle = \Delta\beta \langle I \rangle$, where $\Delta\beta = \frac{1}{T_L} - \frac{1}{T_R}$ is the thermodynamic affinity, driving the system out-of-equilibrium in an irreversible manner. In this setting, the TUR (5.1) simplifies to

$$\Delta\beta \frac{\langle I^2 \rangle_c}{\langle I \rangle} \geq 2. \quad (5.3)$$

The objective of this work is to understand the behavior of current fluctuations in thermal transport junctions by providing insights on the validity of the TUR, Eq. (5.3). First, based on the steady state fluctuation symmetry, we show that T-TUR violations are linked to the behavior of the skewness, the third cumulant of the heat current. This derivation holds for both classical and quantum systems. We exemplify this observation and examine the T-TUR in two central quantum thermal transport models (see Fig. 5.1): (i) system of coupled harmonic oscillators and further coupled at two edges to harmonic baths. In this case we prove that the T-TUR is always satisfied. (ii) a tight-binding fermionic chain, where we study electronic heat transport. Furthermore, in a particular regime or interests, known as the resonant transport regime, we provide an analytic condition for T-TUR violations, and is further supported by numerical simulations.

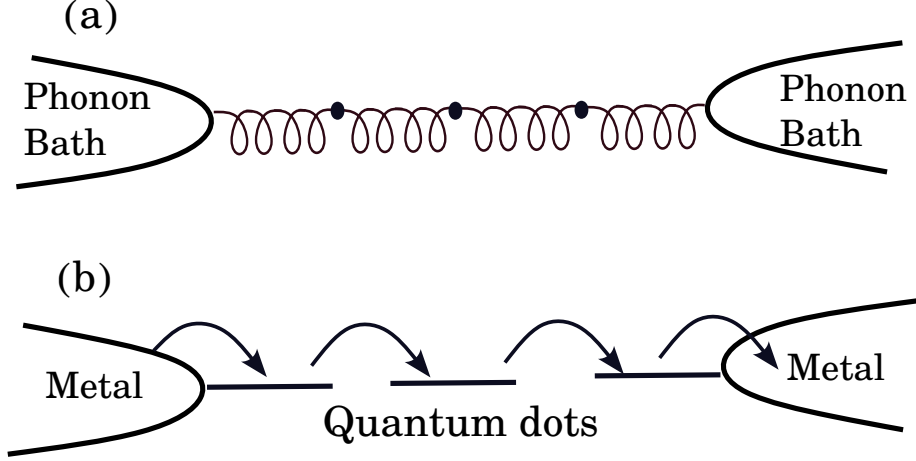


Figure 5.1: Representation of thermal transport models investigated in this study: (a) System of coupled harmonic oscillators attached at two points to phonon baths. (b) Noninteracting tight-binding electron transport model. Here, the first and last electronic sites are coupled to metallic baths that are maintained at different temperatures but identical chemical potential.

This chapter is organized as follows: In Section 5.2, we employ the universal steady state fluctuation relation (Gallavotti-Cohen symmetry) for heat exchange and present a $\Delta\beta$ perturbative expansion of the TUR ratio. In Section 5.3, we study the non-interacting harmonic oscillator model. In Section 5.4 we investigate the T-TUR in electronic heat transport. We conclude the chapter in Section 5.6.

5.2 Perturbative expansion for the TUR from fluctuation symmetry

The steady state fluctuation symmetry relates the probability of integrated heat current, $Q(t) = \int_0^t d\tau I(\tau)$, flowing in the forward direction (from hot to cold) $p(Q = It)$ to that of the probability of heat flowing in the reverse direction $p(Q = -It)$ (from cold to hot). The precise statement of SSFS is

$$\lim_{t \rightarrow \infty} \frac{1}{t} \ln \left[\frac{p(Q = It)}{p(Q = -It)} \right] = \Delta\beta I. \quad (5.4)$$

Here, $\sigma = \Delta\beta I$ is the stochastic entropy production rate. Note that, the above fluctuation symmetry is valid in the absence of any time-dependent driving and/or odd-parity fields for example, magnetic field. In terms of the cumulant generating function (CGF), defined as

$\mathcal{G}(\chi) = \lim_{t \rightarrow \infty} \frac{1}{t} \ln Z(\chi)$ where $Z(\chi) \equiv \int dQ e^{i\chi Q} p(Q)$, the SSFS leads to the symmetry $\mathcal{G}(\chi) = \mathcal{G}(-\chi + i\Delta\beta)$. Here, χ is the counting parameter which keeps track of the net amount of thermal energy flowing between a bath to the system. The cumulants for current are then obtained by taking derivatives, $\langle I^n \rangle_c = \left. \frac{\partial^n \mathcal{G}(\chi)}{\partial (i\chi)^n} \right|_{\alpha=0}$. Invoking this steady state fluctuation symmetry for heat exchange [51, 57], we will derive here a perturbative expression for the ratio $\Delta\beta \langle I^2 \rangle_c / \langle I \rangle$ in orders of the affinity $\Delta\beta$.

In steady state, we can formally expand the averaged heat current and its higher order cumulants, $\langle I^n \rangle_c$, $n = 1, 2, 3, \dots$ in powers of the affinity $\Delta\beta$ as

$$\begin{aligned}
\langle I \rangle &= G_0 + G_1 \Delta\beta + \frac{1}{2!} G_2 (\Delta\beta)^2 + \frac{1}{3!} G_3 (\Delta\beta)^3 + \frac{1}{4!} G_4 (\Delta\beta)^4 + \dots \\
\langle I^2 \rangle_c &= S_0 + S_1 (\Delta\beta) + \frac{1}{2!} S_2 (\Delta\beta)^2 + \frac{1}{3!} S_3 (\Delta\beta)^3 + \dots \\
\langle I^3 \rangle_c &= R_0 + R_1 \Delta\beta + \frac{1}{2!} R_2 (\Delta\beta)^2 + \dots \\
\langle I^4 \rangle_c &= T_0 + T_1 (\Delta\beta) + \dots
\end{aligned} \tag{5.5}$$

The four cumulants are the average current, its variance, skewness, and the kurtosis. For the average current, G_1 is the linear transport coefficient, or the thermal conductance which is always non-negative, G_2, G_3, \dots are nonlinear transport coefficients. Heat current fluctuations include the equilibrium noise component S_0 and higher order nonequilibrium terms, S_1, S_2, \dots . Other coefficients appearing in the skewness and the kurtosis, such as R_1, R_2, T_0, \dots can be similarly described.

As a consequence of this SSFS, it can be shown that linear and higher order transport coefficients in Eq. (5.5) are in fact related to each other [176],

$$\begin{aligned}
S_0 &= 2G_1, & S_1 &= G_2, \\
T_0 &= 2R_1, & T_1 &= R_2, \\
3S_2 - 2G_3 &= R_1, \\
2S_3 - G_4 &= R_2, \\
\dots & & &
\end{aligned} \tag{5.6}$$

and so on. Note that $S_0 = 2G_1$ is the famous Green-Kubo formula. Also, equilibrium component of all the odd-cumulants are zero as a result of SSFS i.e, $G_0 = 0$, $R_0 = 0$, etc.

We substitute the expansion for the current and its fluctuations Eq. (5.5) into Eq. (5.3) and simplify it using the relationships (5.6). As a result, we obtain the left hand side of the TUR as a perturbative series in $\Delta\beta$,

$$\Delta\beta \frac{\langle I^2 \rangle_c}{\langle I \rangle} = 2 + \frac{(\Delta\beta)^2}{6G_1} R_1 + \mathcal{O}(\Delta\beta)^3 + \dots \quad (5.7)$$

This expression is one of the central results of the chapter. Note that $G_1 > 0$ and since there is no fundamental constraint on the sign of the skewness coefficient, R_1 , it is clear that from the above expression that the tighter version of TUR (5.3) may be violated in nonequilibrium systems—within a certain range of the affinity $\Delta\beta$.

We point out the following observations:

- The expansion (5.32) is valid for both classical and quantum systems.
- The linear order term in $\Delta\beta$ does not contribute to the TUR. This is a consequence of the relation $S_1 = G_2$, which stems from the time-reversal symmetry of the underlying Hamiltonian.
- Coefficients for orders $(\Delta\beta)^n$, $n = 2, 3, \dots$ include heat current cumulants that are greater than two. Therefore, if the probability distribution for heat exchange is Gaussian the TUR precisely saturates to the value 2, since all higher order cumulants greater than two vanish.
- It is evident from this expression that for noninteracting setups (missing a diode effect) only even orders in $\Delta\beta$ contribute since the current is an odd function of the thermal bias, while the second cumulant involves only even powers in $\Delta\beta$. This may not be the situation for interacting junctions.

Equation (5.32) reveals that the TUR (5.3) is violated if $R_1 < 0$. Of course, one may observe that $R_1 > 0$ but the TUR is still violated due to the impact of higher cumulants. However, in this work, we examine the breakdown of the TUR within the leading order of the affinity i.e., up to $(\Delta\beta)^2$, and we therefore focus on the sign of R_1 . In what follows we study the TUR for two paradigmatic thermal transport problems: harmonic oscillator system coupled to harmonic baths and a tight-binding electronic junction.

5.3 Coupled harmonic oscillators: Proof for the validity of the TUR

We consider a noninteracting thermal transport model consisting of coupled harmonic oscillators (see Fig. 5.1(a)). We assume that the first and last oscillators are coupled to independent heat baths, L and R , which are maintained at different temperatures, T_L and T_R , respectively. The baths include a collection of harmonic oscillators which are bilinearly coupled to the system. The model is fully harmonic and the total Hamiltonian for this setup can be written as

$$\begin{aligned} \hat{H} = & \sum_{\nu=L,R} \left(\frac{1}{2} \hat{p}_\nu^T \hat{p}_\nu + \frac{1}{2} \hat{u}_\nu^T K^\nu \hat{u}_\nu \right) + \frac{1}{2} \hat{p}_C^T \hat{p}_C + \frac{1}{2} \hat{u}_C^T K^C \hat{u}_C \\ & + \hat{u}_L^T V^{LC} \hat{u}_C + \hat{u}_R^T V^{RC} \hat{u}_C. \end{aligned} \quad (5.8)$$

Here \hat{u}_ν and \hat{p}_ν are column vectors of mass weighted coordinate operators and momenta for regions $\nu = L, R$. K^ν is the corresponding force constant matrix. Similar definitions hold for the central (C) region. V^{LC} and V^{RC} are the force constants matrices between the central system and the left and right regions; recall that the left bath is coupled to a single ('first') oscillator in the system, and similarly the right bath is connected to a specific ('last') oscillator. T stands for the transpose operation.

The integrated thermal energy current is defined as the net change of thermal energy in the reservoir, say the left one, $Q \equiv \hat{H}_R(0) - \hat{H}_R^H(t)$. The superscript H represents the operators in the Heisenberg picture. An exact expression for the steady state CGF, $\mathcal{G}_{\text{HO}}(\alpha)$ for the integrated thermal energy current can be obtained by following the two-time measurement protocol and employing the Keldysh non-equilibrium Green's function approach [61, 62]. The scaled CGF is given by

$$\begin{aligned} \mathcal{G}_{\text{HO}}(\chi) = & - \int_{-\infty}^{\infty} \frac{d\omega}{4\pi} \ln \left\{ 1 - \mathcal{T}_{\text{HO}}(\omega) [n_R(\omega) \bar{n}_L(\omega) \times \right. \\ & \left. (e^{i\chi\hbar\omega} - 1) + n_L(\omega) \bar{n}_R(\omega) (e^{-i\chi\hbar\omega} - 1)] \right\}, \end{aligned} \quad (5.9)$$

with the transmission function $\mathcal{T}_{\text{HO}}(\omega)$, which is expressed in terms of the Green's function of the central region and the self-energies of the baths [61]. We highlight that the transmission function is derived for a harmonic system, but the oscillators within could be coupled

to each other with any geometry and force constants. The baths are maintained at thermal equilibrium with the Bose-Einstein distribution function $n_\nu(\omega) = [\exp(\beta_\nu \hbar \omega) - 1]^{-1}$; $\bar{n}_\nu(\omega) \equiv 1 + n_\nu(\omega)$. Note that the transmission function does not depend on temperature due to the non-interacting nature of the model. As a consequence, the above CGF satisfies the following symmetry

$$\mathcal{G}_{\text{HO}}(\alpha; T_L, T_R) = \mathcal{G}_{\text{HO}}(-\alpha; T_R, T_L), \quad (5.10)$$

which ensures that the energy current and the associated noise are odd and even functions of the affinity $\Delta\beta$, respectively. Therefore, for a fully harmonic model only even powers in $\Delta\beta$ survive in the TUR expression, Eq. (5.32).

The analytical forms for the first and second cumulants can be readily obtained from Eq. (5.9), and are given by

$$\langle I \rangle = \int_0^\infty \frac{d\omega}{2\pi} \hbar \omega \mathcal{T}_{\text{HO}}(\omega) [n_R(\omega) - n_L(\omega)], \quad (5.11)$$

$$\begin{aligned} \langle I^2 \rangle_c &= \int_0^\infty \frac{d\omega}{2\pi} (\hbar \omega)^2 \left\{ \mathcal{T}_{\text{HO}}(\omega) [n_R(\omega) \bar{n}_L(\omega) + n_L(\omega) \bar{n}_R(\omega)] \right. \\ &\quad \left. + \mathcal{T}_{\text{HO}}^2(\omega) [n_R(\omega) - n_L(\omega)]^2 \right\}. \end{aligned} \quad (5.12)$$

Expanding the current and the variance in powers of $\Delta\beta$, we construct the coefficient $R_1 = 3S_2 - 2G_3$, which is always positive

$$R_1 = \int_0^\infty \frac{d\omega}{2\pi} (\hbar \omega)^4 \mathcal{T}_{\text{HO}}(\omega) n(\omega) \bar{n}(\omega) \left[1 + 6 \mathcal{T}_{\text{HO}}(\omega) n(\omega) \bar{n}(\omega) \right] > 0. \quad (5.13)$$

Here, $n(\omega)$ is the Bose-Einstein distribution function evaluated at the average temperature $T = (T_L + T_R)/2$. Since the transmission function and the thermal distribution functions are positive, the coefficient R_1 is always positive. Therefore, up to $\mathcal{O}(\Delta\beta)^2$ the TUR is satisfied for quantum harmonic networks consisting of an arbitrary number of oscillators with general connectivity and arbitrary coupling strengths to the baths.

Moreover, we now prove that for harmonic systems the TUR is valid arbitrarily far from equilibrium. From Eq. (5.12), we note that the second cumulant obeys the inequality,

$$\langle I^2 \rangle_c \geq \int_0^\infty \frac{d\omega}{2\pi} (\hbar \omega)^2 \mathcal{T}_{\text{HO}}(\omega) [n_L(\omega) \bar{n}_R(\omega) + n_R(\omega) \bar{n}_L(\omega)].$$

An equality is satisfied at thermal equilibrium, $\beta_L = \beta_R$. Interestingly, one can show the following inequality involving the Bose-Einstein distribution function for $\forall \omega > 0$,

$$\left[n_L(\omega) \bar{n}_R(\omega) + n_R(\omega) \bar{n}_L(\omega) \right] \geq \frac{2}{\Delta\beta \hbar\omega} [n_R(\omega) - n_L(\omega)]. \quad (5.14)$$

Using this inequality in the noise expression immediately implies that

$$\begin{aligned} \langle I^2 \rangle_c &\geq \frac{2}{\Delta\beta} \int_0^\infty \frac{d\omega}{2\pi} \hbar\omega \mathcal{T}_{\text{HO}}(\omega) [n_L(\omega) - n_R(\omega)] \\ &= \frac{2}{\Delta\beta} \langle I \rangle, \end{aligned} \quad (5.15)$$

which is the TUR, Eq. (5.3). This derivation is entirely independent of the details of the transmission function. The proof only emerges from the formal structure of the CGF in Eq. (5.9). We conclude that for harmonic junctions the TUR is satisfied in the quantum and classical (high temperature) limits irrespective of the underlying dynamics, which could be Markovian or non-Markovian. While this proof holds for classical and quantum systems alike, in Appendix D we separately study classical harmonic systems by directly studying the classical CGF.

5.4 Thermal transport of noninteracting electrons: TUR violation in the resonant transport regime

After analyzing the validity of the TUR for bosonic heat transport, in this Section we study electronic heat transport. For simplicity, we focus on a one-dimensional noninteracting tight-binding chain model for fermions (see Fig. 5.1(b)) with the Hamiltonian

$$\hat{H} = \sum_{\nu=L,C,R} \hat{c}_\nu^\dagger h^\nu \hat{c}_\nu + \sum_{\nu=L,R} \left(\hat{c}_\nu^\dagger V_e^{\nu C} \hat{c}_C + \text{h.c.} \right). \quad (5.16)$$

Here, $\hat{c}_\nu^\dagger (\hat{c}_\nu)$ is the row (column) vector consisting of electronic creation (annihilation) operators in the ν region, with h^ν the single-particle Hamiltonian matrix in that domain. $V_e^{\nu C}$ is the coupling matrix between the metals and the central system. The baths ($\nu = L, R$) and the central system are initially decoupled and are prepared at their respective grand canonical equilibrium state with temperature T_ν and chemical potential μ_ν .

As mentioned in chapter 2, exact CGF can be obtained for this non-interacting setup

and is given by the famous Levitov-Lesovik formula stated in Eq.2.35. Since we are only interested in thermal transport, the CGF for heat exchange can be obtained from Eq.2.35 by simply replacing $\chi_e = -\mu_R\chi$ and $\chi_u = \chi$, where χ keeps track of net amount heat transfer at the right contact, which

$$\begin{aligned} \mathcal{G}_{\text{el}}(\chi) &= \int_{-\infty}^{\infty} \frac{d\epsilon}{2\pi\hbar} \ln \left\{ 1 + \mathcal{T}_{\text{el}}(\epsilon) [f_R(\epsilon)\bar{f}_L(\epsilon)(e^{i\chi(\epsilon-\mu_R)} - 1) \right. \\ &\quad \left. + f_L(\epsilon)\bar{f}_R(\epsilon)(e^{-i\chi(\epsilon-\mu_R)} - 1)] \right\}. \end{aligned} \quad (5.17)$$

$f_\nu(\epsilon) = 1/[e^{\beta_\nu(\epsilon-\mu_\nu)} + 1]$ is the Fermi-Dirac distribution function for the leads, $\nu = L, R$, $\bar{f}_\nu(\epsilon) = 1 - f_\nu(\epsilon)$, μ_ν is the corresponding chemical potential and $\mathcal{T}_{\text{el}}(\epsilon)$ is the transmission function, containing the structural information of the electrodes and the system. Since our focus here is on the heat current, we consider identical chemical potentials ($\mu = \mu_R = \mu_L$) but different temperatures ($T_L \neq T_R$) for the leads. In this case, the CGF follows the symmetry $\mathcal{G}_{\text{el}}(\chi) = \mathcal{G}_{\text{el}}(-\chi + i\Delta\beta)$. Note that, similarly to the non-interacting bosonic case, the CGF here also satisfies

$$\chi_{\text{el}}(\alpha; \mu, T_L, T_R) = \chi_{\text{el}}(-\alpha; \mu, T_R, T_L), \quad (5.18)$$

which implies that the TUR expression in Eq. (5.32) contains only even powers in $\Delta\beta$. Using Eq. (5.17), the heat current and the associated noise are given by

$$\langle I \rangle = \int_{-\infty}^{\infty} \frac{d\epsilon}{2\pi\hbar} (\epsilon - \mu) \mathcal{T}_{\text{el}}(\epsilon) [f_R(\epsilon) - f_L(\epsilon)], \quad (5.19)$$

$$\begin{aligned} \langle I^2 \rangle_c &= \int_{-\infty}^{\infty} \frac{d\epsilon}{2\pi\hbar} (\epsilon - \mu)^2 \left\{ \mathcal{T}_{\text{el}}(\epsilon) [f_R(\epsilon)\bar{f}_L(\epsilon) \right. \\ &\quad \left. + f_L(\epsilon)\bar{f}_R(\epsilon)] - \mathcal{T}_{\text{el}}^2(\epsilon) (f_L(\epsilon) - f_R(\epsilon))^2 \right\}. \end{aligned} \quad (5.20)$$

As before, we compute R_1 , which is given by,

$$\begin{aligned} R_1 &= \int_{-\infty}^{\infty} \frac{d\epsilon}{2\pi\hbar} (\epsilon - \mu)^4 \mathcal{T}_{\text{el}}(\epsilon) f(\epsilon) [1 - f(\epsilon)] \times \\ &\quad \left[1 - 6\mathcal{T}_{\text{el}}(\epsilon) f(\epsilon) [1 - f(\epsilon)] \right]. \end{aligned} \quad (5.21)$$

The Fermi function $f(\epsilon)$ is evaluated at the averaged temperature. It is important to note that the above obtained expressions are valid for arbitrary temperatures, bias voltage, system-

bath coupling and the details of the chain, encapsulated within the transmission function. In what follows, we once again consider different limiting cases to analyze the TUR.

Low-transmission. In the limit when $\mathcal{T}_{\text{el}}(\epsilon) \ll 1$ for all values of ϵ , one can discard the term $\mathcal{T}_{\text{el}}^2(\epsilon)$ in Eq. (5.21) relative to $\mathcal{T}_{\text{el}}(\epsilon)$. This immediately implies that the TUR is satisfied.

Indeed, in the context of charge transport, low transmission probability is associated with a Poisson process, which further implies uncorrelated electron transport through the junction. In this limit, one simplifies Eq. (5.17) by approximating $\ln(1+x) \approx x$ and writes the CGF as

$$\begin{aligned} \chi_{\text{el}}(\alpha) = & \int_{-\infty}^{\infty} \frac{d\epsilon}{2\pi\hbar} \mathcal{T}_{\text{el}}(\epsilon) \left\{ f_R(\epsilon) \bar{f}_L(\epsilon) (e^{i\alpha(\epsilon-\mu_R)} - 1) \right. \\ & \left. + f_L(\epsilon) \bar{f}_R(\epsilon) (e^{-i\alpha(\epsilon-\mu_R)} - 1) \right\}. \end{aligned} \quad (5.22)$$

We can further prove that the TUR is valid arbitrarily far from equilibrium in this low transmission transport regime as follows,

We start from Eqs. (5.19)-(5.20), shift the energy around μ , and take the limit of $\mathcal{T}_{\text{el}}(\epsilon) \ll 1$,

$$\begin{aligned} \langle I \rangle &= \int_0^{\infty} \frac{d\epsilon}{2\pi\hbar} \epsilon \left[\mathcal{T}_{\text{el}}(\epsilon+\mu) + \mathcal{T}_{\text{el}}(\epsilon-\mu) \right] [f_R(\epsilon) - f_L(\epsilon)], \\ \langle I^2 \rangle_c &= \int_0^{\infty} \frac{d\epsilon}{2\pi\hbar} \epsilon^2 \left[\mathcal{T}_{\text{el}}(\epsilon+\mu) + \mathcal{T}_{\text{el}}(\epsilon-\mu) \right] [f_R(\epsilon) \bar{f}_L(\epsilon) \\ &+ f_L(\epsilon) \bar{f}_R(\epsilon)]. \end{aligned} \quad (5.23)$$

We notice the following inequality involving the Fermi functions for $\epsilon \geq 0$.

$$\begin{aligned} \left[f_L(\epsilon) \bar{f}_R(\epsilon) + f_R(\epsilon) \bar{f}_L(\epsilon) \right] &= \coth \left(\frac{\Delta\beta\epsilon}{2} \right) [f_R(\epsilon) - f_L(\epsilon)], \\ &\geq \frac{2}{\Delta\beta\epsilon} [f_R(\epsilon) - f_L(\epsilon)]. \end{aligned} \quad (5.24)$$

Introducing this inequality in the above noise expression immediately implies that $\Delta\beta \frac{\langle I^2 \rangle_c}{\langle I \rangle} \geq 2$, completing our proof on the validity of the TUR in the limit of low transmission probability for far from equilibrium also.

Constant transmission. If the transmission is a constant i.e., $\mathcal{T}_{\text{el}}(\epsilon) = \tau$, the integration in Eq. (5.21) can be performed analytically and the expression for TUR up to $\mathcal{O}(\Delta\beta)^2$

simplifies to

$$\Delta\beta \frac{\langle I^2 \rangle_c}{\langle I \rangle} = 2 + \frac{(\Delta\beta)^2}{\beta^2} \left[\frac{7}{5} \pi^2 (1 - \tau) + 12\tau \right] \geq 2, \quad (5.25)$$

which once again validates the TUR. For perfect transmission $\tau = 1$, the above expression simplifies to $\Delta\beta \frac{\langle I^2 \rangle_c}{\langle I \rangle} = 2 + 12 \frac{(\Delta\beta)^2}{\beta^2} \geq 2$.

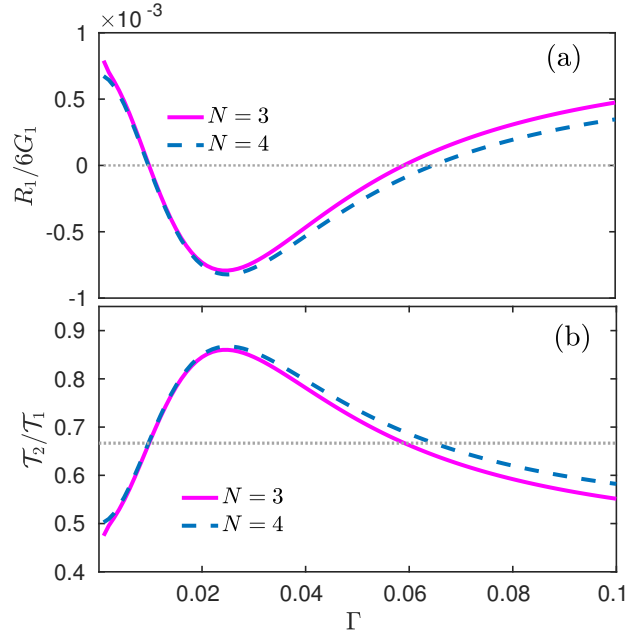


Figure 5.2: TUR violation in electronic thermal transport junctions. (a) Simulation of R_1 using Eq. (5.21), demonstrating TUR violation within a certain range for Γ for $N = 3$ (full) and $N = 4$ (dashed). (b) This violation is in accordance with the observation of $\mathcal{T}_2/\mathcal{T}_1 > 2/3$, where the dotted line marks the value $2/3$. Parameters are $\beta = 1/4$, $\Omega = 1/80$, $\mu = 0$. $\epsilon_d = 1/8$. Figure reproduced with permission from Ref. [73].

Weak coupling- Resonant tunneling limit. Another experimentally realizable case is the weak system-bath coupling limit, also known as the sequential tunneling or the resonant tunneling regime. In this case, the transmission function is sharply peaked about resonance frequencies (corresponding to molecular/quantum dot electronic levels), while the Fermi functions are relatively broad (constant) in the range where the transmission function is non-zero i.e., $k_B T_\nu > \Gamma, \epsilon_d$, where Γ is the hybridization energy and ϵ_d the characteristic energy level of the quantum dots. As a precaution we note that while for charge transport we assess the width of the transmission function itself—relative to the Fermi function—for thermal energy transport we need instead to confirm that the combined function $(\epsilon - \mu)^4 \mathcal{T}_{\text{el}}(\epsilon)$ is

sufficiently narrow relative to the alteration of the Fermi functions.

Assuming for simplicity that the central region includes electronic resonances clustered around the energy ϵ_d , Eq. (5.21) simplifies to

$$R_1 = f(\epsilon_d)[1 - f(\epsilon_d)]\mathcal{T}_1 - 6f(\epsilon_d)^2[1 - f(\epsilon_d)]^2\mathcal{T}_2, \quad (5.26)$$

where we define

$$\mathcal{T}_n = \int_{-\infty}^{\infty} \frac{d\epsilon}{2\pi\hbar} (\epsilon - \mu)^4 \mathcal{T}_{el}^n(\epsilon). \quad (5.27)$$

These integrals converge if the transmission $\mathcal{T}_{el}(\epsilon)$ decays faster than $1/\epsilon^5$. Based on Eq. (5.26) and the inequality $0 \leq f(1 - f) \leq 1/4$, violation of the TUR ($R_1 < 0$) occurs when

$$\boxed{\frac{\mathcal{T}_2}{\mathcal{T}_1} > \frac{2}{3}}. \quad (5.28)$$

This inequality can be satisfied by tuning the electronic parameters of the chain and its hybridization to the metals, as we show below.

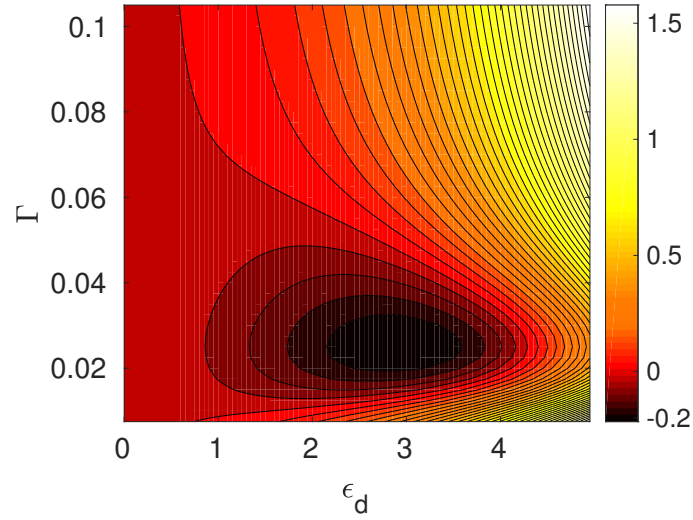


Figure 5.3: Contour plot of the ratio $R_1/6G_1$ in electronic thermal transport junctions as a function of dots onsite energy ϵ_d and the hybridization energy to the leads Γ , beyond the resonant tunneling limit. The TUR is violated (to the order $(\Delta\beta)^2$) when $R_1 < 0$. Other parameters are $\beta = 1/4$, $\Omega = 1/80$, $\mu = 0$, $N = 3$. Figure reproduced with permission from Ref. [73].

In Figs. 5.2-5.3 we present numerical results for the TUR in electronic heat transport following Eq. (5.21). The model consists a junction with its central part including quantum

dots in a serial configuration, and we set the spectral function for the baths to be constant and identical, $\Gamma = \Gamma_L = \Gamma_R$. The N serial quantum dots are described by a tight-binding model with onsite energy ϵ_d and hopping parameter Ω . The transmission function is calculated in a standard way from the Green's function of the system and self energy of the baths [151, 177].

In Fig. 5.2(a), we display the ratio $R_1/6G_1$ as a function of Γ and demonstrate the violation ($R_1/6G_1 < 0$) of the TUR within a certain range of this coupling. We compute R_1 following Eq. (5.21) and G_1 , the linear response coefficient of the current, is computed using Eq. (5.19). Here we present results for $N = 3$ and $N = 4$. Interestingly, the violation weakly depends on the number of quantum dots in the setup, and in fact for the present parameters, results saturate beyond $N = 4$. We further show in Fig. 5.2(b) that the condition of Eq. (5.28), which was derived under the assumption of resonant tunneling, very well captures the violation region. Note that for $N = 3$ and $N = 4$ the transmission function $\mathcal{T}_{el}(\epsilon)$ for large ϵ decays as $1/\epsilon^6$ and $1/\epsilon^8$ respectively and therefore the integrals in Eq. (5.27) converge.

Figure 5.3 displays a map of $R_1/6G_1$, while extending beyond the resonant tunneling limit, with ϵ_d exceeding T . Negative values correspond to the breakdown of the TUR, and we identify a significant basin of TUR violation when $\Gamma \ll \epsilon_d < T$.

5.5 Fate of single-affinity TUR in presence of magnetic field

A similar analysis for the TUR ratio expressed in terms of the transport coefficients like before can be performed in the case when an external magnetic field B is applied, leading to a breakdown of time-reversal symmetry. In this case, the SSFS modifies to [176]

$$\lim_{t \rightarrow \infty} \frac{1}{t} \ln \left[\frac{p(Q = It, B)}{p(Q = -It, -B)} \right] = \Delta\beta I. \quad (5.29)$$

As a result, symmetry relations among various transport coefficients, see Eq.(5.6), that were derived using SSFS, Eq.(5.4), will no longer be true with the exception of Green-Kubo formula. Instead the symmetric/antisymmetric combination of transport coefficients will satisfy symmetry relation similar to Eq.(5.6). More concretely symmetrized transport

coefficient corresponding to average current is defines as,

$$G_i^\pm \equiv G_i \pm \bar{G}_i \quad (5.30)$$

where over-bar represents transport coefficient in presence of reversed magnetic field. Similarly one can define symmetrized transport coefficients for higher order cumulants. Note that in absence of the magnetic field all the antisymmetric transport component will be zero. Interestingly, for symmetric combination we recover all the symmetry relation that were derived in absence of magnetic field in Eq.(5.6). And we get following relations for antisymmetric combination,

$$G_2^- = \frac{S_1^-}{3} = \frac{R_0^-}{6} \quad (5.31)$$

Note that in general, the equilibrium component of the odd cumulants except average is not zero in the presence of the magnetic field. Utilizing above relations, TUR ratio can be expressed as

$$\Delta\beta \frac{\langle I^2 \rangle_c}{\langle I \rangle} = 2 + \frac{(\Delta\beta)}{3G_1} R_0 + \frac{(\Delta\beta)^2}{6G_1} \left[\frac{G_2 R_0}{G_1} + (3S_2 - 2G_3) \right] + \mathcal{O}(\Delta\beta)^3 + \dots$$

(5.32)

From the above expression, we make the following observations:

- Validity of T-TUR now depends on the equilibrium component of skewness in linear order regime and can be possibly violated by just reversing the sign of $\Delta\beta$.
- For two terminal non-interacting models scaled cumulant generating function $\mathcal{G}(\chi, B)$ is an even function of magnetic field B [178–180]. As a result all the antisymmetrized transport coefficients are zero and we recover all the results derived in absence of magnetic field.
- For interacting models one can have very general dependence of $\mathcal{G}(\chi, B)$ on magnetic field B . Consequently, T-TUR can have linear dependence in $\Delta\beta$. Now this property can be used to probe the many body interaction in the system.

As a final remark, if we symmetrize the TUR ratio then we recover the perturbative series which we obtained for time-reversal symmetric case but with transport coefficients also symmetrized. More precisely,

$$\Delta\beta \frac{\langle I^2 \rangle_c + \langle \bar{I}^2 \rangle_c}{\langle I \rangle + \langle \bar{I} \rangle} = 2 + \frac{(\Delta\beta)^2}{6G_1^+} R_1^+ + \mathcal{O}(\Delta\beta)^3 + \dots \quad (5.33)$$

5.6 Summary

We used the universal steady state fluctuation symmetry (SSFS) to explore the validity of the TUR in thermal transport problems. From the SSFS, we wrote down relationships between transport coefficients and organized an expression for the TUR, which was perturbative in the affinity $\Delta\beta$, and given in terms of nonlinear transport coefficients. The first central result of this work is that the negative skewness (to the lowest order in the perturbative expansion around equilibrium) reveals TUR violations. Our expansion, building the TUR, is universally valid for quantum and classical problems, as well as for arbitrary interactions in the conducting system.

The second important result of our work is the proof that the TUR is satisfied in harmonic junctions, classical and quantum, irrespective of the underlying stochastic dynamics.

Finally, we studied the TUR in fermionic chains. Here, we focused on the resonant transport limit where an analytical condition for TUR violation was derived, demonstrated to be in quantitative agreement with simulations. The TUR was satisfied when electron transmission probability was small (Poissonian statistics). Violations were identified within a certain range of the system-bath hybridization energy.

The thermodynamic uncertainty relation attracts significant interest given its impact on the performance of thermal machines. Unlike in [70], which was focused on quantum charge transport and assumed noninteracting electrons, the present deals with heat exchange in classical and quantum systems, and it exposes that the validity of the TUR depends on the statistics of the participating particles.

CHAPTER 6

Thermodynamic uncertainty relation for energy transport in transient regime

Abstract

We investigate the transient version of the thermodynamic uncertainty relation (TUR) which provides a precision-cost trade-off relation for certain out-of-equilibrium thermodynamic observables in terms of net entropy production. We explore this relation in the context of energy transport in a bipartite setting for three exactly solvable toy model systems (two coupled harmonic oscillators, two coupled qubits, and a hybrid coupled oscillator-qubit system) and analyze the role played by the underlying statistics of the transport carriers in the TUR. Interestingly, for all these models, depending on the statistics, the TUR ratio can be expressed as a sum or a difference of a universal term which is always greater than or equal to 2 and a corresponding entropy production term. We find that the generalized version of the TUR, originating from the universal fluctuation symmetry, is always satisfied. However, interestingly, the specialized TUR, a tighter bound, is always satisfied for the coupled harmonic oscillator system obeying Bose-Einstein statistics. Whereas, for both the coupled qubit, obeying Fermi-like statistics, and the hybrid qubit-oscillator system with mixed Fermi-Bose statistics, violation of the tighter bound is observed in certain parameter regimes. We also provide a rigorous proof following the nonequilibrium Green's function approach that the tighter bound is always satisfied in the weak-coupling regime for generic bipartite systems.

Reported in

S. Saryal, O. Sadekar, and B. K. Agarwalla, *Thermodynamic uncertainty relation for energy transport in a transient regime: A model study*, [Phys. Rev. E 103, 022141 \(2021\)](#).

6.1 Introduction

In previous chapter we assessed the tightest version of the TUR for steady-state thermal transport junction and showed that its validity relies on the statistics of the participating carriers. In this chapter we will investigate the transient version of TUR for energy transport in a bipartite setting for three exactly solvable toy model systems, two coupled harmonic oscillators, two coupled qubits, and a hybrid coupled oscillator-qubit system, and analyze the role played by the underlying statistics of the transport carriers. Since it is well known that quantum statistics plays a key role in the transport properties, we ask how does it affect the transient TUR bounds?

We will consider energy exchange that takes place between two quantum systems which are initially equilibrated at different temperatures. For such transport, a non-universal tighter version of the TUR bound (T-TUR) is given as

$$\frac{\langle Q^2 \rangle_c}{\langle Q \rangle^2} \geq \frac{2}{\langle \Sigma \rangle}, \quad (6.1)$$

where Q , a stochastic variable, is the integrated energy current over a certain time duration T . $\langle Q \rangle$, $\langle Q^2 \rangle_c$ represents the average energy exchange and the corresponding noise, respectively. $\langle \Sigma \rangle \geq 0$ represents the average entropy production in the energy exchange process which is always non-negative and further characterizes how far the composite system is driven away from the initial condition.

A loose but a generalized version of the bound (G-TUR1) compared to Eq. (6.1) [72] was recently derived following the fundamental energy exchange fluctuation relation (XFT) [59] where the RHS of Eq. (6.1) was modified to

$$\frac{\langle Q^2 \rangle_c}{\langle Q \rangle^2} \geq \frac{2}{\exp \langle \Sigma \rangle - 1}. \quad (6.2)$$

In fact, a tighter version (still loose compared to Eq. (6.1)) of the generalized bound in Eq. (6.2) was obtained by Timpanaro *et al.* [71](G-TUR2), given as

$$\frac{\langle Q^2 \rangle_c}{\langle Q \rangle^2} \geq f(\langle \Sigma \rangle), \quad (6.3)$$

where $f(x) = \text{csch}^2(g(x/2))$ and $g(x)$ is the inverse function of $x \tanh(x)$.

Of course, it is clear that, systems satisfying XFT will follow the G-TUR1 and G-TUR2. However, it is still an interesting question to ask under what conditions the tighter version i.e., the T-TUR bound in Eq. (6.1) will be preserved. Very recently, the usefulness of the T-TUR bound was proposed to infer the net entropy production for complex non-equilibrium systems [76].

Interestingly, we find that when energy exchange takes place between two simple quantum harmonic oscillators, obeying Bose-Einstein statistics, the T-TUR in Eq. (6.1) is always satisfied. Whereas, in the other extreme scenario, i.e., when each system consists of a single qubit, following Fermi-like statistics, violation for the T-TUR is observed in certain parameter regimes. As a final interesting example, we consider a hybrid setup consisting of a single quantum harmonic oscillator and a qubit and analyze the impact of hybrid-statistics on TUR. These findings are reminiscent of the results obtained in the previous chapter where steady state T-TUR was shown to be valid for coupled harmonic-oscillator system and violation of T-TUR was reported for non-interacting electrons. We also show that for general bipartite setup, the T-TUR is always satisfied in the weak-coupling regime. Expectedly, in all these setups, the generalized version of TUR (GTUR-1, GTUR-2) is always satisfied due to the validity of underlying XFT for energy exchange for these models.

We organize the chapters as follows: In Sec. (6.2) we introduce three toy models, provide derivation for the exact characteristic function, and analyze the corresponding TUR. In Sec. (6.3) we provide a proof for the T-TUR in the weak-coupling regime in both transient and steady-state limits. In Sec. (6.4) we examine the quadratic-bound proposed for cumulant generating function in [136] for our model systems. We summarize our main findings in Sec. (6.5).

6.2 Models and TUR

6.2.1 Two-oscillator system

As a first example, we consider a bipartite setup where each system consists of a single quantum harmonic oscillator (see Fig. (6.1a)). The total Hamiltonian is given as

$$H_{\text{osc}} = \omega_0 a_1^\dagger a_1 \otimes \mathbb{1}_2 + \mathbb{1}_1 \otimes \omega_0 a_2^\dagger a_2 + J (a_1^\dagger \otimes a_2 + a_1 \otimes a_2^\dagger). \quad (6.4)$$

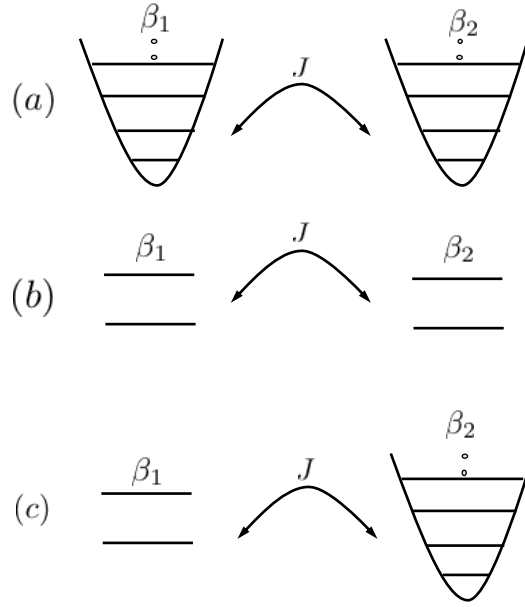


Figure 6.1: Schematic for three different toy models that we investigate in this chapter: (a) coupled two-oscillator system, (b) coupled two-qubit system, and (c) coupled hybrid qubit-oscillator system. Each system is prepared initially in equilibrium at a particular inverse temperature $\beta_i = 1/k_B T_i$, $i = 1, 2$. A finite thermal coupling with coupling strength J allows energy exchange between the systems. Figure reproduced with permission from Ref. [75].

where the first two terms ($H_1 = \omega_0 a_1^\dagger a_1 \otimes 1_2$ and $H_2 = 1_1 \otimes \omega_0 a_2^\dagger a_2$) correspond to two non-interacting quantum harmonic oscillators with $a_i (a_i^\dagger)$ being the bosonic annihilation (creation) operator for the i -th oscillator. The last term, we denote here as V , represents a bilinear interaction between the oscillators with coupling strength J . Note that the frequency of both the oscillators (ω_0) is chosen to be identical which ensures the thermal coupling condition i.e., $[V, H_1 + H_2] = 0$. Recall that, before turning on the interaction V , each oscillator is thermalized independently at a particular temperature which can be achieved by placing the system in weak contact with a thermal bath. After that, the oscillators are separated from the bath and the interaction between them is turned on to allow energy exchange for a certain duration T . The corresponding Cumulant Generating Function (CGF) $\mathcal{G}_T^{\text{osc}}(u) = \ln Z_T^{\text{osc}}(u)$ can be obtained exactly using the Keldysh non-equilibrium Green's function (NEGF) approach [181, 182], given by,

$$\mathcal{G}_T^{\text{osc}}(u) = -\ln \left[1 - \sin^2(JT) \left\{ n_1(\omega_0)(1 + n_2(\omega_0))(e^{iu\omega_0} - 1) + n_2(\omega_0)(1 + n_1(\omega_0))(e^{-iu\omega_0} - 1) \right\} \right], \quad (6.5)$$

where $n_i(\omega_0) = (e^{\beta_i \omega_0} - 1)^{-1}$, $i = 1, 2$ is the Bose-Einstein distribution function. Note that, a similar model was previously studied in the context of fluctuation symmetry where the CGF was obtained only in the weak-coupling regime [63]. Very recently, this model is studied in the context of quantum heat engines [183]. It is easy to verify that the above CGF expression preserves the XFT for arbitrary T, J, β_1 and β_2 . We now lay down the derivation for $\mathcal{G}_T^{\text{osc}}(u)$ following the Keldysh formalism: We begin with Eq. (1.14) and organize the characteristic function in the interaction picture as,

$$\begin{aligned} Z_T(u) &= \int dQ e^{iuQ} p_T(Q), \\ &= \text{Tr} \left[\mathcal{U}_I^\dagger(T, 0) (e^{-iuH_1} \otimes 1_2) \mathcal{U}_I(T, 0) (e^{iuH_1} \otimes 1_2) \rho(0) \right], \end{aligned}$$

where $U_I(t, 0) = \mathcal{T} \exp \left[-i \int_0^t V_I(t') dt' \right]$ with \mathcal{T} being the time-ordered operator and $V_I(t) = e^{iH_0 t} V e^{-iH_0 t}$, $H_0 = H_1 + H_2$. Recall that, the composite density matrix is decoupled at the initial time $t = 0$ with each system is in thermal equilibrium at a particular temperature i.e., $\rho(0) = \rho_1 \otimes \rho_2 = \frac{e^{-\beta_1 H_1}}{\mathcal{Z}_1} \otimes \frac{e^{-\beta_2 H_2}}{\mathcal{Z}_2}$. This condition imply $[\rho(0), H_0] = 0$. The above equation then can be organized as

$$Z_T(u) = \text{Tr} \left[\rho(0) [U_I^\dagger]^{u/2}(T, 0) U_I^{-u/2}(T, 0) \right], \quad (6.6)$$

where now both the forward and backward evolution operators are dressed by the counting field u . This expression can be recast on a Keldysh contour as (see Fig. (6.2))

$$Z_T(u) = \text{Tr} \left[\rho(0) T_c e^{-i \int_c V_I^x(\tau) d\tau} \right], \quad (6.7)$$

where T_c is the contour-ordered operator, which orders operators according to their contour time argument: an earlier (later) contour time places the operator to the right (left). Therefore, the upper (lower) branch corresponds to the forward (backward) evolution. $x(\tau)$ is a contour time dependent function which can take two possible values depending on the location of τ on the contour branch. Here $x^+(t) = -u/2$ for the upper branch (denoted by the $+$ sign) and $x^-(t) = u/2$ for the lower branch (denoted by the $-$ sign) within the measurement time interval $[0, \tau]$. $x^\pm(t) = 0$ outside the measurement time. Finally $V_I^x(\tau) = e^{ixH_1} V_I(\tau) e^{-ixH_1}$ is the modified contour-time dependent operator dressed by the counting field. Note that, the operator V^x is time-independent even in the interaction picture

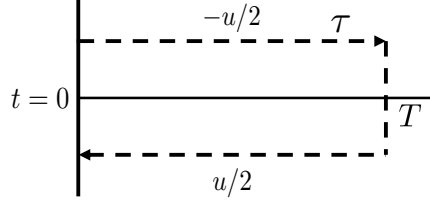


Figure 6.2: The complex time Keldysh Contour with upper and lower branch. The contour path begins from $t = 0$, goes to maximum time $t = T$ and then comes back to $t = 0$ again. The upper (lower) branch corresponds to time-ordered forward (anti-time-ordered backward) evolution propagator. For energy counting statistics problem the Hamiltonian is dressed differently in the upper ($-u/2$) and the lower ($+u/2$) branch by the counting parameter u . τ is the contour-time parameter. Figure reproduced with permission from Ref. [75].

due to the commutable coupling symmetry. Note that, the operator V^x is time-independent even in the interaction picture due to the commutable coupling symmetry.

Invoking the linked-cluster theorem for the CGF, $\mathcal{G}_T^{\text{osc}}(u) = \ln Z_T(u)$, we receive a formal exact expression for the model in contour-time τ as,

$$\mathcal{G}_T^{\text{osc}}(u) = -\text{Tr}_\tau \ln \left[1 - g_{22} \Sigma_{11}^x \right]. \quad (6.8)$$

Here the Green functions are understood as matrices in discretized contour time. In continuous time version the trace operation means $\text{Tr}_\tau[A B] = \int d\tau \int d\tau' A(\tau, \tau') B(\tau', \tau)$. In the above expression, following the standard notations for the Green functions, we define

$$g_{ii}(\tau, \tau') = -i \langle T_c a_i(\tau) a_i^\dagger(\tau') \rangle, \quad i = 1, 2 \quad (6.9)$$

$$g_{ii}^x(\tau, \tau') = -i \langle T_c a_i^x(\tau) a_i^{x\dagger}(\tau') \rangle, \quad i = 1, 2 \quad (6.10)$$

as the bare (Eq. 6.9) and the counting field dependent (Eq. 6.10) Greens function, respectively. Recall that, the counting field appears only for system 1 operators. The self-energy term is then given as $\Sigma_{11}^x(\tau, \tau') = J^2 g_{11}^x(\tau, \tau')$ with J being the coupling strength between the oscillators. Since $a_1^x(\tau) = e^{ixH_1} a_1(\tau) e^{-ixH_1} = a_1(\tau + x(\tau))$, it is thus clear that the effect of measuring or counting energy leads to a shift in contour-time and correspondingly the self-energy is shifted as

$$\Sigma_{11}^x(\tau, \tau') = \Sigma_{11}(\tau + x(\tau), \tau' + x(\tau')). \quad (6.11)$$

Eq. (6.8) doesn't explicitly satisfy the normalization condition $\mathcal{G}_T^{\text{osc}}(u = 0) = 0$. To enforce

this condition, one can further simplify the above expression and write

$$\begin{aligned}
1 - g_{22}\Sigma_{11}^x &= g_{22}\left(g_{22}^{-1} - \Sigma_{11}^x\right) \\
&= g_{22}\left(g_{22}^{-1} - \Sigma - \Sigma_{11}^A\right) \\
&= g_{22}\left(G_{22}^{-1} - \Sigma_{11}^A\right) \\
&= g_{22}G_{22}^{-1}\left(1 - G_{22}\Sigma_{11}^A\right) \\
&= \left(1 - g_{22}\Sigma_{11}\right)\left(1 - G_{22}\Sigma_{11}^A\right), \tag{6.12}
\end{aligned}$$

where in the second line we define a useful quantity $\Sigma_{11}^A = \Sigma_{11}^x - \Sigma_{11}$ which is zero in the absence of the counting field. The third line motivates one to introduce a new Green's function $G_{22}^{-1} = g_{22}^{-1} - \Sigma_{11}$ which in continuous contour-time version satisfies the following Dyson equation:

$$G_{22}(\tau, \tau') = g_{22}(\tau, \tau') + \int_c \int_c d\tau_1 d\tau_2 g_{22}(\tau, \tau_1) \Sigma_{11}(\tau_1, \tau_2) G_{22}(\tau_2, \tau'). \tag{6.13}$$

Notice that, this Green's function is nothing but the dressed Greens function of system 2, taking into account the presence of system 1 in terms of the self-energy Σ_{11} . With the help of Eq. (6.12), Eq. (6.8) then simplifies to

$$\mathcal{G}_T^{\text{osc}}(u) = -\text{Tr}_\tau \ln \left[1 - G_{22} \Sigma_{11}^A \right] \tag{6.14}$$

as $\text{Tr}_\tau \ln \left[1 - g_{22} \Sigma_{11} \right] = 0$ following Eq. (6.8), ensuring the normalization condition.

The next important task from here on is to go from the contour-time to the real time following the Langreth's theorem. Furthermore, a more transparent and simplified framework is obtained by performing an orthogonal Keldysh rotation (rotation in the space of real time by 45°) which gives

$$\mathcal{G}_T^{\text{osc}}(u) = -\text{Tr}_{t,\sigma} \ln \left[1 - \check{G}_{22} \check{\Sigma}_{11}^A \right]. \tag{6.15}$$

The breve symbol indicates that the Green's functions are written in the rotated Keldysh frame. Also note that, the orthogonal Keldysh rotation preserves the trace in the above CGF expressions. In Eq. (6.15) the meaning of trace is now in terms of the real time and as well as over the branch index, denoted as σ . Explicitly, it means, for example, $\text{Tr}_{t,\sigma}[\check{A} \check{B}] =$

$\int_0^T dt_1 \int_0^T dt_2 \text{Tr}[\check{A}(t_1, t_2)\check{B}(t_2, t_1)]$. We receive the \check{G}_{22} as,

$$\check{G}_{22} = \begin{bmatrix} G_{22}^r & G_{22}^k \\ 0 & G_{22}^a \end{bmatrix}, \quad (6.16)$$

where r, a, k are the retarded, advanced and the Keldysh components for the Green function. These various components can be obtained exactly and are given as follows:

$$\begin{aligned} G_{22}^r(t, t') &= -i\theta(t-t')e^{-i\omega_0(t-t')} \cos(J(t-t')), \\ G_{22}^a(t, t') &= i\theta(t'-t)e^{-i\omega_0(t-t')} \cos(J(t-t')), \\ G_{22}^<(t, t') &= -i \left[n_2 \cos(Jt) \cos(Jt') + n_1 \sin(Jt) \sin(Jt') \right], \\ G_{22}^>(t, t') &= -i \left[(1+n_2) \cos(Jt) \cos(Jt') + (1+n_1) \right. \\ &\quad \left. \sin(Jt) \sin(Jt') \right], \end{aligned} \quad (6.17)$$

and the Keldysh component is given as $G_{22}^k = G_{22}^< + G_{22}^>$. Interestingly, the retarded and the advanced components are time-translational invariant which is not the case for other components. It is easy to check that the lesser and greater components satisfy the correct initial condition, given as $iG_{22}^<(t=t'=0) = \langle a_2^\dagger a_2 \rangle = n_2$ and $iG_{22}^>(t=t'=0) = \langle a_2 a_2^\dagger \rangle = (1+n_2)$. Similarly we receive for the counting field dependent self-energy as

$$\check{\Sigma}_{11}^A = \frac{1}{2} \begin{bmatrix} a-b & a+b \\ -(a+b) & b-a \end{bmatrix}, \quad (6.18)$$

where

$$\begin{aligned} a &= \Sigma_{11}^>(t-t'+u) - \Sigma_{11}^>(t, t'), \\ b &= \Sigma_{11}^<(t-t'-u) - \Sigma_{11}^<(t, t'). \end{aligned} \quad (6.19)$$

The calculation further simplifies upon performing a two-time Fourier transformation, defined here as

$$\check{G}_{22}(\omega_1, \omega_2) = \int_0^T dt \int_0^T dt' e^{i\omega_1 t} e^{i\omega_2 t'} \check{G}_{22}(t, t'). \quad (6.20)$$

One then finally obtains from Eq. (6.15)

$$\mathcal{G}_T^{\text{osc}}(u) = -\ln \det \left[1 - \check{G}_{22}(\omega_0, -\omega_0) \check{\Sigma}_{11}^A(\omega_0) \right]. \quad (6.21)$$

Note that, the above formula is exact for arbitrary coupling J . This expression can be easily extended for many-oscillator setup also. One can now write down the Fourier version of the Green functions components which are given as,

$$\begin{aligned}
G_{22}^r(\omega_0, -\omega_0) &= -\frac{2i}{J^2} \sin^2\left(\frac{JT}{2}\right), \\
G_{22}^a(\omega_0, -\omega_0) &= \frac{2i}{J^2} \sin^2\left(\frac{JT}{2}\right), \\
G_{22}^<(\omega_0, -\omega_0) &= -\frac{i}{J^2} \left[n_2 \sin^2(JT) + n_1 (1 - \cos(JT))^2 \right], \\
G_{22}^>(\omega_0, -\omega_0) &= -\frac{i}{J^2} \left[(1 + n_2) \sin^2(JT) + (1 + n_1) \right. \\
&\quad \left. (1 - \cos(JT))^2 \right], \tag{6.22}
\end{aligned}$$

and similarly for the self-energy components,

$$\begin{aligned}
a &= \Sigma_{11}^>(\omega_0) (e^{-i\hbar\omega_0} - 1) \\
&= -i J^2 (1 + n_1(\omega_0)) (e^{-i\hbar\omega_0} - 1), \tag{6.23}
\end{aligned}$$

$$\begin{aligned}
b &= \Sigma_{11}^<(\omega_0) (e^{i\hbar\omega_0} - 1) \\
&= -i J^2 n_1(\omega_0) (e^{i\hbar\omega_0} - 1). \tag{6.24}
\end{aligned}$$

Knowing these analytical expressions for the Green functions one can simply compute the determinant in Eq. (6.21), which finally gives the CGF expression in Eq. (6.5).

To analyze the TUR bound, we now get the expressions for the average energy change and the associated noise. These are easily obtained by taking successive derivatives of $\mathcal{G}_T^{\text{osc}}(u)$ with respect to iu . We receive, (for notational compactness, below we denote $n_i(\omega_0)$ as n_i)

$$\langle Q \rangle^{\text{osc}} = \omega_0 \mathcal{T}_T(J) [n_1 - n_2], \tag{6.25}$$

$$\langle Q^2 \rangle_c^{\text{osc}} = \omega_0^2 \left[\mathcal{T}_T(J) (n_1(1+n_2) + n_2(1+n_1)) + \mathcal{T}_T^2(J) (n_1 - n_2)^2 \right], \tag{6.26}$$

where we define $\mathcal{T}_T(J) = \sin^2(JT)$. Since the second term in Eq. (6.26) is always positive, we receive the following inequality,

$$\langle Q^2 \rangle_c^{\text{osc}} \geq \omega_0^2 \mathcal{T}_T(J) (n_1(1+n_2) + n_2(1+n_1)), \tag{6.27}$$

where the equality sign corresponds to equilibrium situation i.e., $\beta_1 = \beta_2$. We now make use of the following important relation involving the Bose-Einstein distribution function,

$$n_1(1+n_2) + n_2(1+n_1) = \coth\left(\frac{\Delta\beta\omega_0}{2}\right) (n_1 - n_2) \quad (6.28)$$

$$\geq \frac{2}{\Delta\beta\omega_0} (n_1 - n_2), \quad (6.29)$$

where $\Delta\beta = \beta_2 - \beta_1$. In the second line we have used the inequality $x \coth(x) \geq 1$. Substituting this in Eq. (6.27) and using Eq. (6.25), it is easy to see that

$$\Delta\beta \frac{\langle Q^2 \rangle_c^{\text{osc}}}{\langle Q \rangle^{\text{osc}}} \geq 2 \quad (6.30)$$

which imply that for the coupled quantum harmonic oscillator setup displaying bosonic statistics the T-TUR is always satisfied. In fact, an interesting observation can be made by arranging the TUR ratio $\left(\Delta\beta \frac{\langle Q^2 \rangle_c^{\text{osc}}}{\langle Q \rangle^{\text{osc}}}\right)$ using the expressions for the cumulants (Eq. (6.25) and Eq. (6.26)) and Eq. (6.28). One receives,

$$\Delta\beta \frac{\langle Q^2 \rangle_c^{\text{osc}}}{\langle Q \rangle^{\text{osc}}} = \Delta\beta\omega_0 \coth \frac{\Delta\beta\omega_0}{2} + \langle \Sigma \rangle^{\text{osc}} \geq 2. \quad (6.31)$$

Interestingly, the first term here is independent of the coupling information between the systems and is always greater or equal to 2 (equality holds in equilibrium). In contrast, the second term, is exactly the average entropy production for the oscillator system which along with the temperature difference also importantly depends on the dimensionless coupling JT . As the average entropy production always remains positive, $\langle \Sigma \rangle^{\text{osc}} \geq 0$, once again we arrive at the same conclusion that the T-TUR for this setup is always satisfied. Also note that the validity T-TUR immediately implies that the GTUR-1 (Eq. (6.2)) and G-TUR2 (6.3) are also trivially obeyed.

In Fig. (6.3(a)) we plot the first two cumulants and the corresponding TUR ratio as a function of JT . Fig. (6.3(b)) corresponds to a two-dimensional plot for the TUR ratio as a function of JT and $\beta_2\omega_0$. We set $\beta_1\omega_0 = 0.1$ in the simulation. The cumulants as well as the TUR ratio oscillates with JT with periodicity π . The value for TUR ratio is always larger than 2 and matches with the theoretical prediction. For a fixed value of JT , the TUR ratio increases monotonically with increasing $\Delta\beta$.

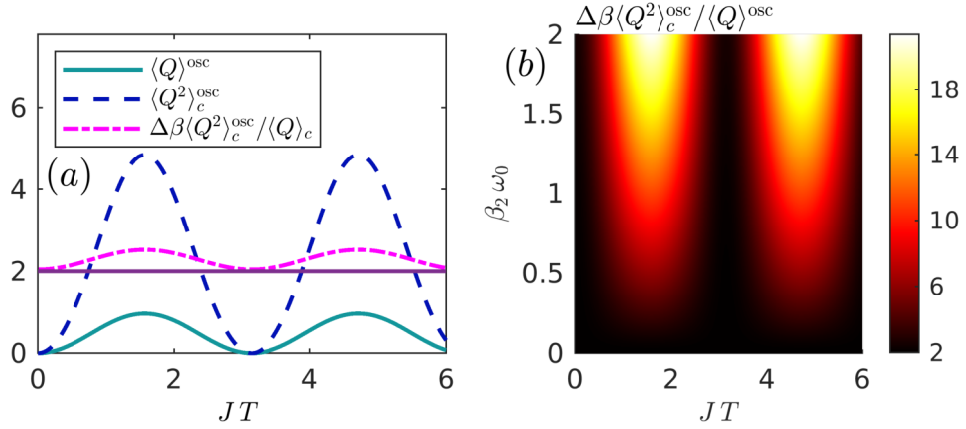


Figure 6.3: (a) Plot for average energy change $\langle Q \rangle_c^{\text{osc}}$ (solid), fluctuation $\langle Q^2 \rangle_c^{\text{osc}}$ (dashed) and the corresponding TUR ratio $\Delta\beta\langle Q^2 \rangle_c^{\text{osc}}/\langle Q \rangle_c^{\text{osc}}$ (dashed-dotted) as a function of JT . For reference a line is drawn at the value 2. The parameters are $\beta_1\omega_0 = 0.5$, $\beta_2\omega_0 = 1$. (b) Two-dimensional plot for TUR ratio $\Delta\beta\langle Q^2 \rangle_c^{\text{osc}}/\langle Q \rangle_c^{\text{osc}}$ as a function of JT and $\beta_2\omega_0$. We set $\beta_1\omega_0 = 0.1$. Figure reproduced with permission from Ref. [75].

6.2.2 Two-qubit system

We next consider another toy model, which we refer here as the XY-model, consisting of two qubits (see Fig. (6.1b)). We write the total Hamiltonian as

$$H_{XY} = \frac{\omega_0}{2}\sigma_1^z \otimes 1_2 + 1_1 \otimes \frac{\omega_0}{2}\sigma_2^z + \frac{J}{2}(\sigma_1^x \otimes \sigma_2^y - \sigma_1^y \otimes \sigma_2^x). \quad (6.32)$$

$\sigma_i, i = x, y, z$ are the standard Pauli matrices. Once again, this model satisfies the thermal coupling condition.

One can analytically compute the CGF of energy exchange following Eq. (1.14) by performing simple algebraic manipulations of the Pauli matrices which yield [184]

$$\mathcal{G}_T^{\text{spin}}(u) = \ln \left[1 + \sin^2(JT) \left\{ f_1(\omega_0)(1 - f_2(\omega_0))(e^{iu\omega_0} - 1) + f_2(\omega_0)(1 - f_1(\omega_0))(e^{-iu\omega_0} - 1) \right\} \right], \quad (6.33)$$

where $f_i(\omega_0) = (e^{\beta_i\omega_0} + 1)^{-1}$, $i = 1, 2$ is the Fermi like distribution function. Once again the XFT is obeyed for arbitrary J, T, β_1 and β_2 due to the thermal coupling symmetry. At this point, it is important to compare the CGF in eq. (6.33) with the CGF for the coupled oscillator (Eq. (6.5)). First of all, for both these models, interestingly the JT dependence appears in the same functional form $\mathcal{T}_T(J) = \sin^2(JT)$. In fact, in this context it is simply

the transition probability between states $|01\rangle$ and $|10\rangle$ i.e., $\mathcal{T}_T(J) = |\langle 10|\mathcal{U}(T,0)|01\rangle|^2$ [$|0\rangle$ ($|1\rangle$) refers to the ground (excited) state for the qubit]. Second and most importantly, there are crucial sign differences in terms of the Bose and Fermi like functions, reflecting the key difference between a two-level spin system and an infinite-level harmonic oscillator system. In fact, because of this crucial sign change for the qubit setup, a looser bound for TUR appears, as we show below. We once again write down the first two cumulants following the CGF as

$$\langle Q \rangle^{\text{spin}} = \omega_0 \mathcal{T}_T(J) [f_1 - f_2], \quad (6.34)$$

$$\langle Q^2 \rangle_c^{\text{spin}} = \omega_0^2 \left[\mathcal{T}_T(J) (f_1(1-f_2) + f_2(1-f_1)) - \mathcal{T}_T^2(J) (f_1 - f_2)^2 \right], \quad (6.35)$$

Interestingly, for Fermi like function also a relation similar to Eq. (6.28) exists, given as

$$f_1(1-f_2) + f_2(1-f_1) = \coth \frac{\Delta\beta\omega_0}{2} (f_1 - f_2). \quad (6.36)$$

This helps us to organize the cumulants and to receive the TUR ratio as

$$\Delta\beta \frac{\langle Q^2 \rangle_c^{\text{spin}}}{\langle Q \rangle^{\text{spin}}} = \Delta\beta\omega_0 \coth \left[\frac{\Delta\beta\omega_0}{2} \right] - \langle \Sigma \rangle^{\text{spin}}. \quad (6.37)$$

Once again this expression should be compared with Eq. (6.31). The first term is the same as before. However, the apparent sign differences between the two models reflects in the second term where the average entropy production term appears as a negative contribution to TUR ratio. It is therefore not immediately obvious that, this coupled two-qubit model will satisfy the T-TUR bound. In what follows we therefore first get an upper bound on the average entropy production and thereby provide a lower bound for the TUR. Interestingly, this helps us to find a condition on $\mathcal{T}_T(J)$ for which the T-TUR is respected.

We first note that, the Fermi-like function can be alternatively written as,

$$f_i = \frac{1}{e^{\beta_i\omega_0} + 1} = \frac{1}{2} \left(1 - \tanh \frac{\beta_i\omega_0}{2} \right). \quad (6.38)$$

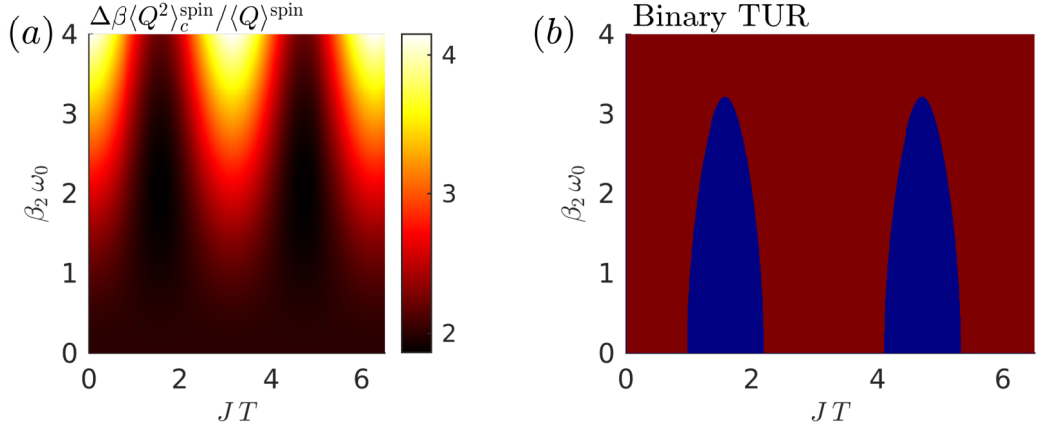


Figure 6.4: (a) Two-dimensional plot for TUR ratio ($\Delta\beta\frac{\langle Q^2 \rangle_c^{\text{spin}}}{\langle Q \rangle^{\text{spin}}}$) for the coupled two-qubit system as a function of JT and $\beta_2\omega_0$. We set $\beta_1 = 0$. (b) Corresponding binary plot of TUR. The violation (validity) regime of the T-TUR bound is colored by blue (dark red). Figure reproduced with permission from Ref. [75].

With the help of this expression, we write down the net entropy production as,

$$\begin{aligned} \langle \Sigma \rangle^{\text{spin}} &= \frac{\Delta\beta\omega_0\mathcal{T}_T(J)}{2} \left[\tanh \frac{\beta_2\omega_0}{2} - \tanh \frac{\beta_1\omega_0}{2} \right] \\ &= \frac{\Delta\beta\omega_0\mathcal{T}_T(J)}{2} \left[\left(\tanh \frac{\Delta\beta\omega_0}{2} \right) \left(1 - \tanh \frac{\beta_1\omega_0}{2} \tanh \frac{\beta_2\omega_0}{2} \right) \right]. \end{aligned} \quad (6.39)$$

Now since β_i is always positive and $\tanh x$ is bounded function between (0,1) for $x > 0$, the second term in the product in the above equation is always < 1 , which gives us

$$\tanh \frac{\Delta\beta\omega_0}{2} \geq \tanh \frac{\beta_2\omega_0}{2} - \tanh \frac{\beta_1\omega_0}{2} \quad (6.40)$$

and therefore, we receive an upper bound for the average entropy production,

$$\langle \Sigma \rangle^{\text{spin}} \leq \frac{\Delta\beta\omega_0\mathcal{T}_T(J)}{2} \tanh \frac{\Delta\beta\omega_0}{2}, \quad (6.41)$$

which finally translates to a lower bound on TUR ratio for this model as

$$\Delta\beta\frac{\langle Q^2 \rangle_c^{\text{spin}}}{\langle Q \rangle^{\text{spin}}} \geq \Delta\beta\omega_0 \left[\coth \frac{\Delta\beta\omega_0}{2} - \frac{\mathcal{T}_T(J)}{2} \tanh \frac{\Delta\beta\omega_0}{2} \right]. \quad (6.42)$$

The equality sign here holds for $\beta_1 = 0$ or at equilibrium. Since the TUR ratio is periodic as a function of JT , we focus our attention within the first period $[0, \pi]$. The obtained bound indicates that, in the weak-coupling limit, i.e., $JT \ll 1$ which implies $\mathcal{T}_T(J) \ll 1$, the

second term in the above expression can be ignored and the T-TUR will be satisfied. In fact, it is easy to check that the T-TUR will remain to be valid for $\mathcal{T}_T(J) < 2/3$ which gives an allowed range for JT , ($JT \leq 0.95$ and $JT \geq 2.19$, within the first period). Therefore, to observe a violation for the T-TUR, a necessary condition is to tune the value of JT such that $\mathcal{T}_T(J) > 2/3$. However, note that, this condition is not a sufficient one. This can be seen as follows: following the RHS of Eq. (6.42), the minimum value for the TUR bound corresponds to $\mathcal{T}_T(J) = 1$. Now for large $\Delta\beta$ ($\Delta\beta\omega_0 \gg 1$), both \coth and \tanh functions saturate to value unity ($\Delta\beta\omega_0 \approx 6$) which imply that the TUR bound scales as $\Delta\beta\omega_0/2$ and the T-TUR will be satisfied. Therefore, along with the condition $\mathcal{T}_T(J) > 2/3$, the violation of T-TUR in this case requires a careful tuning of β_1, β_2 , and ω_0 .

In Fig. (6.4(a)) we display a two-dimensional plot for TUR as a function of $\beta_2\omega_0$ and JT . We set $\beta_1\omega_0 = 0$. Fig (6.4(b)) is the corresponding binary plot differentiating the validity (dark-red) and the violation regimes (blue) of the T-TUR. We clearly observe a regime for which T-TUR is not valid and the results nicely match with our theoretical predictions. As mentioned earlier, for sufficiently large $\Delta\beta$ ($\Delta\beta\omega_0 > 3.2$), the T-TUR bound is always satisfied. In contrast, the minimum value of the TUR bound is found to be ≈ 1.86 which occurs for maximum transition probability $\mathcal{T}_T(J) = 1$ i.e, $JT = \pi/2$ and $\Delta\beta\omega_0 \approx 2.01$.

In Fig. (6.5) we show that the TUR bound obtained in Eq. (6.42) is in fact a tighter one compared to the generalized bound (Eq. (6.2) and Eq. (6.3)). More importantly, we observe that the generalized bound obtained from fluctuation symmetry becomes loose with increasing $\Delta\beta$ whereas the obtained bound closely follow the actual TUR trend. In fact, for large $\Delta\beta$, the net entropy production $\langle \Sigma \rangle$ scales as $\Delta\beta$, hence the G-TUR1 behaves as $2\langle \Sigma \rangle / e^{\langle \Sigma \rangle}$ which tends to zero whereas the TUR bound obtained in Eq. (6.42) scales as $\Delta\beta\omega_0/2$. As expected, G-TUR2 performs a bit better than G-TUR1.

Recently, we collaborated with an experimental group and realized this model in the nuclear magnetic resonance (NMR) setup to assess the validity of the transient T-TUR by obtaining the cumulants of energy exchange following the quantum state tomography technique [109]. We found out that the experimental findings were in a very good agreement with our theoretical predictions. Also, we were able to experimentally access the regimes where T-TUR was not respected. The same model was also used earlier to examine the

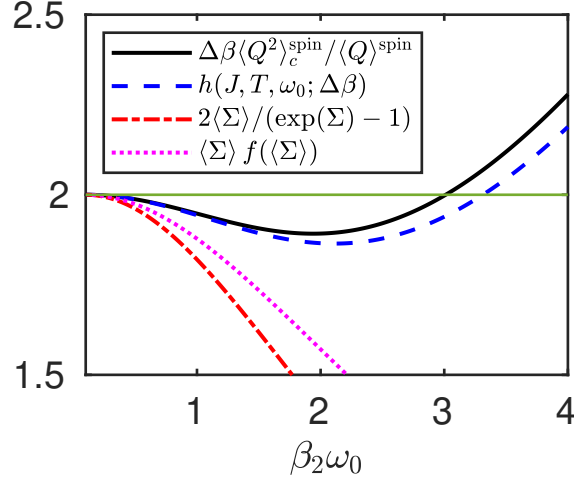


Figure 6.5: Comparison between the TUR bounds obtained in Eq. (6.42), (blue, dashed), denoted here by $h(J, T, \omega_0; \Delta\beta) = \Delta\beta\omega_0 \left[\coth \frac{\Delta\beta\omega_0}{2} - \frac{\mathcal{T}_T(J)}{2} \tanh \frac{\Delta\beta\omega_0}{2} \right]$, the generalized bounds, GTUR-1 (red, dashed-dotted) in Eq. (6.2) and GTUR-2 (magenta, dotted) in Eq. (6.3) with the actual TUR value (black, solid). For reference a line is drawn at the value 2. The parameters are $\beta_1\omega_0 = 0.1$, and $JT = \pi/2$. The bound in Eq. (6.42) closely follow the actual TUR trend. Figure reproduced with permission from Ref. [75].

XFT by measuring the CF for heat exchange employing the ancilla-based interferometric technique [184–187].

6.2.3 Hybrid spin-oscillator system

As a final toy model example we consider a hybrid system consisting of a single qubit and a single quantum harmonic oscillator (see Fig. (6.1(c)), once again interacting via a thermal coupling term. The total Hamiltonian is given as

$$H_{\text{JC}} = \frac{\omega_0}{2} \sigma_z \otimes 1_1 + 1_2 \otimes \omega_0 a^\dagger a + J (a^\dagger \otimes \sigma^- + a \otimes \sigma^+). \quad (6.43)$$

where $\sigma^\pm = \frac{\sigma_x \pm i\sigma_y}{2}$ are the spin ladder operators. This model is in fact the famous Jaynes-Cummings (JC) model and is one of the most well studied setup in quantum optics. We are interested here to analyze the quantum thermodynamics properties for this model and compute the exact CGF for the energy exchange. We provide here a brief outline of the derivation.

Starting from Eq. (1.14) we switch to the interaction picture with respect to the bare part of the Hamiltonian (the first two terms of Eq. (6.43)) and compute the total unitary

propagator in the qubit basis. We receive [188]

$$U_I(t) = e^{-iVt} = \begin{bmatrix} \cos(\sqrt{aa^\dagger}Jt) & -i\frac{\sin(\sqrt{aa^\dagger}Jt)}{\sqrt{aa^\dagger}}a \\ -i\frac{\sin(\sqrt{a^\dagger a}Jt)}{\sqrt{a^\dagger a}}a^\dagger & \cos(\sqrt{a^\dagger a}Jt) \end{bmatrix}, \quad (6.44)$$

where we have used the convention that $[U_I(t)]_{11} = \langle e|U_I(t)|e\rangle$, $[U_I(t)]_{12} = \langle e|U_I(t)|g\rangle$, $[U_I(t)]_{21} = \langle g|U_I(t)|e\rangle$, and $[U_I(t)]_{22} = \langle g|U_I(t)|g\rangle$. Note that because of the commutable coupling condition, in the interaction picture, the time-ordered operator in the unitary propagator does not play any role. With the help of this exact unitary operator and carrying out the calculation in the qubit basis, the exact CGF can be written down as,

$$\mathcal{G}_T^{\text{JC}}(u) = \ln \left[1 + \mathcal{Q} \left\{ \frac{f_1}{n_2} (e^{iu\omega_0} - 1) + \frac{(1 - f_1)}{(1 + n_2)} (e^{-iu\omega_0} - 1) \right\} \right], \quad (6.45)$$

where we define the function $\mathcal{Q} = \mathcal{Q}(J, T, \omega_0; \beta_2)$ as

$$\mathcal{Q}(J, T, \omega_0; \beta_2) = \sum_{n=0}^{\infty} e^{-\beta_2 n \omega_0} \sin^2(\sqrt{n}JT). \quad (6.46)$$

We make the following observations here: (i) Unlike the coupled oscillator or the coupled qubit model, for this hybrid setup the transition probability is weighted by the oscillator temperature β_2 as captured by the \mathcal{Q} function. (ii) Because of the hybrid nature of the setup both the Fermi like and the Bose functions appears in the CGF expression. Once again, it is easy to check the validity of XFT for arbitrary J, T and the initial temperatures β_1, β_2 . Note that, in the low-temperature limit of the oscillator i.e., $\beta_2\omega_0 \gg 1$, it is expected that the above result should reproduce the two-qubit CGF. This can be seen as follows: for $\beta_2\omega_0 \gg 1$ only $n = 1$ term contributes to Eq. (6.46). Therefore, the \mathcal{Q} function simplifies to $\mathcal{Q} \approx e^{-\beta_2\omega_0} \sin^2(JT)$ and correspondingly the Bose functions simplifies to $n_2 \approx e^{-\beta_2\omega_0} (1 + e^{-\beta_2\omega_0})$ and $1 + n_2 \approx 1 + e^{-\beta_2\omega_0}$ which gives $\mathcal{Q}/n_2 = (1 - f_2) \sin^2(JT)$ and $\mathcal{Q}/(1 + n_2) = f_2 \sin^2(JT)$ and thus one correctly recovers the two-qubit model CGF, given in Eq. (6.33).

We now investigate the TUR bound and write down the cumulants as,

$$\langle Q \rangle^{\text{JC}} = \omega_0 \mathcal{Q} \left(\frac{f_1}{n_2} - \frac{1-f_1}{1+n_2} \right) = \omega_0 \mathcal{Q} \frac{f_1}{1+n_2} \left(e^{\beta_2 \omega_0} - e^{\beta_1 \omega_0} \right), \quad (6.47)$$

$$\langle Q^2 \rangle_c^{\text{JC}} = \omega_0^2 \mathcal{Q} \left[\left(\frac{f_1}{n_2} + \frac{1-f_1}{1+n_2} \right) - \mathcal{Q} \left(\frac{f_1}{n_2} - \frac{1-f_1}{1+n_2} \right)^2 \right]. \quad (6.48)$$

As expected, the energy exchange in Eq. (6.47) vanishes when both the spin and the oscillator are initially kept at the same temperature. Interestingly, we once again receive a similar identity as in Eq (6.29) but now involving both the Fermi and Bose functions,

$$f_1(1+n_2) + n_2(1-f_1) = \coth \left[\frac{\Delta\beta\omega_0}{2} \right] (f_1(1+n_2) - n_2(1-f_1)), \quad (6.49)$$

which helps us to write the TUR ratio as

$$\Delta\beta \frac{\langle Q^2 \rangle_c^{\text{JC}}}{\langle Q \rangle^{\text{JC}}} = \Delta\beta\omega_0 \coth \frac{\Delta\beta\omega_0}{2} - \langle \Sigma \rangle^{\text{JC}}. \quad (6.50)$$

This expression once again should be compared with Eq. (6.31) and Eq. (6.37). Interestingly, analogous to the previous cases, the first term remains the same. Whereas, the average entropy production term for the hybrid case produces a negative contribution to the TUR ratio, as was the case for the two-qubit model. Therefore, the breakdown of the T-TUR bound can be expected even for this setup. However, note that, in the limit when $\mathcal{Q} \ll 1$, i.e., in the weak-coupling limit, the T-TUR is once again preserved. In Fig. (6.6) we display the two-dimensional plots for the first and second cumulant and the corresponding TUR ratio. Notice that, the cumulants and the corresponding TUR ratio is not entirely periodic as a function of JT , especially in the high-temperature regime $\beta_2\omega_0 \ll 1$. This is clear from the expression for the function \mathcal{Q} . The violation for the T-TUR bound is clearly observed in the binary plot (Fig. (6.6(d))). Expectedly, the low temperature behavior for the TUR ratio is found to be similar with the two-qubit case with clear validity of T-TUR bound beyond $\Delta\beta\omega_0 \approx 3.4$. However, in the high temperature regime the violation regime for the JC model is broader (comparing TUR ratio vs JT within the first period in both Fig. (6.4(b)) and Fig. (6.6(d)) in comparison to the two-qubit case. This is because of the availability of many states for the oscillator leading a significant contribution of the average entropy production.

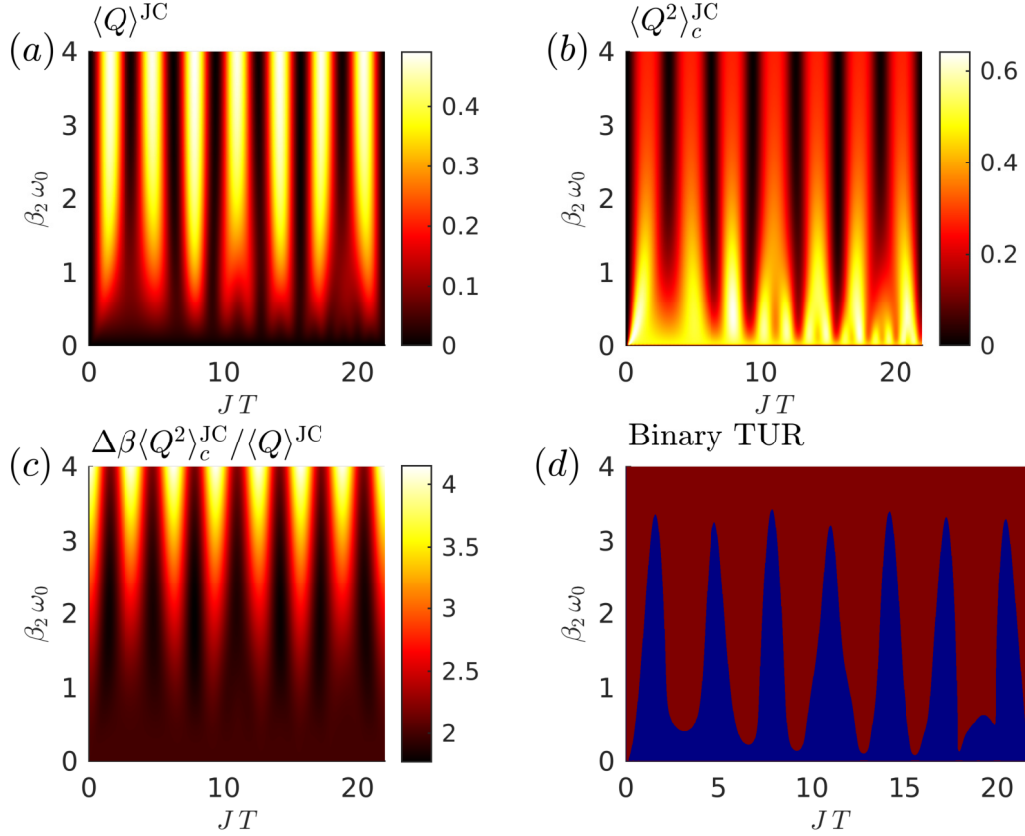


Figure 6.6: Two-dimensional plots for the JC model: (a) average energy change $\langle Q \rangle^{\text{JC}}$, (b) corresponding noise $\langle Q^2 \rangle_c^{\text{JC}}$, (c) the TUR ratio $\Delta\beta \langle Q^2 \rangle_c^{\text{JC}} / \langle Q \rangle^{\text{JC}}$ and (d) binary plot of the same TUR data where the violation (validity) regime of the T-TUR bound is colored by blue (dark red), as a function of JT and $\beta_2 \omega_0$. We set $\beta_1 = 0$. Figure reproduced with permission from Ref. [75].

6.3 Proof of T-TUR for generic bipartite systems in the weak coupling regime

In this section we provide a proof for the tighter bound of TUR (T-TUR) in the weak coupling regime for generic bipartite setup. We again employ here the Keldysh non-equilibrium Green's function approach [181, 182, 189] for the proof. This method is useful to receive a bound in transient as well as in the steady-state regime, as we show below. As mentioned earlier, it is more convenient to work with the logarithm of the characteristic function, $\mathcal{G}_T(u) \equiv \log Z_T(u)$, which according to the linked-cluster theorem [190] contains only the connected diagrams. Since our focus is in weak-coupling regime, we therefore expand the exponential and collect terms up to the leading order in the coupling V that produces non-

zero contribution. It turns out that the first order contribution in V vanishes. This can be shown as follows: The CGF in the first order, denoted by $\mathcal{G}_T^{(1)}(u)$ is given as

$$\begin{aligned}\mathcal{G}_T^{(1)}(u) &= -i \int d\tau \langle V_I^x(\tau) \rangle \\ &= -i \int_0^T dt \left[\langle V_I^{x+}(t) \rangle - \langle V_I^{x-}(t) \rangle \right],\end{aligned}\quad (6.51)$$

where in the second line we transform back to the real time (t) from the contour time (τ) using the Langreth's rule [182, 191]. Note that, in this order the contour-ordered operator does not play any role. Now since $V_I^{x\pm}(t_1) = e^{\mp i\xi/2H_1} V_I(t) e^{\mp i\xi/2H_1}$ and furthermore because $[\rho(0), H_1] = 0$, the counting field dependent phase factors cancels out exactly leaving $\langle V_I^{x+}(t) \rangle = \langle V_I^{x-}(t) \rangle$, i.e., independent of the branch index and thus the above contribution vanishes.

Next, the second order contribution to the CGF is given as,

$$\begin{aligned}\mathcal{G}_T^{(2)}(u) &= \frac{(-i)^2}{2} \int d\tau_1 \int d\tau_2 \langle T_c V_I^x(\tau_1) V_I^x(\tau_2) \rangle_c \\ &= \int d\tau_1 \int d\tau_2 \tilde{G}_c(\tau_1, \tau_2),\end{aligned}\quad (6.52)$$

where $\tilde{G}_c(\tau_1, \tau_2)$ indicates the connected part of the correlation function with the tilde symbol referring to the counting field dependence. Since the normalization condition demands that $\mathcal{G}_T^{(2)}(u=0) = 0$, one can explicitly enforce the normalization in the above expression as

$$\mathcal{G}_T^{(2)}(u) = \int d\tau_1 \int d\tau_2 \left[\tilde{G}_c(\tau_1, \tau_2) - G_c(\tau_1, \tau_2) \right],\quad (6.53)$$

where recall that Green functions without the tilde symbol refers to $u = 0$. We once again transform back to the real time following the same procedure as mentioned earlier and obtain,

$$\begin{aligned}\mathcal{G}_T^{(2)}(u) &= \int_0^T dt_1 \int_0^T dt_2 \left[G_c^<(t_1, t_2) + G_c^>(t_1, t_2) \right. \\ &\quad \left. - \tilde{G}_c^<(t_1, t_2) - \tilde{G}_c^>(t_1, t_2) \right],\end{aligned}\quad (6.54)$$

where $< (>)$ symbol corresponds to the lesser (greater) component of the Green function. In order to proceed from here, we choose a generic form for the coupling, given as $V =$

$J A \otimes B$, where $A (B)$ corresponds to Hermitian operator involving system 1 (system 2). For simplicity, we consider single degree of freedom and systems with Bosonic degree of freedom. However, the calculation can be straightforwardly extended for fermionic as well as for hybrid systems.

Now since the average in the Green functions are taken over $\rho(0)$ i.e., decoupled initial state, the connected part of the correlation function in the contour-time reduces to

$$\tilde{G}_c(\tau_1, \tau_2) = \frac{J^2}{2} \tilde{g}_A(\tau_1, \tau_2) g_B(\tau_2, \tau_1), \quad (6.55)$$

where $\tilde{g}_A(\tau_1, \tau_2) = -i \langle T_c A^x(\tau_1) A^x(\tau_2) \rangle$ is the bare but counting field dependent correlation function for system 1 with average taken over the equilibrium density operator $\rho_1 = \frac{e^{-\beta_1 H_1}}{\mathcal{Z}_1}$ and similarly $g_B(\tau_1, \tau_2) = -i \langle T_c B(\tau_1) B(\tau_2) \rangle$ with average taken over the equilibrium density operator $\rho_2 = \frac{e^{-\beta_2 H_2}}{\mathcal{Z}_2}$. Following Eq. (6.53), in the real time we are interested only in the lesser and the greater components which are given as

$$\begin{aligned} \tilde{G}_c^<(t_1, t_2) &= \frac{J^2}{2} g_A^<(t_1 - t_2 - u) g_B^>(t_2 - t_1), \\ \tilde{G}_c^>(t_1, t_2) &= \frac{J^2}{2} g_A^>(t_1 - t_2 + u) g_B^<(t_2 - t_1). \end{aligned} \quad (6.56)$$

Since each of the bare Green functions are time-translational invariant, we can work in the frequency domain by performing Fourier transformation which gives,

$$\begin{aligned} Z_T(u) &= -\frac{J^2}{2} \int_{-\infty}^{\infty} \frac{d\omega_1}{2\pi} \int_{-\infty}^{\infty} \frac{d\omega_2}{2\pi} \frac{\sin^2 \left[\frac{(\omega_1 - \omega_2)T}{2} \right]}{\frac{(\omega_1 - \omega_2)^2}{4}} \\ &\times \left[g_A^<(\omega_1) g_B^>(\omega_2) (e^{iu\omega_1} - 1) + g_A^>(\omega_1) g_B^<(\omega_2) (e^{-iu\omega_1} - 1) \right]. \end{aligned} \quad (6.57)$$

Notice that since bare Green functions are computed with respect to their respective equilibrium state, they follow the standard Kubo-Martin-Schwinger boundary condition [191] given as $g_A^>(\omega) = e^{\beta_1 \omega} g_A^<(\omega)$ and similarly for system 2 Green function $g_B^>(\omega) = e^{\beta_2 \omega} g_B^<(\omega)$. Using this condition, one can rewrite the expressions for first and second cumulant by tak-

ing derivative of Eq. (6.57) with respect to iu and receive,

$$\begin{aligned}\langle Q \rangle &= -\frac{J^2}{2} \int_{-\infty}^{\infty} \frac{d\omega_1}{2\pi} \int_{-\infty}^{\infty} \frac{d\omega_2}{2\pi} \omega_1 \mathcal{F}(\omega_1, \omega_2; T) \\ &\quad g_A^>(\omega_1) g_B^<(\omega_2) \left[e^{-\beta_1 \omega_1} e^{\beta_2 \omega_2} - 1 \right],\end{aligned}\quad (6.58)$$

$$\begin{aligned}\langle Q^2 \rangle_c &= -\frac{J^2}{2} \int_{-\infty}^{\infty} \frac{d\omega_1}{2\pi} \int_{-\infty}^{\infty} \frac{d\omega_2}{2\pi} \omega_1^2 \mathcal{F}(\omega_1, \omega_2; T) \\ &\quad g_A^>(\omega_1) g_B^<(\omega_2) \left[e^{-\beta_1 \omega_1} e^{\beta_2 \omega_2} + 1 \right],\end{aligned}\quad (6.59)$$

where we define $\mathcal{F}(\omega_1, \omega_2; T) = \frac{\sin^2 \left[\frac{(\omega_1 - \omega_2)T}{2} \right]}{\frac{(\omega_1 - \omega_2)^2}{4}}$. Up to this point the only approximation made was the weak-coupling. However, this does not automatically ensure current conservation or the XFT, as reflected in the above equation. In order to meet these criteria one needs to further impose resonant condition for energy exchange. In order to achieve this, we use many-body quantum state representation for the individual system Hamiltonian H_1 , and H_2 , and write the lesser and greater components of the Green functions explicitly. For system 1,

$$\begin{aligned}g_A^<(t) &= -i \sum_{mn} \frac{e^{-\beta_1 E_m}}{Z_A} |A_{m,n}|^2 e^{i\omega_{nm}t}, \\ g_A^>(t) &= -i \sum_{mn} \frac{e^{-\beta_1 E_m}}{Z_A} |A_{m,n}|^2 e^{-i\omega_{nm}t},\end{aligned}\quad (6.60)$$

where $\omega_{nm} = E_n - E_m$, $|A_{mn}|^2 = |\langle m|A|n \rangle|^2$ with $|m\rangle, |n\rangle$ being the energy eigenstates for system 1 with Hamiltonian H_1 and E_m, E_n are the corresponding eigenvalues. One receives similar expression for $g_B^<,>(t)$ but with inverse temperature β_2 . We denote the corresponding energy eigenstates with $|p\rangle, |q\rangle$. Using Fourier transformed version of these Green functions we receive for the average energy change

$$\begin{aligned}\langle Q \rangle &= 2\pi^2 J^2 \sum_{mn} \sum_{pq} \omega_{mn} \mathcal{F}(\omega_{mn}, \omega_{qp}; T) |A_{mn}|^2 |B_{pq}|^2 \\ &\quad \left[e^{-\beta_1 \omega_{mn}} e^{\beta_2 \omega_{qp}} - 1 \right] \frac{e^{-\beta_1 E_m}}{Z_A} \frac{e^{-\beta_2 E_p}}{Z_B}.\end{aligned}\quad (6.61)$$

We now impose the resonant energy exchange condition between the two systems which

imply $E_m - E_n \approx E_q - E_p$ i.e., $\omega_{mn} \approx \omega_{qp}$ leading to $\mathcal{F}(\omega_{mn}, \omega_{qp}; T) \approx T^2$ and we receive,

$$\begin{aligned} \langle Q \rangle &= 2\pi^2 J^2 T^2 \sum_{mn} \sum_{pq} \omega_{mn} |A_{mn}|^2 |B_{pq}|^2 \\ &\quad \left[e^{\Delta\beta\omega_{qp}} - 1 \right] \frac{e^{-\beta_1 E_m}}{Z_A} \frac{e^{-\beta_2 E_p}}{Z_B}. \end{aligned} \quad (6.62)$$

Using the same resonant condition, we receive for the noise

$$\begin{aligned} \langle Q^2 \rangle_c &= 2\pi^2 J^2 T^2 \sum_{mn} \sum_{pq} \omega_{mn}^2 |A_{mn}|^2 |B_{pq}|^2 \frac{e^{-\beta_1 E_m}}{Z_A} \frac{e^{-\beta_2 E_p}}{Z_B} \\ &\quad \times \left[e^{\Delta\beta\omega_{qp}} + 1 \right] \\ &= 2\pi^2 J^2 T^2 \sum_{mn} \sum_{pq} \omega_{mn} |A_{mn}|^2 |B_{pq}|^2 \frac{e^{-\beta_1 E_m}}{Z_A} \frac{e^{-\beta_2 E_p}}{Z_B} \\ &\quad \times \omega_{qp} \coth \left[\frac{\Delta\beta\omega_{qp}}{2} \right] \left[e^{\Delta\beta\omega_{qp}} - 1 \right], \\ &\geq \frac{2}{\Delta\beta} \langle Q \rangle \end{aligned} \quad (6.63)$$

where going from the first to the third line we write $\omega_{mn}^2 \approx \omega_{mn} \omega_{qp}$. Notice the important term $\omega_{qp} \coth \left[\frac{\Delta\beta\omega_{qp}}{2} \right]$ in the fourth line which is always greater or equal to $2/\Delta\beta$ using which we receive the T-TUR bound. Also, note that the cumulants in this limit scales with T^2 and the entire analysis remains valid for $JT \ll 1$.

The another key importance of the expression in Eq. (6.57) is that one can readily discuss results for the long-time limit $T \rightarrow \infty$. In fact, if a unique long-time limit of Eq. (6.57) exists that supports a non-equilibrium steady-state for the bipartite setup (imagining each system to be macroscopic bath) in which case all cumulants scale with T , as

$$\lim_{T \rightarrow \infty} \frac{\sin^2 \left[\frac{(\omega_1 - \omega_2)T}{2} \right]}{\frac{(\omega_1 - \omega_2)^2}{4}} = 2\pi T \delta(\omega_1 - \omega_2) \quad (6.65)$$

and one receives the following expressions for the cumulants following Eq. (6.57)

$$\begin{aligned}
\frac{\langle Q \rangle}{T} &= -J^2 \int_{-\infty}^{\infty} \frac{d\omega}{4\pi} \omega g_A^>(\omega) g_B^<(\omega) [e^{\Delta\beta\omega} - 1], \\
\frac{\langle Q^2 \rangle_c}{T} &= -J^2 \int_{-\infty}^{\infty} \frac{d\omega}{4\pi} \omega^2 g_A^>(\omega) g_B^<(\omega) [e^{\Delta\beta\omega} + 1] \\
&= -J^2 \int_{-\infty}^{\infty} \frac{d\omega}{4\pi} \omega^2 \coth [\Delta\beta\omega/2] g_A^>(\omega) g_B^<(\omega) \\
&\quad \times [e^{\Delta\beta\omega} - 1], \\
&\geq -\frac{2}{\Delta\beta} J^2 \int_{-\infty}^{\infty} \frac{d\omega}{4\pi} \omega g_A^>(\omega) g_B^<(\omega) [e^{\Delta\beta\omega} - 1] \\
&\geq \frac{2}{\Delta\beta} \frac{\langle Q \rangle}{T}
\end{aligned} \tag{6.66}$$

$$\tag{6.67}$$

where once again, like in the previous case, in the third line of $\langle Q^2 \rangle_c/T$ expression we use the inequality $\omega \coth[\Delta\beta\omega/2] \geq 2/\Delta\beta$. Therefore for weakly coupled bipartite setup in the steady-state the T-TUR is preserved. It is crucial to note that both the G-TUR1 and G-TUR2 in this long-time limit fails to predict any non-trivial bound for the TUR ratio as the average entropy-production $\langle \Sigma \rangle$ diverges as $T \rightarrow \infty$.

6.4 Comparison with Quadratic Bound

In Ref. [136] based on extensive numerical simulation a quadratic bound (lower bound) was proposed for a scaled cumulant generating function for a multiaffinity time-homogeneous discrete state continuous-time Markov process in steady state. Later on, in Ref. [65], a rigorous proof for the quadratic bound was given for systems following continuous-time Markov jump processes in steady state. For our single-affinity problem and transient dynamics, the quadratic bound (QB) in terms of the CGF translates to

$$\mathcal{G}^{QB}(u) = u \langle Q \rangle \left[1 + \frac{u \langle Q \rangle}{\langle \Sigma \rangle} \right] \tag{6.68}$$

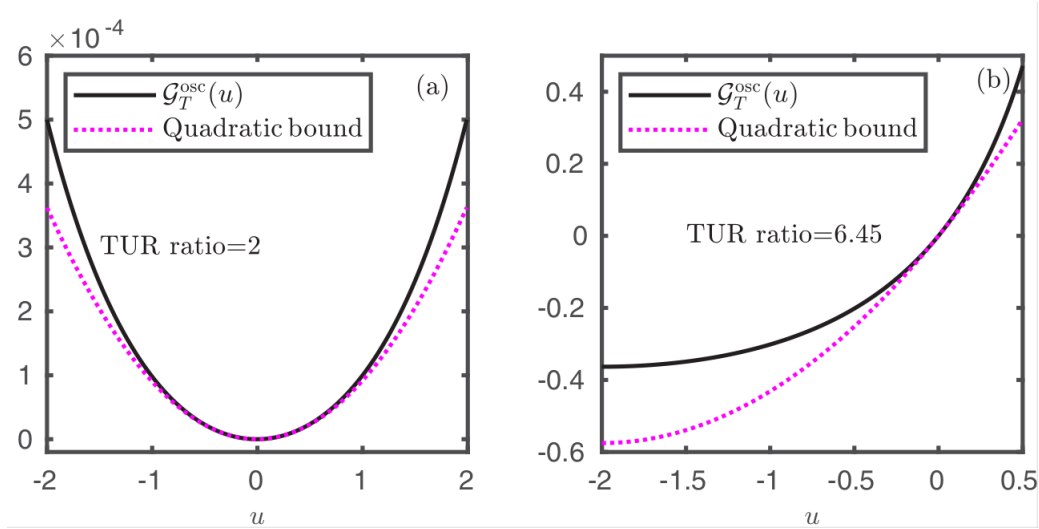


Figure 6.7: Comparison between the exact CGF $\mathcal{G}_T^{\text{osc}}(u)$ in Eq. (6.5) and the quadratic CGF in Eq. (6.68) for the two-oscillator problem for two different values for the TUR ratio: (a) TUR ratio = 2 and (b) TUR ratio = 6.45. Figure reproduced with permission from Ref. [75].

where u is treated as a real variable (the CGFs obtained in the main text should be analytically continued, $iu \rightarrow u$). Once any CGF satisfies the above quadratic bound one can immediately prove the T-TUR in Eq. (6.1). Since we have the exact expressions for the CGFs for three exactly solvable model systems, we compare numerically the CGFs with the quadratic bound in Eq. (6.68). We found that, for the harmonic oscillator problem since T-TUR is always valid, the above quadratic bound is always respected as shown in Fig.(6.7) for two different values of the TUR ratio.

In contrast, for the two-qubit and the hybrid spin-oscillator model we observe that whenever the T-TUR is valid the above quadratic bound is respected, see Figs. 6.8(a) and 6.9(a), and, expectedly, the violation of the quadratic bound is observed whenever the T-TUR ratio is smaller than 2, as shown in Figs. 6.8(b) and 6.9(b).

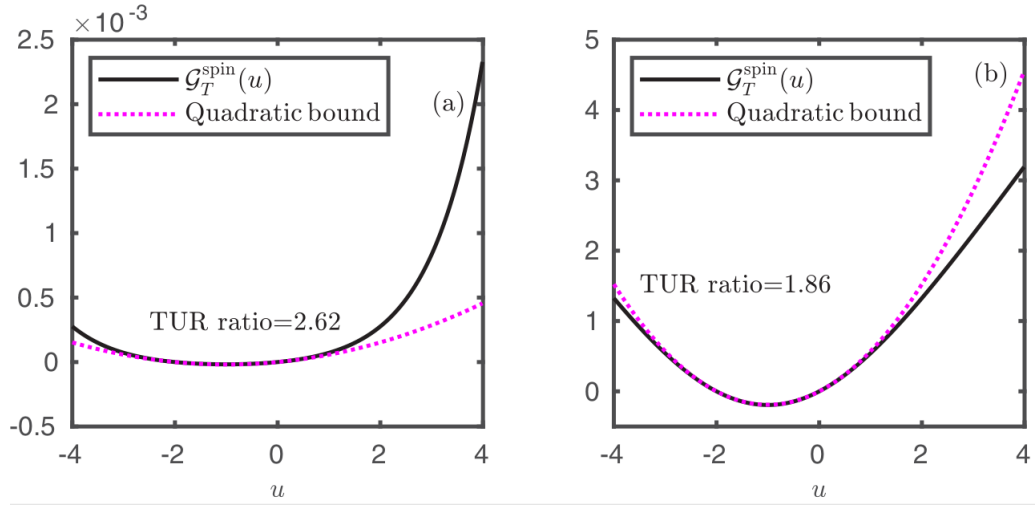


Figure 6.8: Same as in Fig. (6.7) but for the two-qubit model with exact CGF for two different values for the TUR ratio: (a) TUR ratio = 2.62 and (b) TUR ratio = 1.86. Figure reproduced with permission from Ref. [75].

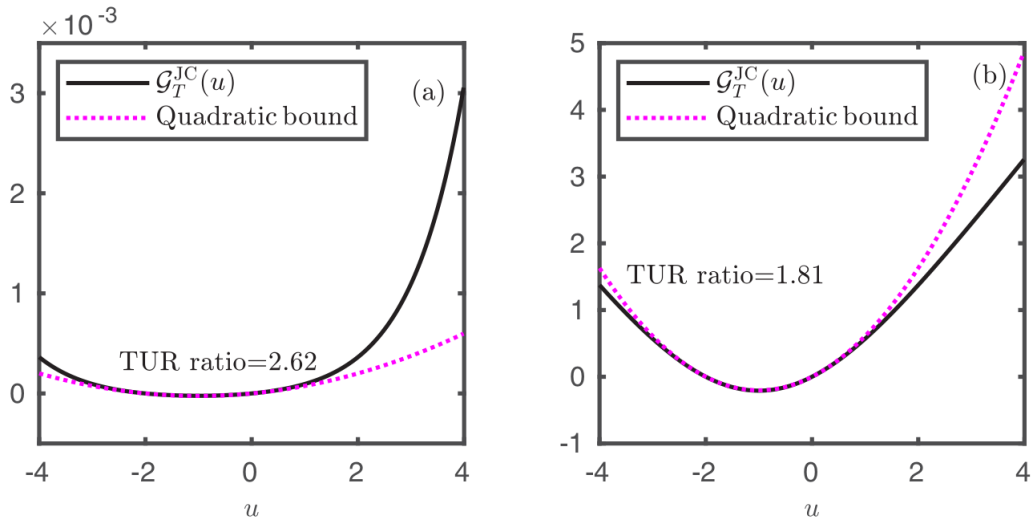


Figure 6.9: Same as in Fig. 6.7) but for the hybrid spin-oscillator model for two different values for the TUR ratio: (a) TUR ratio = 2.62 and (b) TUR ratio = 1.81. Figure reproduced with permission from Ref. [75].

6.5 Summary

In this chapter we examined the TUR bound for energy exchange for three simple model systems characterized by different underlying statistics for the transport carriers. We obtained exact analytical expressions for the heat exchange characteristic function for all three cases which hands over the cumulants to analyze the different versions of transient TUR.

One of the interesting observations was the similarity in the expressions for the CGF for the two- qubit and two-oscillator model where they differ by crucial sign differences arising from the underlying Fermi-like and the Bose statistics. We found that, much like the steady-state case, the transient TUR ratio in general is sensitive to the statistics and the validity or violation of the T-TUR is critically dependent on this. In all three cases, interestingly, the TUR ratio was organized in terms of a universal term which is always greater than or equal to 2 and a net entropy production term. The deviation from the T-TUR bound largely depends on the contribution of this average entropy production to the TUR ratio. For a coupled oscillator system, displaying pure bosonic statistics, this contribution turned out to be always positive and thus the tighter bound is always preserved. In contrast, the appearance of the Fermi like statistics for both the qubit and the hybrid model leads to a negative contribution, leading to a lower bound (smaller than the T-TUR) for the TUR. However, in the weak-coupling regime, all these models satisfy the T-TUR bound. We provided a rigorous proof for the T-TUR, in the weak-coupling regime, by deriving a general expression for the CGF following the NEGF approach.

CHAPTER 7

Concluding remarks and Future prospects

This dissertation presents a detailed theoretical study on the bounds on fluctuations for non-equilibrium systems and its consequence in the context of general, quantum or classical, thermal machines. Our results unravel a novel relationship among the much studied thermodynamic uncertainty relations for the individual currents when the setup under consideration is operating as a thermal machine. Let us briefly summarize the central results obtained in this thesis.

We first examined autonomous continuous thermal machines with time-reversal symmetry in chapter 2 and established that the relative fluctuations of the output current (power output) is always lower bounded by the relative fluctuations of the input current (heat current absorbed from the hot bath). As an immediate consequence, thermodynamic uncertainty relation for input and output current received strict hierarchy. Furthermore, we showed that the obtained upper bound on the efficiency is tighter than the upper bound obtained using the thermodynamic uncertainty relations. Next in chapter 3 we generalized our findings of previous chapter to broken time-reversal symmetric thermal machines. We showed that, in the linear response regime the relative fluctuation of the sum of output currents for time-forward and time-reversed processes is always lower bounded by the corresponding relative fluctuation of the sum of input currents. Consequently, we established a connection between our results and the generalized thermodynamic uncertainty relations for time-reversal symmetry-broken systems. We also provided physically relevant bounds on individual forward and backward processes. As a consequence of this, we also showed that the bounds exactly like the time-reversal symmetric case will hold true for at least one of the processes.

In chapter 4 we examined the bounds on the fluctuations for finite-time quantum Otto cycle which is a discrete thermal machine. Following two-point measurement scheme we obtained exact full statistics of heat and work in the adiabatic driving limit for a class of

working fluids that follow a scale-invariant energy eigenspectra . As a result we derived a universal expression for the ratio of nth cumulant of output work and input heat in terms of the Otto efficiency in the adiabatic driving limit. Furthermore, for nonadiabatic driving of quantum Otto engine with working fluid consisting of either (i) a qubit or (ii) a harmonic oscillator, we showed that the relative fluctuation of output work is always greater than the corresponding relative fluctuation of input heat absorbed from the hot bath that we also obtained for time-reversal symmetric continuous thermal machines in chapter 2.

In the later part of the thesis we focused our attention on the fate of of the T-TUR in steady-state and transient-state transport junctions. In chapter 5, we employed the fundamental non-equilibrium steady state fluctuation symmetry and derived a condition on the validity T-TUR for single affinity driven systems. We showed that the validity of the T-TUR relies on the statistics of the participating carriers. In chapter 6 we assessed the validity of transient version of T-TUR. We explored T-TUR in the context of energy transport in a bipartite setting for three exactly solvable toy model systems (two coupled harmonic oscillators, two coupled qubits, and a hybrid coupled oscillator-qubit system) and analyzed the role played by the underlying statistics of the transport carriers in the TUR. Interestingly, for all these models, depending on the statistics, the TUR ratio can be expressed as a sum or a difference of a universal term which is always greater than or equal to 2 and a corresponding entropy production term. We also provided a rigorous proof following the non-equilibrium Green's function approach that the tighter bound is always satisfied in the weak-coupling regime for generic bipartite systems.

After summarizing the thesis, let us point out some future prospects originating from the thesis.

Future Prospects

- Exploring the impact of fluctuations and assessing the validity of universal bounds on non-equilibrium fluctuations and the connection to TUR in a broader and general setting. It will be important and interesting to explore (a) continuous machines operating beyond the linear response regime, (b) non-autonomous continuously coupled quantum engines i.e., for systems following driven-dissipative dynamics by incorporating Floquet prescription for periodically driven systems, and (c) discrete engines.

- Extension of our approach for multi-terminal transport setup is an interesting avenue to explore for the continuous thermal machines. Especially, it would be interesting to understand how the relative fluctuations of individual currents can be controlled in multi-terminal setting.
- Building thermodynamically consistent framework for other quantum analogs of discrete thermal machines like Carnot cycle, Stirling cycle etc. And then investigating the universality of bounds on $\eta^{(2)}$ for these machines.
- Experimental verification's of these novel bounds using state-of-the-art experiments.
- Exploring universal bounds for broken time-reversal symmetric situations in case of the discrete thermal machines, for example asymmetric driving in finite-time Otto engine.
- Exploring the role of many-body interaction on the validity/violation of T-TUR, both in steady-state and transient-state using the state-of-the-art numerical methods like, numerically exact path integral technique [192], and tensor-network methods [193].

APPENDIX A

Quantum XFT in thermal-coupling limit

To take advantage of the thermal coupling limit i.e., the commutable coupling condition $[H_1 + H_2, V] = 0$, one can rewrite the above expression along with the consideration that initially both the systems are in their respective Gibbs thermal state, i.e., $\rho(0) = \frac{e^{-\beta_1 H_1}}{\mathcal{Z}_1} \otimes \frac{e^{-\beta_2 H_2}}{\mathcal{Z}_2}$ which further imply $[\rho(0), H_1] = 0$. One then receives,

$$Z_T(u) = \frac{1}{\mathcal{Z}_1 \mathcal{Z}_2} \text{Tr} \left[(e^{iuH_1} \otimes 1_2) e^{\Delta\beta H_1} e^{-\beta_2(H_1+H_2)} \mathcal{U}^\dagger(T, 0) (e^{-iuH_1} \otimes 1_2) \mathcal{U}(T, 0) \right], \quad (\text{A.1})$$

where recall that $\Delta\beta = \beta_2 - \beta_1$. The thermal coupling condition allows swapping the third and the fourth term. Next performing cyclic permutation under the trace operation, we receive,

$$Z_T(u) = \frac{1}{\mathcal{Z}_1 \mathcal{Z}_2} \text{Tr} \left[\mathcal{U}(T, 0) (e^{-i(-u+i\Delta\beta)H_1} \otimes 1_2) \mathcal{U}^\dagger(T, 0) (e^{i(-u+i\Delta\beta)H_1} \otimes 1_2) \rho(0) \right], \quad (\text{A.2})$$

where $\Delta\beta = \beta_2 - \beta_1$. This expression still does not give us the XFT that we are looking for. In fact, at this point the above expression satisfies a fluctuation relation given as $Z_T(u) = Z_{-T}(-u + i\Delta\beta)$ connecting forward and reversed protocol.

In order to proceed, we now assume that the composite and the individual systems are time reversal invariant, which is the case considered in this paper. We then have $\Theta \mathcal{U}(T, 0) = \mathcal{U}^\dagger(T, 0) \Theta$, $\Theta e^{-iuH_1} = e^{iu^*H_1} \Theta$ and $[\Theta, H_{1,2}] = 0$. Θ is time reversal

operator. Now inserting $\Theta^{-1}\Theta$ inside the trace and using eq. (A.2) we receive

$$\begin{aligned}
Z_T(u) &= \frac{1}{\mathcal{Z}_1\mathcal{Z}_2} \text{Tr} \left[\Theta^{-1}\Theta \mathcal{U}(T, 0) (e^{-i(-u+i\Delta\beta)H_1} \otimes 1_2) \right. \\
&\quad \left. \mathcal{U}^\dagger(T, 0) (e^{i(-u+i\Delta\beta)H_1} \otimes 1_2) \rho(0) \right], \\
&= \frac{1}{\mathcal{Z}_1\mathcal{Z}_2} \text{Tr} \left[\Theta^{-1}\mathcal{U}^\dagger(T, 0) (e^{i(-u^*-i\Delta\beta)H_1} \otimes 1_2) \right. \\
&\quad \left. \mathcal{U}(T, 0) (e^{-i(-u^*-i\Delta\beta)H_1} \otimes 1_2) \rho(0)\Theta \right]. \tag{A.3}
\end{aligned}$$

Now due to the antilinear nature of Θ we have $\text{Tr}[\Theta^{-1} A \Theta] = \text{Tr}[A^\dagger]$ [51]. Therefore we finally receive

$$\begin{aligned}
Z_T(u) &= \frac{1}{\mathcal{Z}_1\mathcal{Z}_2} \text{Tr} \left[\mathcal{U}^\dagger(T, 0) (e^{-i(-u+i\Delta\beta)H_1} \otimes 1_2) \mathcal{U}(T, 0) (e^{i(-u+i\Delta\beta)H_1} \otimes 1_2) \rho(0) \right] \\
&= Z_T(-u + i\Delta\beta) \tag{A.4}
\end{aligned}$$

for arbitrary time duration T and coupling strength. In other words, quantum XFT is valid exactly under thermal-coupling for arbitrary coupling strength and arbitrary time duration.

APPENDIX B

Tight-coupling limit beyond linear response

In this appendix we focus on the tight coupling (TC) limit. We prove the upper bound $\eta^{(2)} \leq \eta_C^2$ and that the lower bound is saturated. Both results hold beyond linear response. We further derive bounds on ratios (output power to heat) of high order cumulants.

In the tight-coupling limit, the energy current flowing through the junction is proportional to the electron flux. While commonly, this limit is assumed for the averaged currents, here we enforce it for the stochastic currents. i.e., $I_u = \epsilon_d I_e$ with ϵ_d the energy of the single quantum dot. Since the currents here are proportional (coupled), this limit is commonly referred to as the “tight-coupling limit”. Such a situation can be easily realized when a single quantum level is weakly coupled to the reservoirs. The dynamics and thermodynamics of the model can be obtained from stochastic thermodynamics using Markovian master equations. The TC limit is of great interest in nanoelectronics since the system in this limit has the ability to operate at the Carnot efficiency [194]. Furthermore, various universal features in nonlinear response such as the universality of the efficiency at maximum power were proved in this regime [195].

We now study the ratio between work and heat fluctuations in the TC limit for a thermoelectric engine, arbitrarily far from equilibrium. First, we calculate the average thermodynamic efficiency in the TC limit,

$$\begin{aligned}\langle \eta \rangle &= \frac{-\langle I_w \rangle}{\langle \dot{I}_q^h \rangle} \\ &= \frac{\Delta\mu \langle I_e \rangle}{\langle I_u \rangle - \mu_R \langle I_e \rangle} = \frac{\Delta\mu}{(\epsilon_d - \mu_R)}.\end{aligned}\tag{B.1}$$

The upper bound for the mean efficiency is given by the Carnot value $\eta_C = 1 - \frac{T_L}{T_R}$. This can be proved by enforcing the positivity requirement for the average entropy production rate. In steady state, it is defined as $\langle \sigma \rangle = \sum_{i=e,u} A_i \langle I_i \rangle$ where $A_e = (\beta_R \mu_R - \beta_L \mu_L)$ and $A_u = (\beta_L - \beta_R)$ are the two thermodynamic affinities corresponding to particle and energy

current, respectively. In the TC limit, this reduces to

$$\langle \sigma \rangle = [\beta_L(\epsilon_d - \mu_L) - \beta_R(\epsilon_d - \mu_R)] \langle I_e \rangle \geq 0, \quad (\text{B.2})$$

which is always non-negative. The zero net entropy production limit corresponds to a quasi-static situation, which, interestingly, in TC limit can be achieved without requiring the individual affinities to go to zero. The above condition in the context of thermoelectric engine yields,

$$\beta_L(\epsilon_d - \mu_L) \geq \beta_R(\epsilon_d - \mu_R), \quad (\text{B.3})$$

which implies that

$$\langle \eta \rangle = \frac{\Delta\mu}{(\epsilon_d - \mu_R)} \leq 1 - \frac{\beta_R}{\beta_L} = \eta_C. \quad (\text{B.4})$$

As expected, the mean efficiency of the engine is limited by the Carnot value $\langle \eta \rangle \leq \eta_C$.

We now generalize this result for higher order ($n \geq 1$) cumulants. Since the stochastic energy current goes hand in hand with the stochastic electron flux i.e., $I_u = \epsilon_d I_e$, higher order cumulants satisfy $\langle I_u^n \rangle_c = \epsilon_d^n \langle I_e^n \rangle$ and $\langle I_q^n \rangle_c = (\epsilon_d - \mu_R)^n \langle I_e^n \rangle_c$ resulting in

$$\begin{aligned} \eta^{(n)} &\equiv \frac{\langle (-I_w)^n \rangle_c}{\langle (I_q^h)^n \rangle_c} \\ &= \frac{(\Delta\mu)^n}{(\epsilon_d - \mu_R)^n} = \langle \eta \rangle^n \leq \eta_C^n. \end{aligned} \quad (\text{B.5})$$

Since $\langle \eta \rangle \leq \eta_C$ we conclude that in the TC limit, $\eta^{(n)} \leq \eta_C^n$. This result holds arbitrarily far from equilibrium.

APPENDIX C

Single affinity limit in time-reversal symmetric continuous machines

Here we discuss the behavior of the Q ratio in the single affinity limit. Let us first turn off the affinity corresponding to the input channel, i.e., $A_1 = 0$. One then receives in the linear-response limit,

$$Q_{A_1=0} \equiv \frac{\langle I_1 \rangle^2}{\langle I_1^2 \rangle_c} \frac{\langle \langle I_2^2 \rangle \rangle}{\langle \langle I_2 \rangle \rangle} = \frac{L_{12}^2}{L_{22}^2} \frac{L_{22}}{L_{11}} = \frac{\mathcal{L}_{12}^2}{\mathcal{L}_{22} \mathcal{L}_{11}} \leq 1, \quad (\text{C.1})$$

where the inequality follows from the positivity of entropy production in a spontaneous process. This result implies that the relative fluctuation or the precision of the current related to the applied bias (I_2) is always upper bounded by the corresponding precision for the current of the coupled phenomena (I_1). This further indicates that in the linear response limit, the TUR ratio for a current under its bias, is always upper bounded by the corresponding TUR ratio for the coupled current i.e., $\langle \sigma \rangle \frac{\langle I_2^2 \rangle_c}{\langle I_2 \rangle^2} \leq \langle \sigma \rangle \frac{\langle I_1^2 \rangle_c}{\langle I_1 \rangle^2}$. Similarly, in the opposite limit, i.e., for $A_2 = 0$, following similar steps, it is easy to see that $Q_{A_2=0} \geq 1$ i.e., we reach the same conclusion: the current that corresponds to the applied bias is upper bounded by the relative fluctuation of the coupled current.

APPENDIX D

Harmonic junctions in the classical limit

In this Appendix, we prove the validity of T-TUR directly in the classical limit for harmonic systems starting from the classical generating function for heat exchange obtained by Kundu et al. [196]. One can as well reach the classical result from the exact quantum CGF in Eq. (5.9) by taking the high temperature limit, $\beta_L \hbar \omega \ll 1, \beta_R \hbar \omega \ll 1$. The CGF in the classical limit, $\chi_{\text{HO}}^{\text{cl}}(\alpha)$, is given by,

$$\mathcal{G}_{\text{HO}}^{\text{cl}}(\chi) = - \int_{-\infty}^{\infty} \frac{d\omega}{4\pi} \ln \left[1 - \mathcal{T}_{\text{HO}}(\omega) \frac{i\chi}{\beta_L \beta_R} (i\chi + (\beta_R - \beta_L)) \right] \quad (\text{D.1})$$

Of course, this classical version also satisfies the steady state fluctuation relation i.e., $\mathcal{G}_{\text{HO}}^{\text{cl}}(\chi) = \mathcal{G}_{\text{HO}}^{\text{cl}}(-\chi + i\Delta\beta)$. Using this CGF, one can immediately derive the current and its noise,

$$\begin{aligned} \langle I \rangle &\equiv \left. \frac{\partial \mathcal{G}_{\text{HO}}^{\text{cl}}(\chi)}{\partial (i\chi)} \right|_{\chi=0} = k_B (T_L - T_R) \mathcal{T}_1, \\ \langle I^2 \rangle_c &\equiv \left. \frac{\partial^2 \mathcal{G}_{\text{HO}}^{\text{cl}}(\chi)}{\partial (i\chi)^2} \right|_{\chi=0} = 2k_B^2 T_L T_R \mathcal{T}_1 + k_B^2 (T_L - T_R)^2 \mathcal{T}_2, \end{aligned} \quad (\text{D.2})$$

where $\mathcal{T}_n = \int_{-\infty}^{\infty} \frac{d\omega}{4\pi} \mathcal{T}_{\text{HO}}^n(\omega)$. Since the last term in the noise expression is positive, one can then write

$$\langle I^2 \rangle_c \geq 2 T_L T_R \mathcal{T}_1 = 2 \frac{\langle I \rangle}{\Delta\beta}, \quad (\text{D.3})$$

which recovers the TUR (5.3). The equality is reached in the equilibrium limit. The TUR is therefore satisfied for a coupled harmonic oscillator system in the classical limit. The proof is general for arbitrary spectral function of the baths and internal parameters for the system. Thus, the TUR is valid independent of the nature of the underlying stochastic dynamics of the oscillators.

Bibliography

- [1] Sadi Carnot. *Reflections on the motive power of fire, and on machines fitted to develop that power.* 1824.
- [2] Herbert B Callen. *Thermodynamics and an introduction to thermostatistics; 2nd ed.* Wiley, New York, NY, 1985.
- [3] S Whalen, M Thompson, D Bahr, C Richards, and R Richards. Design, fabrication and testing of the p3 micro heat engine. *Sensors and Actuators A: Physical*, 104(3):290–298, 2003. Selected papers based on contributions revised from the Technical Digest of the 2002 Solid-State Sensors, Actuators and Microsystems workshop.
- [4] P. G. Steeneken, K. Le Phan, M. J. Goossens, G. E. J. Koops, G. J. A. M. Brom, C. van der Avoort, and J. T. M. van Beek. Piezoresistive heat engine and refrigerator. *Nature Physics*, 7(4):354–359, Apr 2011.
- [5] Jean-Philippe Brantut, Charles Grenier, Jakob Meineke, David Stadler, Sebastian Krinner, Corinna Kollath, Tilman Esslinger, and Antoine Georges. A thermoelectric heat engine with ultracold atoms. *Science*, 342(6159):713–715, 2013.
- [6] Valentin Blickle and Clemens Bechinger. Realization of a micrometre-sized stochastic heat engine. *Nature Physics*, 8(2):143–146, Feb 2012.
- [7] I. A. Martínez, É Roldán, L. Dinis, D. Petrov, J. M. R. Parrondo, and R. A. Rica. Brownian carnot engine. *Nature Physics*, 12(1):67–70, Jan 2016.
- [8] Sudeesh Krishnamurthy, Subho Ghosh, Dipankar Chatterji, Rajesh Ganapathy, and A. K. Sood. A micrometre-sized heat engine operating between bacterial reservoirs. *Nature Physics*, 12(12):1134–1138, Dec 2016.

- [9] Thorsten Hugel, Nolan B. Holland, Anna Cattani, Luis Moroder, Markus Seitz, and Hermann E. Gaub. Single-molecule optomechanical cycle. *Science*, 296(5570):1103–1106, 2002.
- [10] Johannes Roßnagel, Samuel T. Dawkins, Karl N. Tolazzi, Obinna Abah, Eric Lutz, Ferdinand Schmidt-Kaler, and Kilian Singer. A single-atom heat engine. *Science*, 352(6283):325–329, 2016.
- [11] D. von Lindenfels, O. Gräß, C. T. Schmiegelow, V. Kaushal, J. Schulz, Mark T. Mitchison, John Goold, F. Schmidt-Kaler, and U. G. Poschinger. Spin heat engine coupled to a harmonic-oscillator flywheel. *Phys. Rev. Lett.*, 123:080602, Aug 2019.
- [12] Gleb Maslennikov, Shiqian Ding, Roland Hablützel, Jaren Gan, Alexandre Roulet, Stefan Nimmrichter, Jibo Dai, Valerio Scarani, and Dzmitry Matsukevich. Quantum absorption refrigerator with trapped ions. *Nature Communications*, 10(1):202, Jan 2019.
- [13] James Klatzow, Jonas N. Becker, Patrick M. Ledingham, Christian Weinzetl, Krzysztof T. Kaczmarek, Dylan J. Saunders, Joshua Nunn, Ian A. Walmsley, Raam Uzdin, and Eilon Poem. Experimental demonstration of quantum effects in the operation of microscopic heat engines. *Phys. Rev. Lett.*, 122:110601, Mar 2019.
- [14] John P. S. Peterson, Tiago B. Batalhão, Marcela Herrera, Alexandre M. Souza, Roberto S. Sarthour, Ivan S. Oliveira, and Roberto M. Serra. Experimental characterization of a spin quantum heat engine. *Phys. Rev. Lett.*, 123:240601, Dec 2019.
- [15] Rogério J. de Assis, Taysa M. de Mendonça, Celso J. Villas-Boas, Alexandre M. de Souza, Roberto S. Sarthour, Ivan S. Oliveira, and Norton G. de Almeida. Efficiency of a quantum otto heat engine operating under a reservoir at effective negative temperatures. *Phys. Rev. Lett.*, 122:240602, Jun 2019.
- [16] Quentin Bouton, Jens Nettersheim, Sabrina Burgardt, Daniel Adam, Eric Lutz, and Artur Widera. A quantum heat engine driven by atomic collisions. *Nature Communications*, 12(1):2063, Apr 2021.

- [17] William Sutherland. Xviii. ionization, ionic velocities, and atomic sizes. *The London, Edinburgh, and Dublin Philosophical Magazine and Journal of Science*, 3(14):161–177, 1902.
- [18] William Sutherland. Lxxv. a dynamical theory of diffusion for non-electrolytes and the molecular mass of albumin. *The London, Edinburgh, and Dublin Philosophical Magazine and Journal of Science*, 9(54):781–785, 1905.
- [19] A. Einstein. On the motion of small particles suspended in liquids at rest required by the molecular-kinetic theory of heat. *Annalen der Physik*, 322(8):549–560, 1905. <https://onlinelibrary.wiley.com/doi/pdfdirect/10.1002/andp.19053220806>.
- [20] A. Einstein. Eine neue bestimmung der moleküldimensionen. *Annalen der Physik*, 324(2):289–306, 1906.
- [21] A. Einstein. Zur theorie der brownschen bewegung. *Annalen der Physik*, 324(2):371–381, 1906.
- [22] J. B. Johnson. Thermal agitation of electricity in conductors. *Phys. Rev.*, 32:97–109, Jul 1928.
- [23] H. Nyquist. Thermal agitation of electric charge in conductors. *Phys. Rev.*, 32:110–113, Jul 1928.
- [24] Herbert B. Callen and Theodore A. Welton. Irreversibility and generalized noise. *Phys. Rev.*, 83:34–40, Jul 1951.
- [25] Melville S. Green. Markoff random processes and the statistical mechanics of time-dependent phenomena. *The Journal of Chemical Physics*, 20(8):1281–1295, 1952.
- [26] Melville S. Green. Markoff random processes and the statistical mechanics of time-dependent phenomena. ii. irreversible processes in fluids. *The Journal of Chemical Physics*, 22(3):398–413, 1954.
- [27] Ryogo Kubo. Statistical-mechanical theory of irreversible processes. i. general theory and simple applications to magnetic and conduction problems. *Journal of the Physical Society of Japan*, 12(6):570–586, 1957.

- [28] Peter Hänggi. Nonlinear fluctuations: The problem of deterministic limit and reconstruction of stochastic dynamics. *Phys. Rev. A*, 25:1130–1136, Feb 1982.
- [29] Peter Hänggi and Harry Thomas. Stochastic processes: Time evolution, symmetries and linear response. *Physics Reports*, 88(4):207–319, 1982.
- [30] G. M. Wang, J. C. Reid, D. M. Carberry, D. R. M. Williams, E. M. Sevick, and Denis J. Evans. Experimental study of the fluctuation theorem in a nonequilibrium steady state. *Phys. Rev. E*, 71:046142, Apr 2005.
- [31] S. Schuler, T. Speck, C. Tietz, J. Wrachtrup, and U. Seifert. Experimental test of the fluctuation theorem for a driven two-level system with time-dependent rates. *Phys. Rev. Lett.*, 94:180602, May 2005.
- [32] E. H. Trepagnier, C. Jarzynski, F. Ritort, G. E. Crooks, C. J. Bustamante, and J. Liphardt. Experimental test of hatano and sasa’s nonequilibrium steady-state equality. *Proceedings of the National Academy of Sciences*, 101(42):15038–15041, 2004.
- [33] Jan Liphardt, Sophie Dumont, Steven B. Smith, Ignacio Tinoco, and Carlos Bustamante. Equilibrium information from nonequilibrium measurements in an experimental test of jarzynski’s equality. *Science*, 296(5574):1832–1835, 2002.
- [34] D. Collin, F. Ritort, C. Jarzynski, S. B. Smith, I. Tinoco, and C. Bustamante. Verification of the crooks fluctuation theorem and recovery of rna folding free energies. *Nature*, 437(7056):231–234, Sep 2005.
- [35] C. Tietz, S. Schuler, T. Speck, U. Seifert, and J. Wrachtrup. Measurement of stochastic entropy production. *Phys. Rev. Lett.*, 97:050602, Aug 2006.
- [36] Denis J. Evans, E. G. D. Cohen, and G. P. Morriss. Probability of second law violations in shearing steady states. *Phys. Rev. Lett.*, 71:2401–2404, Oct 1993.
- [37] Denis J. Evans and Debra J. Searles. Equilibrium microstates which generate second law violating steady states. *Phys. Rev. E*, 50:1645–1648, Aug 1994.

- [38] G. Gallavotti and E. G. D. Cohen. Dynamical ensembles in nonequilibrium statistical mechanics. *Phys. Rev. Lett.*, 74:2694–2697, Apr 1995.
- [39] C. Jarzynski. Nonequilibrium equality for free energy differences. *Phys. Rev. Lett.*, 78:2690–2693, Apr 1997.
- [40] Chris Jarzynski. Nonequilibrium work theorem for a system strongly coupled to a thermal environment. *Journal of Statistical Mechanics: Theory and Experiment*, 2004(09):P09005, sep 2004.
- [41] Michele Campisi, Peter Talkner, and Peter Hänggi. Fluctuation theorem for arbitrary open quantum systems. *Phys. Rev. Lett.*, 102:210401, May 2009.
- [42] Peter Talkner, Michele Campisi, and Peter Hänggi. Fluctuation theorems in driven open quantum systems. *Journal of Statistical Mechanics: Theory and Experiment*, 2009(02):P02025, feb 2009.
- [43] G.N. Bochkov and Yu.E. Kuzovlev. Nonlinear fluctuation-dissipation relations and stochastic models in nonequilibrium thermodynamics: I. generalized fluctuation-dissipation theorem. *Physica A: Statistical Mechanics and its Applications*, 106(3):443–479, 1981.
- [44] G.N. Bochkov and Yu.E. Kuzovlev. Nonlinear fluctuation-dissipation relations and stochastic models in nonequilibrium thermodynamics: I. generalized fluctuation-dissipation theorem. *Physica A: Statistical Mechanics and its Applications*, 106(3):443–479, 1981.
- [45] R. L. Stratonovich. *Nonlinear nonequilibrium thermodynamics II : advanced theory*. Springer series in synergetics ; v. 59. Springer, Berlin ;, 1994.
- [46] T. Monnai and S. Tasaki. Quantum correction of fluctuation theorem, 2003.
- [47] Vladimir Chernyak and Shaul Mukamel. Effect of quantum collapse on the distribution of work in driven single molecules. *Phys. Rev. Lett.*, 93:048302, Jul 2004.

- [48] A. E. Allahverdyan and Th. M. Nieuwenhuizen. Fluctuations of work from quantum subensembles: The case against quantum work-fluctuation theorems. *Phys. Rev. E*, 71:066102, Jun 2005.
- [49] M. F. Gelin and D. S. Kosov. Unified approach to the derivation of work theorems for equilibrium and steady-state, classical and quantum hamiltonian systems. *Phys. Rev. E*, 78:011116, Jul 2008.
- [50] Peter Talkner, Eric Lutz, and Peter Hänggi. Fluctuation theorems: Work is not an observable. *Phys. Rev. E*, 75:050102, May 2007.
- [51] Michele Campisi, Peter Hänggi, and Peter Talkner. Colloquium: Quantum fluctuation relations: Foundations and applications. *Rev. Mod. Phys.*, 83:771–791, Jul 2011.
- [52] Jorge Kurchan. A quantum fluctuation theorem, 2000.
- [53] Hal Tasaki. Jarzynski relations for quantum systems and some applications, 2000.
- [54] Shaul Mukamel. Quantum extension of the jarzynski relation: Analogy with stochastic dephasing. *Phys. Rev. Lett.*, 90:170604, May 2003.
- [55] Peter Talkner and Peter Hänggi. The tasaki–crooks quantum fluctuation theorem. *Journal of Physics A: Mathematical and Theoretical*, 40(26):F569–F571, jun 2007.
- [56] Peter Talkner, Peter Hänggi, and Manuel Morillo. Microcanonical quantum fluctuation theorems. *Phys. Rev. E*, 77:051131, May 2008.
- [57] Massimiliano Esposito, Upendra Harbola, and Shaul Mukamel. Nonequilibrium fluctuations, fluctuation theorems, and counting statistics in quantum systems. *Rev. Mod. Phys.*, 81:1665–1702, Dec 2009.
- [58] Michele Campisi, Peter Talkner, and Peter Hänggi. Influence of measurements on the statistics of work performed on a quantum system. *Phys. Rev. E*, 83:041114, Apr 2011.

- [59] Christopher Jarzynski and Daniel K. Wójcik. Classical and quantum fluctuation theorems for heat exchange. *Phys. Rev. Lett.*, 92:230602, Jun 2004.
- [60] Bijay Kumar Agarwalla, Huanan Li, Baowen Li, and Jian-Sheng Wang. Exchange fluctuation theorem for heat transport between multiterminal harmonic systems. *Phys. Rev. E*, 89:052101, May 2014.
- [61] Bijay Kumar Agarwalla, Baowen Li, and Jian-Sheng Wang. Full-counting statistics of heat transport in harmonic junctions: Transient, steady states, and fluctuation theorems. *Phys. Rev. E*, 85:051142, May 2012.
- [62] Keiji Saito and Abhishek Dhar. Fluctuation theorem in quantum heat conduction. *Phys. Rev. Lett.*, 99:180601, Oct 2007.
- [63] Shiho Akagawa and Naomichi Hatano. The Exchange Fluctuation Theorem in Quantum Mechanics. *Progress of Theoretical Physics*, 121(6):1157–1172, 06 2009.
- [64] Andre C. Barato and Udo Seifert. Thermodynamic uncertainty relation for biomolecular processes. *Phys. Rev. Lett.*, 114:158101, Apr 2015.
- [65] Todd R. Gingrich, Jordan M. Horowitz, Nikolay Perunov, and Jeremy L. England. Dissipation bounds all steady-state current fluctuations. *Phys. Rev. Lett.*, 116:120601, Mar 2016.
- [66] Jordan M. Horowitz and Todd R. Gingrich. Proof of the finite-time thermodynamic uncertainty relation for steady-state currents. *Phys. Rev. E*, 96:020103, Aug 2017.
- [67] Karel Proesmans and Christian Van den Broeck. Discrete-time thermodynamic uncertainty relation. *EPL (Europhysics Letters)*, 119(2):20001, jul 2017.
- [68] Patrick Pietzonka and Udo Seifert. Universal trade-off between power, efficiency, and constancy in steady-state heat engines. *Phys. Rev. Lett.*, 120:190602, May 2018.
- [69] Katarzyna Macieszczak, Kay Brandner, and Juan P. Garrahan. Unified thermodynamic uncertainty relations in linear response. *Phys. Rev. Lett.*, 121:130601, Sep 2018.

- [70] Bijay Kumar Agarwalla and Dvira Segal. Assessing the validity of the thermodynamic uncertainty relation in quantum systems. *Phys. Rev. B*, 98:155438, Oct 2018.
- [71] André M. Timpanaro, Giacomo Guarnieri, John Goold, and Gabriel T. Landi. Thermodynamic uncertainty relations from exchange fluctuation theorems. *Phys. Rev. Lett.*, 123:090604, Aug 2019.
- [72] Yoshihiko Hasegawa and Tan Van Vu. Fluctuation theorem uncertainty relation. *Phys. Rev. Lett.*, 123:110602, Sep 2019.
- [73] Sushant Saryal, Hava Meira Friedman, Dvira Segal, and Bijay Kumar Agarwalla. Thermodynamic uncertainty relation in thermal transport. *Phys. Rev. E*, 100:042101, Oct 2019.
- [74] Giacomo Guarnieri, Gabriel T. Landi, Stephen R. Clark, and John Goold. Thermodynamics of precision in quantum nonequilibrium steady states. *Phys. Rev. Research*, 1:033021, Oct 2019.
- [75] Sushant Saryal, Onkar Sadekar, and Bijay Kumar Agarwalla. Thermodynamic uncertainty relation for energy transport in a transient regime: A model study. *Phys. Rev. E*, 103:022141, Feb 2021.
- [76] Sreekanth K. Manikandan, Deepak Gupta, and Supriya Krishnamurthy. Inferring entropy production from short experiments. *Phys. Rev. Lett.*, 124:120603, Mar 2020.
- [77] Udo Seifert. From stochastic thermodynamics to thermodynamic inference. *Annual Review of Condensed Matter Physics*, 10(1):171–192, 2019.
- [78] R Kubo. The fluctuation-dissipation theorem. *Reports on Progress in Physics*, 29(1):255–284, jan 1966.
- [79] Hugo Touchette. The large deviation approach to statistical mechanics. *Physics Reports*, 478(1):1–69, 2009.
- [80] Simone Pigolotti, Izaak Neri, Édgar Roldán, and Frank Jülicher. Generic properties of stochastic entropy production. *Phys. Rev. Lett.*, 119:140604, Oct 2017.

- [81] Patrick Pietzonka, Felix Ritort, and Udo Seifert. Finite-time generalization of the thermodynamic uncertainty relation. *Phys. Rev. E*, 96:012101, Jul 2017.
- [82] Changbong Hyeon and Wonseok Hwang. Physical insight into the thermodynamic uncertainty relation using brownian motion in tilted periodic potentials. *Phys. Rev. E*, 96:012156, Jul 2017.
- [83] Yoshihiko Hasegawa and Tan Van Vu. Uncertainty relations in stochastic processes: An information inequality approach. *Phys. Rev. E*, 99:062126, Jun 2019.
- [84] Todd R Gingrich, Grant M Rotskoff, and Jordan M Horowitz. Inferring dissipation from current fluctuations. *Journal of Physics A: Mathematical and Theoretical*, 50(18):184004, apr 2017.
- [85] Deepak Gupta and Amos Maritan. Thermodynamic uncertainty relations in a linear system. *The European Physical Journal B*, 93(2):28, Feb 2020.
- [86] Patrick Pietzonka. Classical pendulum clocks break the thermodynamic uncertainty relation. *Phys. Rev. Lett.*, 128:130606, Apr 2022.
- [87] Timur Koyuk, Udo Seifert, and Patrick Pietzonka. A generalization of the thermodynamic uncertainty relation to periodically driven systems. *Journal of Physics A: Mathematical and Theoretical*, 52(2):02LT02, dec 2018.
- [88] Andre C Barato, Raphael Chetrite, Alessandra Faggionato, and Davide Gabrielli. Bounds on current fluctuations in periodically driven systems. *New Journal of Physics*, 20(10):103023, oct 2018.
- [89] Andreas Dechant. Multidimensional thermodynamic uncertainty relations. *Journal of Physics A: Mathematical and Theoretical*, 52(3):035001, dec 2018.
- [90] Wonseok Hwang and Changbong Hyeon. Energetic costs, precision, and transport efficiency of molecular motors. *The Journal of Physical Chemistry Letters*, 9(3):513–520, Feb 2018.

- [91] Robert Marsland, Wenping Cui, and Jordan M. Horowitz. The thermodynamic uncertainty relation in biochemical oscillations. *Journal of The Royal Society Interface*, 16(154):20190098, 2019.
- [92] Sangwon Lee, Changbong Hyeon, and Junghyo Jo. Thermodynamic uncertainty relation of interacting oscillators in synchrony. *Phys. Rev. E*, 98:032119, Sep 2018.
- [93] Mayank Shreshtha and Rosemary J. Harris. Thermodynamic uncertainty for run-and-tumble-type processes. *EPL (Europhysics Letters)*, 126(4):40007, jun 2019.
- [94] Patrick P. Potts and Peter Samuelsson. Thermodynamic uncertainty relations including measurement and feedback. *Phys. Rev. E*, 100:052137, Nov 2019.
- [95] Tan Van Vu and Yoshihiko Hasegawa. Uncertainty relation under information measurement and feedback control. *Journal of Physics A: Mathematical and Theoretical*, 53(7):075001, jan 2020.
- [96] Karel Proesmans and Jordan M Horowitz. Hysteretic thermodynamic uncertainty relation for systems with broken time-reversal symmetry. *Journal of Statistical Mechanics: Theory and Experiment*, 2019(5):054005, may 2019.
- [97] Kay Brandner, Taro Hanazato, and Keiji Saito. Thermodynamic bounds on precision in ballistic multiterminal transport. *Phys. Rev. Lett.*, 120:090601, Mar 2018.
- [98] Hyun-Myung Chun, Lukas P. Fischer, and Udo Seifert. Effect of a magnetic field on the thermodynamic uncertainty relation. *Phys. Rev. E*, 99:042128, Apr 2019.
- [99] Juan P. Garrahan. Simple bounds on fluctuations and uncertainty relations for first-passage times of counting observables. *Phys. Rev. E*, 95:032134, Mar 2017.
- [100] Todd R. Gingrich and Jordan M. Horowitz. Fundamental bounds on first passage time fluctuations for currents. *Phys. Rev. Lett.*, 119:170601, Oct 2017.
- [101] Krzysztof Ptaszyński. Coherence-enhanced constancy of a quantum thermoelectric generator. *Phys. Rev. B*, 98:085425, Aug 2018.

- [102] Junjie Liu and Dvira Segal. Thermodynamic uncertainty relation in quantum thermoelectric junctions. *Phys. Rev. E*, 99:062141, Jun 2019.
- [103] Matteo Polettini, Alexandre Lazarescu, and Massimiliano Esposito. Tightening the uncertainty principle for stochastic currents. *Phys. Rev. E*, 94:052104, Nov 2016.
- [104] Hava Meira Friedman, Bijay K. Agarwalla, Ofir Shein-Lumbroso, Oren Tal, and Dvira Segal. Thermodynamic uncertainty relation in atomic-scale quantum conductors. *Phys. Rev. B*, 101:195423, May 2020.
- [105] James A. McLennan. Statistical mechanics of the steady state. *Phys. Rev.*, 115:1405–1409, Sep 1959.
- [106] Selman Hershfield. Reformulation of steady state nonequilibrium quantum statistical mechanics. *Phys. Rev. Lett.*, 70:2134–2137, Apr 1993.
- [107] Harald Cramér. *Mathematical methods of statistics*. Princeton University Press, Princeton, 1946.
- [108] C. Radhakrishna Rao. *Information and the Accuracy Attainable in the Estimation of Statistical Parameters*, pages 235–247. Springer New York, New York, NY, 1992.
- [109] Soham Pal, Sushant Saryal, Dvira Segal, T. S. Mahesh, and Bijay Kumar Agarwalla. Experimental study of the thermodynamic uncertainty relation. *Phys. Rev. Research*, 2:022044, May 2020.
- [110] Ronnie Kosloff and Amikam Levy. Quantum heat engines and refrigerators: Continuous devices. *Annual Review of Physical Chemistry*, 65(1):365–393, 2014. PMID: 24689798.
- [111] Amikam Levy and David Gelbwaser-Klimovsky. *Quantum Features and Signatures of Quantum Thermal Machines*, pages 87–126. Springer International Publishing, Cham, 2018.
- [112] H Julian Goldsmid. *The Physics of Thermoelectric Energy Conversion*. 2053-2571. Morgan & Claypool Publishers, 2017.

- [113] Joshua P. Small, Kerstin M. Perez, and Philip Kim. Modulation of thermoelectric power of individual carbon nanotubes. *Phys. Rev. Lett.*, 91:256801, Dec 2003.
- [114] Akram I. Boukai, Yuri Bunimovich, Jamil Tahir-Kheli, Jen-Kan Yu, William A. Goddard III, and James R. Heath. Silicon nanowires as efficient thermoelectric materials. *Nature*, 451(7175):168–171, Jan 2008.
- [115] Yonatan Dubi and Massimiliano Di Ventra. Colloquium: Heat flow and thermoelectricity in atomic and molecular junctions. *Rev. Mod. Phys.*, 83:131–155, Mar 2011.
- [116] B. Roche, P. Roulleau, T. Jullien, Y. Jompol, I. Farrer, D. A. Ritchie, and D. C. Glattli. Harvesting dissipated energy with a mesoscopic ratchet. *Nature Communications*, 6(1):6738, Apr 2015.
- [117] Björn Sothmann, Rafael Sánchez, and Andrew N Jordan. Thermoelectric energy harvesting with quantum dots. *Nanotechnology*, 26(3):032001, dec 2014.
- [118] Jeffrey M. Gordon and Kim Choon. Ng. *Cool thermodynamics : the engineering and physics of predictive, diagnostic and optimization methods for cooling systems*. Cambridge International Science Pub., Cambridge, UK, 2001.
- [119] Mark T. Mitchison. Quantum thermal absorption machines: refrigerators, engines and clocks. *Contemporary Physics*, 60(2):164–187, 2019.
- [120] Noah Linden, Sandu Popescu, and Paul Skrzypczyk. How small can thermal machines be? the smallest possible refrigerator. *Phys. Rev. Lett.*, 105:130401, Sep 2010.
- [121] Amikam Levy and Ronnie Kosloff. Quantum absorption refrigerator. *Phys. Rev. Lett.*, 108:070604, Feb 2012.
- [122] Luis A. Correa, José P. Palao, Gerardo Adesso, and Daniel Alonso. Performance bound for quantum absorption refrigerators. *Phys. Rev. E*, 87:042131, Apr 2013.
- [123] Anqi Mu, Bijay Kumar Agarwalla, Gernot Schaller, and Dvira Segal. Qubit absorption refrigerator at strong coupling. *New Journal of Physics*, 19(12):123034, dec 2017.

- [124] Patrick P. Hofer, Martí Perarnau-Llobet, Jonatan Bohr Brask, Ralph Silva, Marcus Huber, and Nicolas Brunner. Autonomous quantum refrigerator in a circuit qed architecture based on a josephson junction. *Phys. Rev. B*, 94:235420, Dec 2016.
- [125] Davide Venturelli, Rosario Fazio, and Vittorio Giovannetti. Minimal self-contained quantum refrigeration machine based on four quantum dots. *Phys. Rev. Lett.*, 110:256801, Jun 2013.
- [126] Mark T Mitchison, Marcus Huber, Javier Prior, Mischa P Woods, and Martin B Plenio. Realising a quantum absorption refrigerator with an atom-cavity system. *Quantum Science and Technology*, 1(1):015001, mar 2016.
- [127] Paolo Andrea Erdman, Bibek Bhandari, Rosario Fazio, Jukka P. Pekola, and Fabio Taddei. Absorption refrigerators based on coulomb-coupled single-electron systems. *Phys. Rev. B*, 98:045433, Jul 2018.
- [128] Sushant Saryal and Bijay Kumar Agarwalla. Bounds on fluctuations for finite-time quantum otto cycle. *Phys. Rev. E*, 103:L060103, Jun 2021.
- [129] H. T. Quan, Yu-xi Liu, C. P. Sun, and Franco Nori. Quantum thermodynamic cycles and quantum heat engines. *Phys. Rev. E*, 76:031105, Sep 2007.
- [130] Armen E. Allahverdyan, Ramandeep S. Johal, and Guenter Mahler. Work extremum principle: Structure and function of quantum heat engines. *Phys. Rev. E*, 77:041118, Apr 2008.
- [131] H. E. D. Scovil and E. O. Schulz-DuBois. Three-level masers as heat engines. *Phys. Rev. Lett.*, 2:262–263, Mar 1959.
- [132] Raam Uzdin and Ronnie Kosloff. The multilevel four-stroke swap engine and its environment. *New Journal of Physics*, 16(9):095003, sep 2014.
- [133] Massimiliano F. Sacchi. Multilevel quantum thermodynamic swap engines. *Phys. Rev. A*, 104:012217, Jul 2021.

- [134] Michele Campisi, Jukka Pekola, and Rosario Fazio. Nonequilibrium fluctuations in quantum heat engines: theory, example, and possible solid state experiments. *New Journal of Physics*, 17(3):035012, mar 2015.
- [135] Udo Seifert. Stochastic thermodynamics, fluctuation theorems and molecular machines. *Reports on Progress in Physics*, 75(12):126001, nov 2012.
- [136] Patrick Pietzonka, Andre C. Barato, and Udo Seifert. Universal bounds on current fluctuations. *Phys. Rev. E*, 93:052145, May 2016.
- [137] Udo Seifert. Entropy production along a stochastic trajectory and an integral fluctuation theorem. *Phys. Rev. Lett.*, 95:040602, Jul 2005.
- [138] Izaak Neri, Édgar Roldán, and Frank Jülicher. Statistics of infima and stopping times of entropy production and applications to active molecular processes. *Phys. Rev. X*, 7:011019, Feb 2017.
- [139] Gatién Verley, Tim Willaert, Christian Van den Broeck, and Massimiliano Esposito. Universal theory of efficiency fluctuations. *Phys. Rev. E*, 90:052145, Nov 2014.
- [140] Gatién Verley, Massimiliano Esposito, Tim Willaert, and Christian Van den Broeck. The unlikely carnot efficiency. *Nature Communications*, 5(1):4721, Sep 2014.
- [141] Sreekanth K. Manikandan, Lennart Dabelow, Ralf Eichhorn, and Supriya Krishnamurthy. Efficiency fluctuations in microscopic machines. *Phys. Rev. Lett.*, 122:140601, Apr 2019.
- [142] Marc Suñé and Alberto Imparato. Efficiency fluctuations in steady-state machines. *Journal of Physics A: Mathematical and Theoretical*, 52(4):045003, jan 2019.
- [143] Kosuke Ito, Chao Jiang, and Gentaro Watanabe. Universal bounds for fluctuations in small heat engines, 2019.
- [144] Takuya Kamijima, Shun Otsubo, Yuto Ashida, and Takahiro Sagawa. Higher-order efficiency bound and its application to nonlinear nanothermoelectrics. *Phys. Rev. E*, 104:044115, Oct 2021.

- [145] Lars Onsager. Reciprocal relations in irreversible processes. i. *Phys. Rev.*, 37:405–426, Feb 1931.
- [146] Lars Onsager. Reciprocal relations in irreversible processes. ii. *Phys. Rev.*, 38:2265–2279, Dec 1931.
- [147] Giuliano Benenti, Giulio Casati, Keiji Saito, and Robert S. Whitney. Fundamental aspects of steady-state conversion of heat to work at the nanoscale. *Physics Reports*, 694:1–124, 2017. Fundamental aspects of steady-state conversion of heat to work at the nanoscale.
- [148] C. R. Johnson. Positive definite matrices. *The American Mathematical Monthly*, 77(3):259–264, 1970.
- [149] Lesovik G. B. Levitov L. S. Charge distribution in quantum shot noise. *JETP Lett.*, 58:225, August 1993.
- [150] K. Schönhammer. Full counting statistics for noninteracting fermions: Exact results and the levitov-lesovik formula. *Phys. Rev. B*, 75:205329, May 2007.
- [151] Massimiliano Di Ventra. *Electrical Transport in Nanoscale Systems*. Cambridge University Press, 2008.
- [152] Sushant Saryal, Matthew Gerry, Ilia Khait, Dvira Segal, and Bijay Kumar Agarwalla. Universal bounds on fluctuations in continuous thermal machines. *Phys. Rev. Lett.*, 127:190603, Nov 2021.
- [153] Sandipan Mohanta, Sushant Saryal, and Bijay Kumar Agarwalla. Universal bounds on cooling power and cooling efficiency for autonomous absorption refrigerators. *Phys. Rev. E*, 105:034127, Mar 2022.
- [154] Luis A. Correa, José P. Palao, Daniel Alonso, and Gerardo Adesso. Quantum-enhanced absorption refrigerators. *Scientific Reports*, 4(1):3949, Feb 2014.
- [155] Dvira Segal. Current fluctuations in quantum absorption refrigerators. *Phys. Rev. E*, 97:052145, May 2018.

- [156] Keiji Saito, Giuliano Benenti, Giulio Casati, and Tomaž Prosen. Thermopower with broken time-reversal symmetry. *Phys. Rev. B*, 84:201306, Nov 2011.
- [157] O. Entin-Wohlman and A. Aharony. Three-terminal thermoelectric transport under broken time-reversal symmetry. *Phys. Rev. B*, 85:085401, Feb 2012.
- [158] Kay Brandner, Keiji Saito, and Udo Seifert. Thermodynamics of micro- and nano-systems driven by periodic temperature variations. *Phys. Rev. X*, 5:031019, Aug 2015.
- [159] Viktor Holubec and Artem Ryabov. Cycling tames power fluctuations near optimum efficiency. *Phys. Rev. Lett.*, 121:120601, Sep 2018.
- [160] Kay Brandner, Keiji Saito, and Udo Seifert. Strong bounds on onsager coefficients and efficiency for three-terminal thermoelectric transport in a magnetic field. *Phys. Rev. Lett.*, 110:070603, Feb 2013.
- [161] Kay Brandner and Udo Seifert. Multi-terminal thermoelectric transport in a magnetic field: bounds on onsager coefficients and efficiency. *New Journal of Physics*, 15(10):105003, oct 2013.
- [162] Giuliano Benenti, Keiji Saito, and Giulio Casati. Thermodynamic bounds on efficiency for systems with broken time-reversal symmetry. *Phys. Rev. Lett.*, 106:230602, Jun 2011.
- [163] Jian-Hua Jiang, Bijay Kumar Agarwalla, and Dvira Segal. Efficiency statistics and bounds for systems with broken time-reversal symmetry. *Phys. Rev. Lett.*, 115:040601, Jul 2015.
- [164] Matthew Gerry, Na'im Kalantar, and Dvira Segal. Bounds on fluctuations for ensembles of quantum thermal machines. *Journal of Physics A: Mathematical and Theoretical*, 55(10):104005, feb 2022.
- [165] Sushant Saryal, Sandipan Mohanta, and Bijay Kumar Agarwalla. Bounds on fluctuations for machines with broken time-reversal symmetry: A linear response study. *Phys. Rev. E*, 105:024129, Feb 2022.

- [166] M. Büttiker. Small normal-metal loop coupled to an electron reservoir. *Phys. Rev. B*, 32:1846–1849, Aug 1985.
- [167] M. Büttiker. Role of quantum coherence in series resistors. *Phys. Rev. B*, 33:3020–3026, Mar 1986.
- [168] Tobias Denzler and Eric Lutz. Efficiency fluctuations of a quantum heat engine. *Phys. Rev. Research*, 2:032062, Sep 2020.
- [169] Vladimir Gritsev, Peter Barmettler, and Eugene Demler. Scaling approach to quantum non-equilibrium dynamics of many-body systems. *New Journal of Physics*, 12(11):113005, nov 2010.
- [170] Christopher Jarzynski. Generating shortcuts to adiabaticity in quantum and classical dynamics. *Phys. Rev. A*, 88:040101, Oct 2013.
- [171] Adolfo del Campo. Shortcuts to adiabaticity by counterdiabatic driving. *Phys. Rev. Lett.*, 111:100502, Sep 2013.
- [172] Sebastian Deffner, Christopher Jarzynski, and Adolfo del Campo. Classical and quantum shortcuts to adiabaticity for scale-invariant driving. *Phys. Rev. X*, 4:021013, Apr 2014.
- [173] Mathieu Beau, Juan Jaramillo, and Adolfo Del Campo. Scaling-up quantum heat engines efficiently via shortcuts to adiabaticity. *Entropy*, 18(5), 2016.
- [174] Tobias Denzler. Fluctuations and correlations of quantum heat engines, ph.d. thesis, university of stuttgart, 2020.
- [175] Sebastian Deffner and Eric Lutz. Nonequilibrium work distribution of a quantum harmonic oscillator. *Phys. Rev. E*, 77:021128, Feb 2008.
- [176] Keiji Saito and Yasuhiro Utsumi. Symmetry in full counting statistics, fluctuation theorem, and relations among nonlinear transport coefficients in the presence of a magnetic field. *Phys. Rev. B*, 78:115429, Sep 2008.

- [177] Abraham Nitzan. *Chemical Dynamics in Condensed Phases: Relaxation, Transfer and Reactions in Condensed Molecular Systems*. Oxford Graduate Texts. Oxford University Press, Oxford, 2006.
- [178] David Sánchez and Markus Büttiker. Magnetic-field asymmetry of nonlinear mesoscopic transport. *Phys. Rev. Lett.*, 93:106802, Sep 2004.
- [179] B. Spivak and A. Zyuzin. Signature of the electron-electron interaction in the magnetic-field dependence of nonlinear I-V characteristics in mesoscopic systems. *Phys. Rev. Lett.*, 93:226801, Nov 2004.
- [180] Jürgen König and Yuval Gefen. Aharonov-bohm interferometry with interacting quantum dots: Spin configurations, asymmetric interference patterns, bias-voltage-induced aharonov-bohm oscillations, and symmetries of transport coefficients. *Phys. Rev. B*, 65:045316, Jan 2002.
- [181] Julian Schwinger. Brownian motion of a quantum oscillator. *Journal of Mathematical Physics*, 2(3):407–432, 1961.
- [182] J. Rammer and H. Smith. Quantum field-theoretical methods in transport theory of metals. *Rev. Mod. Phys.*, 58:323–359, Apr 1986.
- [183] Massimiliano F. Sacchi. Thermodynamic uncertainty relations for bosonic otto engines. *Phys. Rev. E*, 103:012111, Jan 2021.
- [184] Soham Pal, T. S. Mahesh, and Bijay Kumar Agarwalla. Experimental demonstration of the validity of the quantum heat-exchange fluctuation relation in an nmr setup. *Phys. Rev. A*, 100:042119, Oct 2019.
- [185] L. Mazzola, G. De Chiara, and M. Paternostro. Measuring the characteristic function of the work distribution. *Phys. Rev. Lett.*, 110:230602, Jun 2013.
- [186] R. Dorner, S. R. Clark, L. Heaney, R. Fazio, J. Goold, and V. Vedral. Extracting quantum work statistics and fluctuation theorems by single-qubit interferometry. *Phys. Rev. Lett.*, 110:230601, Jun 2013.

- [187] Michele Campisi, Ralf Blattmann, Sigmund Kohler, David Zueco, and Peter Hänggi. Employing circuit QED to measure non-equilibrium work fluctuations. *New Journal of Physics*, 15(10):105028, oct 2013.
- [188] Christopher Gerry and Peter Knight. *Introductory Quantum Optics*. Cambridge University Press, 2004.
- [189] Leonid Veniaminovich Keldysh. Diagram technique for nonequilibrium processes. *Sov.Phys.JETP*, 2:052101, 1965.
- [190] Gerald D. Mahan. *Many-particle physics*. Plenum Press, New York, 1993.
- [191] Hartmut Haug and A. P. Jauho. *Quantum Kinetics in Transport and Optics of Semiconductors*. Springer, 2004.
- [192] Michael Kilgour, Bijay Kumar Agarwalla, and Dvira Segal. Path-integral methodology and simulations of quantum thermal transport: Full counting statistics approach. *The Journal of Chemical Physics*, 150(8):084111, 2019.
- [193] Marlon Brenes, Juan José Mendoza-Arenas, Archak Purkayastha, Mark T. Mitchison, Stephen R. Clark, and John Goold. Tensor-network method to simulate strongly interacting quantum thermal machines. *Phys. Rev. X*, 10:031040, Aug 2020.
- [194] T. E. Humphrey, R. Newbury, R. P. Taylor, and H. Linke. Reversible quantum brownian heat engines for electrons. *Phys. Rev. Lett.*, 89:116801, Aug 2002.
- [195] M. Esposito, K. Lindenberg, and C. Van den Broeck. Thermoelectric efficiency at maximum power in a quantum dot. *EPL (Europhysics Letters)*, 85(6):60010, mar 2009.
- [196] Anupam Kundu, Sanjib Sabhapandit, and Abhishek Dhar. Large deviations of heat flow in harmonic chains. *Journal of Statistical Mechanics: Theory and Experiment*, 2011(03):P03007, mar 2011.